

University of Windsor

## Scholarship at UWindor

---

Electronic Theses and Dissertations

Theses, Dissertations, and Major Papers

---

1995

### Numerical analysis of two phase fluid flow and heat transfer in a condenser.

Atish. Bokil  
*University of Windsor*

Follow this and additional works at: <https://scholar.uwindsor.ca/etd>

---

#### Recommended Citation

Bokil, Atish., "Numerical analysis of two phase fluid flow and heat transfer in a condenser." (1995).  
*Electronic Theses and Dissertations*. 2882.  
<https://scholar.uwindsor.ca/etd/2882>

This online database contains the full-text of PhD dissertations and Masters' theses of University of Windsor students from 1954 forward. These documents are made available for personal study and research purposes only, in accordance with the Canadian Copyright Act and the Creative Commons license—CC BY-NC-ND (Attribution, Non-Commercial, No Derivative Works). Under this license, works must always be attributed to the copyright holder (original author), cannot be used for any commercial purposes, and may not be altered. Any other use would require the permission of the copyright holder. Students may inquire about withdrawing their dissertation and/or thesis from this database. For additional inquiries, please contact the repository administrator via email ([scholarship@uwindsor.ca](mailto:scholarship@uwindsor.ca)) or by telephone at 519-253-3000ext. 3208.



National Library  
of Canada

Bibliothèque nationale  
du Canada

Acquisitions and  
Bibliographic Services Branch

Direction des acquisitions et  
des services bibliographiques

395 Wellington Street  
Ottawa, Ontario  
K1A 0N4

395, rue Wellington  
Ottawa (Ontario)  
K1A 0N4

*Your file - Votre référence*

*Our file - Notre référence*

## NOTICE

## AVIS

The quality of this microform is heavily dependent upon the quality of the original thesis submitted for microfilming. Every effort has been made to ensure the highest quality of reproduction possible.

La qualité de cette microforme dépend grandement de la qualité de la thèse soumise au microfilmage. Nous avons tout fait pour assurer une qualité supérieure de reproduction.

If pages are missing, contact the university which granted the degree.

S'il manque des pages, veuillez communiquer avec l'université qui a conféré le grade.

Some pages may have indistinct print especially if the original pages were typed with a poor typewriter ribbon or if the university sent us an inferior photocopy.

La qualité d'impression de certaines pages peut laisser à désirer, surtout si les pages originales ont été dactylographiées à l'aide d'un ruban usé ou si l'université nous a fait parvenir une photocopie de qualité inférieure.

Reproduction in full or in part of this microform is governed by the Canadian Copyright Act, R.S.C. 1970, c. C-30, and subsequent amendments.

La reproduction, même partielle, de cette microforme est soumise à la Loi canadienne sur le droit d'auteur, SRC 1970, c. C-30, et ses amendements subséquents.

Canada

**Numerical Analysis of Two Phase Fluid Flow  
and Heat Transfer in a Condenser**

**by**

**Atish Bokil**

**A Thesis**

**Submitted to the Faculty of Graduate Studies and Research  
through the Department of Mechanical Engineering  
in Partial Fulfillment of the Requirements for  
the Degree of Master of Applied Science at  
the University of Windsor**

**Windsor, Ontario, Canada**

**1994**

**(c) 1994 Atish Bokil**



National Library  
of Canada

Bibliothèque nationale  
du Canada

Acquisitions and  
Bibliographic Services Branch

Direction des acquisitions et  
des services bibliographiques

395 Wellington Street  
Ottawa, Ontario  
K1A 0N4

395, rue Wellington  
Ottawa (Ontario)  
K1A 0N4

*Your file* *Votre référence*

*Our file* *Notre référence*

THE AUTHOR HAS GRANTED AN IRREVOCABLE NON-EXCLUSIVE LICENCE ALLOWING THE NATIONAL LIBRARY OF CANADA TO REPRODUCE, LOAN, DISTRIBUTE OR SELL COPIES OF HIS/HER THESIS BY ANY MEANS AND IN ANY FORM OR FORMAT, MAKING THIS THESIS AVAILABLE TO INTERESTED PERSONS.

L'AUTEUR A ACCORDE UNE LICENCE IRREVOCABLE ET NON EXCLUSIVE PERMETTANT A LA BIBLIOTHEQUE NATIONALE DU CANADA DE REPRODUIRE, PRETER, DISTRIBUER OU VENDRE DES COPIES DE SA THESE DE QUELQUE MANIERE ET SOUS QUELQUE FORME QUE CE SOIT POUR METTRE DES EXEMPLAIRES DE CETTE THESE A LA DISPOSITION DES PERSONNE INTERESSEES.

THE AUTHOR RETAINS OWNERSHIP OF THE COPYRIGHT IN HIS/HER THESIS. NEITHER THE THESIS NOR SUBSTANTIAL EXTRACTS FROM IT MAY BE PRINTED OR OTHERWISE REPRODUCED WITHOUT HIS/HER PERMISSION.

L'AUTEUR CONSERVE LA PROPRIETE DU DROIT D'AUTEUR QUI PROTEGE SA THESE. NI LA THESE NI DES EXTRAITS SUBSTANTIELS DE CELLE-CI NE DOIVENT ETRE IMPRIMES OU AUTREMENT REPRODUITS SANS SON AUTORISATION.

ISBN 0-612-01433-9

Canada

Name ATISH BOKIL

Dissertation Abstracts International is arranged by broad, general subject categories. Please select the one subject which most nearly describes the content of your dissertation. Enter the corresponding four-digit code in the spaces provided.

MECHANICAL

0 5 4 8

U·M·I

SUBJECT TERM

SUBJECT CODE

**Subject Categories**

**THE HUMANITIES AND SOCIAL SCIENCES**

**COMMUNICATIONS AND THE ARTS**

Architecture ..... 0729  
 Art History ..... 0377  
 Cinema ..... 0900  
 Dance ..... 0378  
 Fine Arts ..... 0357  
 Information Science ..... 0723  
 Journalism ..... 0391  
 Library Science ..... 0399  
 Mass Communications ..... 0708  
 Music ..... 0413  
 Speech Communication ..... 0459  
 Theater ..... 0465

**EDUCATION**

General ..... 0515  
 Administration ..... 0514  
 Adult and Continuing ..... 0516  
 Agricultural ..... 0517  
 Art ..... 0273  
 Bilingual and Multicultural ..... 0282  
 Business ..... 0688  
 Community College ..... 0275  
 Curriculum and Instruction ..... 0727  
 Early Childhood ..... 0518  
 Elementary ..... 0524  
 Finance ..... 0277  
 Guidance and Counseling ..... 0519  
 Health ..... 0680  
 Higher ..... 0745  
 History of ..... 0520  
 Home Economics ..... 0278  
 Industrial ..... 0521  
 Language and Literature ..... 0279  
 Mathematics ..... 0280  
 Music ..... 0522  
 Philosophy of ..... 0998  
 Physical ..... 0523

Psychology ..... 0525  
 Reading ..... 0535  
 Religious ..... 0527  
 Sciences ..... 0714  
 Secondary ..... 0533  
 Social Sciences ..... 0534  
 Sociology of ..... 0340  
 Special ..... 0529  
 Teacher Training ..... 0530  
 Technology ..... 0710  
 Tests and Measurements ..... 0288  
 Vocational ..... 0747

**LANGUAGE, LITERATURE AND LINGUISTICS**

Language

General ..... 0679  
 Ancient ..... 0289  
 Linguistics ..... 0290  
 Modern ..... 0291

Literature

General ..... 0401  
 Classical ..... 0294  
 Comparative ..... 0295  
 Medieval ..... 0297  
 Modern ..... 0298  
 African ..... 0316  
 American ..... 0591  
 Asian ..... 0305  
 Canadian (English) ..... 0352  
 Canadian (French) ..... 0355  
 English ..... 0593  
 Germanic ..... 0311  
 Latin American ..... 0312  
 Middle Eastern ..... 0315  
 Romance ..... 0313  
 Slavic and East European ..... 0314

**PHILOSOPHY, RELIGION AND THEOLOGY**

Philosophy ..... 0422  
 Religion

General ..... 0318  
 Biblical Studies ..... 0321  
 Clergy ..... 0319  
 History of ..... 0320  
 Philosophy of ..... 0322  
 Theology ..... 0469

**SOCIAL SCIENCES**

American Studies ..... 0323  
 Anthropology

Archaeology ..... 0324  
 Cultural ..... 0326  
 Physical ..... 0327

Business Administration

General ..... 0310  
 Accounting ..... 0272  
 Banking ..... 0770  
 Management ..... 0454  
 Marketing ..... 0338

Canadian Studies ..... 0385

Economics

General ..... 0501  
 Agricultural ..... 0503  
 Commerce-Business ..... 0505  
 Finance ..... 0508  
 History ..... 0509  
 Labor ..... 0510  
 Theory ..... 0511

Folklore ..... 0358  
 Geography ..... 0366  
 Gerontology ..... 0351  
 History

General ..... 0578

Ancient ..... 0579  
 Medieval ..... 0581  
 Modern ..... 0582  
 Black ..... 0328  
 African ..... 0331  
 Asia, Australia and Oceania ..... 0332  
 Canadian ..... 0334  
 European ..... 0335  
 Latin American ..... 0336  
 Middle Eastern ..... 0333  
 United States ..... 0337  
 History of Science ..... 0585  
 Law ..... 0398  
 Political Science

General ..... 0615  
 International Law and Relations ..... 0616  
 Public Administration ..... 0617  
 Recreation ..... 0814  
 Social Work ..... 0452

Sociology

General ..... 0626  
 Criminology and Penology ..... 0627  
 Demography ..... 0938  
 Ethnic and Racial Studies ..... 0631  
 Individual and Family Studies ..... 0628  
 Industrial and Labor Relations ..... 0629  
 Public and Social Welfare ..... 0630  
 Social Structure and Development ..... 0700  
 Theory and Methods ..... 0344  
 Transportation ..... 0709  
 Urban and Regional Planning ..... 0999  
 Women's Studies ..... 0453

**THE SCIENCES AND ENGINEERING**

**BIOLOGICAL SCIENCES**

Agriculture

General ..... 0473  
 Agronomy ..... 0285  
 Animal Culture and Nutrition ..... 0475  
 Animal Pathology ..... 0476  
 Food Science and Technology ..... 0359  
 Forestry and Wildlife ..... 0478  
 Plant Culture ..... 0479  
 Plant Pathology ..... 0480  
 Plant Physiology ..... 0817  
 Range Management ..... 0777  
 Wood Technology ..... 0746

Biology

General ..... 0306  
 Anatomy ..... 0287  
 Biostatistics ..... 0308  
 Botany ..... 0309  
 Cell ..... 0379  
 Ecology ..... 0329  
 Entomology ..... 0353  
 Genetics ..... 0369  
 Limnology ..... 0793  
 Microbiology ..... 0410  
 Molecular ..... 0307  
 Neuroscience ..... 0317  
 Oceanography ..... 0416  
 Physiology ..... 0433  
 Radiation ..... 0821  
 Veterinary Science ..... 0778  
 Zoology ..... 0472

Biophysics

General ..... 0786  
 Medical ..... 0760

**EARTH SCIENCES**

Biogeochemistry ..... 0425  
 Geochemistry ..... 0996

Geodesy ..... 0370  
 Geology ..... 0372  
 Geophysics ..... 0373  
 Hydrology ..... 0388  
 Mineralogy ..... 0411  
 Paleobotany ..... 0345  
 Paleocology ..... 0426  
 Paleontology ..... 0418  
 Paleozoology ..... 0985  
 Palynology ..... 0427  
 Physical Geography ..... 0368  
 Physical Oceanography ..... 0415

**HEALTH AND ENVIRONMENTAL SCIENCES**

Environmental Sciences ..... 0768  
 Health Sciences

General ..... 0566  
 Audiology ..... 0300  
 Chemotherapy ..... 0992  
 Dentistry ..... 0567  
 Education ..... 0350  
 Hospital Management ..... 0769  
 Human Development ..... 0758  
 Immunology ..... 0982  
 Medicine and Surgery ..... 0564  
 Mental Health ..... 0347  
 Nursing ..... 0569  
 Nutrition ..... 0570  
 Obstetrics and Gynecology ..... 0380  
 Occupational Health and Therapy ..... 0354  
 Ophthalmology ..... 0381  
 Pathology ..... 0571  
 Pharmacology ..... 0419  
 Pharmacy ..... 0572  
 Physical Therapy ..... 0382  
 Public Health ..... 0573  
 Radiology ..... 0574  
 Recreation ..... 0575

Speech Pathology ..... 0460  
 Toxicology ..... 0383  
 Home Economics ..... 0386

**PURE SCIENCES**

Chemistry

General ..... 0485  
 Agricultural ..... 0749  
 Analytical ..... 0486  
 Biochemistry ..... 0487  
 Inorganic ..... 0488  
 Nuclear ..... 0738  
 Organic ..... 0490  
 Pharmaceutical ..... 0491  
 Physical ..... 0494  
 Polymer ..... 0495  
 Radiation ..... 0754

Mathematics ..... 0405

Physics

General ..... 0605  
 Acoustics ..... 0986  
 Astronomy and Astrophysics ..... 0606  
 Atmospheric Science ..... 0608  
 Atomic ..... 0748  
 Electronics and Electricity ..... 0607  
 Elementary Particles and High Energy ..... 0798  
 Fluid and Plasma ..... 0759  
 Molecular ..... 0609  
 Nuclear ..... 0610  
 Optics ..... 0752  
 Radiation ..... 0756  
 Solid State ..... 0611

Statistics ..... 0463

**Applied Sciences**

Applied Mechanics ..... 0346  
 Computer Science ..... 0984

Engineering

General ..... 0537  
 Aerospace ..... 0538  
 Agricultural ..... 0539  
 Automotive ..... 0540  
 Biomedical ..... 0541  
 Chemical ..... 0542  
 Civil ..... 0543  
 Electronics and Electrical ..... 0544  
 Heat and Thermodynamics ..... 0348  
 Hydraulic ..... 0545  
 Industrial ..... 0546  
 Marine ..... 0547  
 Materials Science ..... 0794  
 Mechanical ..... 0548  
 Metallurgy ..... 0743  
 Mining ..... 0551  
 Nuclear ..... 0552  
 Packaging ..... 0549  
 Petroleum ..... 0765  
 Sanitary and Municipal ..... 0554  
 System Science ..... 0790

Geotechnology ..... 0428  
 Operations Research ..... 0796  
 Plastics Technology ..... 0795  
 Textile Technology ..... 0994

**PSYCHOLOGY**

General ..... 0621  
 Behavioral ..... 0384  
 Fluid ..... 0622  
 Clinical ..... 0620  
 Developmental ..... 0620  
 Experimental ..... 0623  
 Industrial ..... 0624  
 Personality ..... 0625  
 Physiological ..... 0989  
 Psychobiology ..... 0349  
 Psychometrics ..... 0632  
 Social ..... 0451



## **ABSTRACT**

A quasi-three-dimensional algorithm is developed to simulate two-phase fluid flow and heat transfer in the shell side of power plant condensers. The simulation method developed is based on the fundamental governing conservation equations of mass and momentum for both gas and liquid phases, and the air mass fraction conservation equation. In the proposed numerical method, the condenser shell side is subdivided into a number of domains normal to the cooling water flow direction. The three-dimensional effects due to the cooling water temperature difference are taken into account by a series of two dimensional calculations, each being for one domain. A porous media concept is employed to model the tube bank. The pressure drop balance concept is used to determine the inlet mass flow rate for each domain. A staggered grid is used to perform the discretization. The resulting discretized equations are solved using the SIMPLEC algorithm.

The numerical predictions of an experimental steam condenser are compared with the available experimental results. The predicted results are in good agreement with the experimental data. The results also show an improvement over the results obtained using a single-phase model. Sensitivity studies are carried out for four different correlations of condensation heat transfer coefficient.

## **ACKNOWLEDGEMENT**

It is a great pleasure for me to express my sincere gratitude to my supervisor, Dr. Chao Zhang, for her invaluable guidance, encouragement and support during the course of this work.

Special thanks go to the other committee members, Dr. Barron, Dr. Rankin and Dr. McCorquodale, for their kind cooperation, helpful suggestions and comments. The assistance rendered by Dr. Sridhar is also gratefully acknowledged.

The assistance rendered by several fellow graduate students, especially Mr. Dinakara Karanth, Mr. Satya Kurada and Mr. Vijayakanthan Damodaran, is greatly appreciated.

The financial assistance from the University of Windsor is gratefully acknowledged. The facilities provided by the University of Windsor Computer Center are also recognized. The assistance rendered by Ms. Jaya Sreedharan is greatly appreciated.

# TABLE OF CONTENTS

<b>ABSTRACT</b>	<b>iii</b>
<b>ACKNOWLEDGEMENTS</b>	<b>iv</b>
<b>LIST OF FIGURES</b>	<b>vii</b>
<b>LIST OF TABLES</b>	<b>ix</b>
<b>NOMENCLATURE</b>	<b>x</b>
<b>CHAPTER</b>	
<b>I. INTRODUCTION</b>	<b>1</b>
1.1 Motivation	1
1.2 Scope of Present Work	2
1.3 Outline of the Thesis	3
<b>II. REVIEW OF PREVIOUS WORK</b>	<b>5</b>
2.1 Prediction of Fluid Flow and Heat Transfer using Single-Phase Models	5
2.2 Prediction of Fluid Flow and Heat Transfer using Two-Phase Models	7
<b>III. NUMERICAL MODEL AND ANALYSIS</b>	<b>11</b>
3.1 Physical Representation	11
3.2 Mathematical Formulation	12
3.3 Boundary Conditions	22
<b>IV. NUMERICAL SOLUTION TECHNIQUE</b>	<b>25</b>
4.1 General Form of Differential Equations	25
4.2 Grid Arrangement	27
4.3 Discretized Equations	27



4.4	Solution of Linear Algebraic Equations	33
4.5	Solution Procedure for One Domain: Sequence of operations	34
4.6	Convergence Criteria for Each Domain	35
4.7	Overall Solution Procedure	36
4.8	Overall Convergence Criteria	37
<b>V.</b>	<b>RESULTS AND DISCUSSION</b>	<b>38</b>
5.1	The Experimental Configuration	38
5.2	Computational Details	39
5.3	Results	39
5.4	Comparison of the Results From Quasi-Three-Dimensional Two-Phase Model and Two-Dimensional Two-Phase Model	44
5.5	Comparison of Results From Quasi-Three-Dimensional Two-Phase Model and Quasi-Three-Dimensional Single-Phase Model	45
5.6	Sensitivity Study of Heat Transfer Coefficient Correlations	46
<b>VI.</b>	<b>CONCLUSION</b>	<b>50</b>
6.1	Concluding Remarks	50
6.2	Future Work	51
	<b>REFERENCES</b>	<b>53</b>
	<b>FIGURES</b>	<b>58</b>
	<b>VITA AUCTORIS</b>	<b>100</b>

## LIST OF FIGURES

4.1	Grid Arrangement	58
4.2	Flow Chart	59
5.1	Configuration of the Experimental Condenser	60
5.2	Position of Tube Rows in the Condenser	61
5.3	Grid Used for the Simulation	62
5.4	Velocity Vector Plots for Plane no.3	63-64
5.5	Contour Map of Gas Velocity Magnitude for Plane no.3	65
5.6	Contour Map of Liquid Velocity Magnitude for Plane no.3	66
5.7	Contour Maps of Air Mass Fraction	67-71
5.8	Contour Maps of Heat Flux	72-76
5.9	Contour Map of Cooling Water Temperature for Plane no.3	77
5.10	Contour Map of Condensation Rate for Plane no.3	78
5.11	Contour Map of Liquid Volume Fraction for Plane no.3 (Droplet Diameter=0.001m)	79
5.12	Contour Map of Interphase Friction Force for Plane no.3 (Droplet Diameter=0.001m)	80

5.13	Contour Map of Interphase Friction Force per unit Gravitational Force for Plane no.3 (Droplet Diameter=0.001m)	81
5.14	Contour Map of Liquid Volume Fraction for Plane no.3 (Droplet Diameter=0.004m)	82
5.15	Contour Map of Interphase Friction Force per unit Gravitational Force for Plane no.3 (Droplet Diameter=0.004m)	83
5.16	Comparison of Predicted Heat Flux with Experimental Data	84-87
5.17	Comparison of Predicted Heat Flux with Bush's Results	88-91
5.18	Comparison of Predicted Heat Flux with Results Obtained From Two Different Methodologies of Quasi- Three-Dimensional Single-Phase Model	92-95
5.19	Comparison of Predicted Heat Flux for Different Correlations of Condensation Heat Transfer Coefficient	96-99

## LIST OF TABLES

5.1	Geometrical Parameters of the Experimental Condenser	38
5.2	Operating Parameters of the Experimental Condenser	39
5.3	Predicted Total Condensation Rates by Using Different Correlations of Condensation Heat Transfer Coefficient for Quasi-Three-Dimensional Two-Phase Model	48
5.4	Predicted Total Condensation Rates by Using Different Correlations of Condensation Heat Transfer Coefficient for Quasi-Three-Dimensional Single-Phase Model(Method I)	48
5.5	Predicted Total Condensation Rates by Using Different Correlations of Condensation Heat Transfer Coefficient for Quasi-Three-Dimensional Single-Phase Model (Method II)	49

# NOMENCLATURE

$A$	heat transfer area of a given control volume
$A_d$	total projected area of droplet in the cell
$A_e$	actual flow area of the control surface
$a$	discretization coefficient
$b$	constant part of the linearized source term in the discretized equations
$C_f$	interphase friction coefficient
$c_p$	specific heat at constant pressure
$c$	condensation rate in the control volume under consideration
$D$	diffusivity of air in vapour
$D_d$	droplet diameter
$D_e$	effective diffusivity of air in vapour
$D_i$	inner diameter of tube
$D_o$	outer diameter of tube
$D_t$	turbulent diffusivity of air in vapour
$Fr$	Froude number
$F_{ui}$	flow resistance force for the phase 'i' in the x-momentum equation
$F_{vi}$	flow resistance force for the phase 'i' in the y-momentum equation
$f$	friction factor
$Gr$	Grashof number
$g$	gravitational acceleration

<b>H</b>	non-dimensional number of condensation
<b>J</b>	total flux of convection and diffusion
<b>k</b>	thermal conductivity
<b>L</b>	latent heat of condensation
<b>M</b>	total number of control volumes in x-direction
<b><math>M_v</math></b>	mass velocity of steam through maximum flow area
<b>m</b>	steam condensation rate per unit volume
<b>N</b>	total number of control volumes in y-direction
<b>Nu</b>	Nusselt number
<b>Pr</b>	Prandtl number
<b><math>P_t</math></b>	tube pitch
<b>p</b>	pressure
<b><math>p^*</math></b>	estimated pressure
<b><math>p'</math></b>	pressure correction
<b>Re</b>	Reynolds number
<b><math>R_a</math></b>	gas constant for air
<b><math>R_c</math></b>	thermal resistance for condensation heat transfer
<b><math>R_f</math></b>	fouling resistance
<b><math>R_g</math></b>	volume fraction of gas
<b><math>R_l</math></b>	volume fraction of liquid
<b><math>R_m</math></b>	gas constant for air-steam mixture

$R_s$	gas constant for steam
$R_t$	tube wall resistance
$R_w$	water side thermal resistance
$Rs_a$	air resistance
$ra$	$\rho\mu$ ratio
$S_\phi$	source term in the general differential equation
$\bar{S}$	average value of source term over control volume
$S_c$	constant part of linearized source
$S_p$	variable dependent part of the linearized source
$T$	temperature
$U_{pi}$	velocity vector magnitude for the phase 'i' = $(u_i^2+v_i^2)^{1/2}$
$u_i$	velocity component in the x-direction for the phase 'i'
$u^*$	estimated velocity component in the x-direction
$u'$	velocity correction in the x-direction velocity component
$V$	volume
$v_i$	velocity component in the y-direction for the phase 'i'
$v^*$	estimated velocity component in the y-direction
$v'$	velocity correction in the y-direction velocity component
$w$	total amount of condensate leaving the particular control volume
$x$	steam main flow direction coordinate
$y$	steam cross flow direction coordinate

## **GREEK LETTERS**

$\alpha$	heat transfer coefficient on the steam side
$\alpha_r$	under-relaxation factor
$\beta$	local volume porosity
$\Gamma_\phi$	diffusion coefficient
$\gamma$	residue reduction factor
$\mu$	laminar dynamic viscosity
$\mu_e$	effective viscosity
$\mu_t$	turbulent viscosity
$\xi$	pressure loss coefficient
$\rho$	density
$\phi$	general dependent variable
$\Phi$	air mass fraction

## **SUBSCRIPTS**

a	air
c	condensate
cs	steam-condensate interface
d	droplet
E,W	grid points
e,w	control volume faces



g	gas
i	phase in question
l	liquid
N,S	grid points
n,s	control volume faces
nb	neighbour grid points
P	grid point
p	parameter in pressure correction equation
s	steam
t	tube
u	parameter in x-momentum equation
v	parameter in y-momentum equation
w	cooling water
x	variable in x-direction
y	variable in y-direction

### **SUPERSCRIPTS**

o	previous iteration
---	--------------------

# CHAPTER I

## INTRODUCTION

---

### 1.1 Motivation

Steam condensers enable the operation of steam power plants in water-steam cycles. The condenser design plays a very important role in the efficient operation of the condenser and the power plant as a whole. There are many important factors which have to be taken into account in a successful condenser design. These are the non-condensable gas blanketing, pressure drop across the tube bundles, vapour velocity and condensate inundation. All these factors affect the heat transfer in a condenser. Over the years, it has become more important and yet more difficult to design the condensers for efficient thermal performance. Accurate and detailed predictions of the shell side flow distribution and heat transfer are of primary importance in performing the hydraulic design analysis.

An efficient and viable approach to improve the design tools is through the development of advanced numerical models using fundamental conservation equations and appropriate constitutive relations. The advantage of numerical models is that they can provide a more detailed picture of the flow, and include the effects of baffles, drip trays,

steam lanes in the nest and other mechanical details. Until now, these models have been of a single-phase two-dimensional and quasi-three-dimensional type or two-phase two-dimensional type.

The liquid phase affects the fluid flow and heat transfer in the condenser by virtue of interphase friction force and forming films on the tubes. There is a need to understand the physical behaviour of the condensate, involving its form and its effect, in condensers. In the design of condensers, the assumption is usually made that heat transfer is reduced in the lower tubes of a tube nest by the increase in film thickness as a result of condensate raining from the tubes above. This condensate would inundate the steam space producing thicker water coatings on the cooling tubes causing a decrease in the heat transfer. However, recent experimental work has indicated that the region of minimum heat transfer was situated in the upper half of the tube nest.

## **1.2 Scope of Present Work**

The purpose of the present work is to develop a model to predict three-dimensional two-phase fluid flow and heat transfer in a power plant condenser more accurately. The simulation method developed in this study is based on the fundamental governing equations of mass, momentum and air mass fraction conservation. Coupled momentum equations for each fluid are solved along with the continuity equations to obtain the volume fractions, velocity fields and shared pressure. The two-phase model

predicts the flow of condensate in droplet form, and its effect on the gas through interphase friction. The objectives of the proposed work can be summed up as follows,

1. To develop a quasi-three-dimensional two-phase model to predict the shell side fluid flow and heat transfer;
2. To validate the proposed model by comparing it with the experimental results of an experimental condenser;
3. To compare the predicted results obtained by the proposed quasi-three-dimensional two-phase model with respect to those obtained from quasi-three-dimensional single phase models.
4. To study the effect of different heat transfer coefficient correlations on the predictions.

The porous media concept is used in the proposed model. A porosity,  $\beta$ , is employed to account for the volume reduction due to the tube bundles, baffles and other internal obstacles. The conversion of the differential equations into equivalent finite-volume equations is carried out by integrating over a small control volume. In the case of discretization of momentum equations, a staggered grid is used. The resulting discretized equations are solved in primitive variables using the SIMPLEC algorithm<sup>[1]</sup>.

### **1.3 Outline of the Thesis**

The thesis is organized as follows:

Chapter 1 - A brief introduction about the present work;

- Chapter 2 - Review of the previous work in the area related to the present work;
- Chapter 3 - Detailed presentation of the numerical model, the governing equations and other auxiliary equations used in the numerical procedure;
- Chapter 4 - General description of the discretization technique and presentation of the numerical procedure used in the work;
- Chapter 5 - Results and discussion;
- Chapter 6 - Conclusions and recommendations for future work.

## **CHAPTER II**

### **REVIEW OF PREVIOUS WORK**

---

#### **2.1 Prediction of Fluid Flow and Heat Transfer Using Single-Phase Models**

Extensive work has been done in the area of simulation of single-phase fluid flow and heat transfer in a condenser. Various models have been constructed to simulate the steam-air mixture flow and heat transfer in condensers. The common characteristic of all these models is the use of a porous media concept in the tubular region. Most of the models use the SIMPLEC algorithm to solve the governing equations.

A numerical technique was developed by Theodossiou et al.<sup>[2]</sup> to predict flow distribution in shell-and-tube heat exchangers. The flow is assumed to be two-dimensional, incompressible and isothermal. The porous media concept is incorporated in the governing equations, for the tubular region. The resulting discretized equations are solved using the SIMPLEC (Semi-Implicit Pressure-Linked Equations Consistent) numerical formulation.

A computational procedure to calculate two-dimensional flow in shell-and-tube

heat exchangers was developed by Carlucci et al<sup>[3]</sup>. The geometry and internal obstacles for different shell-and-tube heat exchangers are modelled by an isotropic porosity distribution. The Semi-Implicit Pressure-Linked Equations (SIMPLE) algorithm is employed for solving the discretized equations.

Davidson and Rowe<sup>[4]</sup> presented a computational method to simulate condenser performance which is based on the assumption that there is no steam flow parallel to the tube axes in the bank. The flow is considered two-dimensional. The governing equations are continuity, momentum and air concentration field equations. A finite difference discretization of the field equations is used.

Caremoli<sup>[5]</sup> presented a computational method to predict the shell side flow in power plant condensers. The governing equations are the equations of conservation of mass, momentum, and air mass fraction. The porous media principle is used to model the tubes and other internal obstacles in the power plant condenser. Steam is assumed to be saturated throughout the condenser and the steam-air mixture is considered as a perfect gas.

A quasi-three-dimensional approach was proposed by Zhang<sup>[6]</sup>. The three-dimensional effects due to the cooling water temperature difference have been taken into consideration by a series of step by step two-dimensional calculations. The inlet mass

flow rate of each domain is determined by the condensation capability in that domain. The effects of inundation and air-blanket are not taken into account.

A numerical model was developed by Zhang<sup>[7]</sup> which not only takes into account the three-dimensional aspects of the fluid flow, but also considers the effect of inundation and air-blanket. An inundation correction factor is applied to the heat transfer coefficient. The steam is considered saturated throughout the condenser. The porous media principle is utilized to model the tube bank inside the condenser. A pressure drop balance concept is used to determine inlet mass flow rate distribution along the cooling water flow direction.

## **2.2 Prediction of Fluid Flow and Heat Transfer Using Two-Phase Models**

A general computational procedure to simulate multiphase fluid flow and heat transfer was proposed by Spalding<sup>[8]</sup>. Detailed information about all the governing equations used in the numerical procedure and all the important parameters used in these equations is provided. The energy equation and species conservation equation are also proposed. The species conservation equation is a partial differential equation which expresses the conservation of species present in various phases. In the solution procedure, a reliably convergent successive-adjustment procedure called IPSA (Inter-Phase Slip Analyser) has been employed.



A mathematical model was described by Singhal and Spalding<sup>[9]</sup>, for the steam generator of a nuclear power plant. It computes three-dimensional unsteady distributions of velocity, pressure, enthalpy, etc, in the shell side of the generator, and the distribution of primary-fluid temperature within the tubes. The mathematical model is formulated on the basis of the IPSA algorithm of Spalding<sup>[10]</sup>. The distributed-resistance concept, described by Patankar and Spalding<sup>[11]</sup> is used. In the calculations, thermal equilibrium is assumed; i.e. the vapour and the liquid have equal temperatures in the two-phase regions. The model has been developed primarily for transient flows by the inclusion of time dependent term of the governing flow equations. Finite difference discretization of the field equations is used. Calculations are obtained from the unequal-velocity (slip) model by assuming fixed value of the interphase friction coefficient. Calculations are also performed with different inter-phase-friction coefficients so as to examine the effects of this parameter on the local and global flow properties.

A stable semi-implicit numerical scheme was developed by Lee<sup>[12]</sup> for solving nonequilibrium two-phase flow problems. The basic two-fluid, six-equation model was employed. During the pressure iteration loop, the changes in pressures as well as the void fractions are computed simultaneously using the mass and momentum equations of both phases.

A two-phase model for flow in condensers was presented by Al Sanea et al<sup>[13]</sup>.

Equations were proposed for the momentum, volume fraction and enthalpy of the gas, the concentration of steam in air, and pressure, which is assumed common to both phases. Only the momentum and volume fraction equations of the second phase (i.e. condensate) have been considered. The model predicts the flow of condensate in droplet form, and its effect on the gas phase through interphase friction. Vapour and liquid phases are assumed to be at saturation temperature throughout the condenser. The model was used to predict the flow and condensation in an experimental condenser having a rectangular tube nest, and air venting arrangements. Empirical correlations were used to calculate the local heat and mass transfer. The results were compared with the measurements for an experimental condenser.

Bush et al.<sup>[14]</sup> reported the predicted flow behaviour of the three-component mixture of air, steam and condensate in an experimental condenser test rig. The coupled momentum equations for each fluid are solved along with the continuity equation to provide the volume fraction, velocity and pressure. It is assumed that saturation conditions prevail throughout the condenser. The liquid condensate is assumed to exist as droplets of a single size. Steam and air are assumed to be perfect gases.

The shell side flow within large power plant condensers, in general, is three-dimensional. The steam flow in different sections along the cooling water flow direction will differ due to the rise of the cooling water temperature. The Quasi-three-dimensional

approach takes into consideration the three-dimensional aspects of the flow due to the cooling water temperature difference. The single-phase model results show the region of minimum heat transfer to be present in the lower half of the tube nest. Recent experimental results, however, have shown that the region of minimum heat transfer is situated in the upper half of the tube nest. There is, therefore, a need to develop a model, in particular for power plant condensers, which includes the effects of both three-dimensional and two-phase flow, to predict the fluid flow and heat transfer in a power condenser more accurately.

## **CHAPTER III**

### **NUMERICAL MODEL AND ANALYSIS**

---

The flow in a steam condenser is two-phase and three-dimensional. Steam-air mixture forms the gas phase while the condensed water forms the liquid phase. The air leaks into the condenser through joints. The liquid condensate exists as film on the tubes and as droplets or columns of liquid between the tubes. Several mechanisms of heat and mass transfer take place between the phases. There is an entrainment of liquid from the films to form droplets. The droplets impinge onto the tubes. Heat transfer from gas to film takes place on account of condensation. There is also a possibility of steam condensing directly into droplets floating in the gaseous phase. Heat is transferred to droplets in this case. Re-evaporation might occur from droplets to gas phase. The heat transfer from film to tubes is in the form of conduction or convection. Interphase friction exists between the gas and the droplets. Similarly there is some friction between the gas and the film and also between the film and the tube.

#### **3.1 Physical Representation**

In general, the flow behaviour within the tube nest of a steam condenser is very complicated and not well understood. It is therefore necessary to make a number of assumptions based on the likely characteristics of the flow. At the present time the

following major elements are proposed for the complete physical model.

- \*The gas phase is comprised of a mixture of steam and air, the proportions being defined by the air mass fraction.
- \*Mixture of air and steam is considered as a perfect gas.
- \*Steam is assumed saturated throughout the condenser.
- \*The model predicts the flow of condensate in droplet form.
- \*Liquid condensate is assumed saturated throughout the condenser.
- \*Liquid condensate exists as droplets of single size so there will be no diffusion terms for the condensate.
- \*There is no heat transfer between the steam and the droplets.
- \*Pressure is assumed common to both phases.
- \*Mass sink term for gas associated with condensation is equal to the mass source term for the liquid due to the local balance between condensation and entrainment (transfer of liquid from film to droplets).
- \*Turbulent viscosity is constant.
- \*Pressure drop from inlet to vent for all domains must be the same.

### **3.2 Mathematical Formulation**

The simulation method developed in this study is based on the fundamental governing equations of mass, momentum and air mass fraction conservation. A two-phase quasi-three-dimensional model including the effects of inundation is proposed to

predict the heat transfer and fluid flow in the shell side of power plant condensers. A porosity factor is incorporated into the governing equations to account for the flow volume reduction, and for the distributed hydraulic and thermal resistance due to the tube bundles, baffles and other internal obstacles.

### 3.2.1. Governing equations

Separate momentum equations are formulated for the gas and the liquid phases. In the liquid phase momentum equations, diffusive terms are neglected. A pressure correction equation is obtained from the gas continuity equation and gas momentum equations. Liquid volume fractions are obtained from the liquid continuity equation. The gas volume fractions are obtained by using an auxiliary equation. There is a separate equation to calculate air mass fraction.

#### Gas mass conservation equation

$$\frac{\partial}{\partial x} (R_g \rho_g u_g) + \frac{\partial}{\partial y} (R_g \rho_g v_g) = -\dot{m} \quad (3.1)$$

#### Gas momentum conservation equation

$$\begin{aligned} \frac{\partial}{\partial x} (R_g \rho_g u_g u_g) + \frac{\partial}{\partial y} (R_g \rho_g v_g u_g) &= \frac{\partial}{\partial x} (R_g \mu_e \frac{\partial u_g}{\partial x}) \\ + \frac{\partial}{\partial y} (R_g \mu_e \frac{\partial u_g}{\partial y}) - R_g \frac{\partial p}{\partial x} - \dot{m} u_g + C_f (u_l - u_g) & \\ - R_g F_{ug} & \end{aligned} \quad (3.2)$$

$$\begin{aligned} \frac{\partial}{\partial x} (R_g \rho_g u_g v_g) + \frac{\partial}{\partial y} (R_g \rho_g v_g v_g) &= \frac{\partial}{\partial x} (R_g \mu_e \frac{\partial v_g}{\partial x}) \\ + \frac{\partial}{\partial y} (R_g \mu_e \frac{\partial v_g}{\partial y}) - R_g \frac{\partial p}{\partial y} - \dot{m} v_g + C_f (v_l - v_g) & \quad (3.3) \\ - R_g F_{vg} \end{aligned}$$

**Droplet mass conservation equation ( Droplet volume fraction equation )**

$$\frac{\partial}{\partial x} (R_l \rho_l u_l) + \frac{\partial}{\partial y} (R_l \rho_l v_l) = \dot{m} \quad (3.4)$$

**Droplet momentum conservation equation**

$$\begin{aligned} \frac{\partial}{\partial x} (R_l \rho_l u_l u_l) + \frac{\partial}{\partial y} (R_l \rho_l v_l u_l) &= -R_l \frac{\partial p}{\partial x} \quad (3.5) \\ + C_f (u_g - u_l) - R_l F_{ul} \end{aligned}$$

$$\begin{aligned} \frac{\partial}{\partial x} (R_l \rho_l u_l v_l) + \frac{\partial}{\partial y} (R_l \rho_l v_l v_l) &= -R_l \frac{\partial p}{\partial y} \quad (3.6) \\ + C_f (v_g - v_l) - R_l F_{vl} + R_l \rho_l g \end{aligned}$$

**Conservation of air mass fraction**

$$\begin{aligned} \frac{\partial}{\partial x} (R_g \rho_g \Phi u_g) + \frac{\partial}{\partial y} (R_g \rho_g \Phi v_g) &= \frac{\partial}{\partial x} (R_g \rho_g D_e \frac{\partial \Phi}{\partial x}) \quad (3.7) \\ + \frac{\partial}{\partial y} (R_g \rho_g D_e \frac{\partial \Phi}{\partial y}) \end{aligned}$$

where  $x, y$  - coordinates in steam main flow and cross flow directions;

$u, v$  - velocity components in  $x, y$  directions;

$p$  - pressure;

$\Phi$  - air mass fraction

### 3.2.2. Auxiliary relations

#### Volume fractions:

The isotropic porosity,  $\beta$ , which is employed to describe the flow volume reduction due to the tube bundle and baffles, is defined as

$\beta$  = Volume occupied by the fluid / total volume

The porosity in the tube bundle region,  $\beta_t$ , is

$$\beta_t = 1 - \frac{\pi}{2\sqrt{3}} \left( \frac{D_o}{P_t} \right)^2 \quad (3.8)$$

In the tube bundle region,  $\beta = \beta_t$ ; in the untubed region,  $\beta = 1$ .

Sum of the gas and liquid volume fractions represents the porosity.i.e

$$R_g + R_l = \beta \quad (3.9)$$

$R_g$  and  $R_l$  are volume fractions for gas and liquid droplets respectively,

$R_g$  is the volume occupied by gas/ total volume,

$R_l$  is the volume occupied by droplets/ total volume.

#### Other properties:

The density of the mixture varies locally according to the relation:



$$\rho = \frac{P}{R_m T} \quad (3.10)$$

where:

$$R_m = \Phi R_a + (1 - \Phi) R_s$$

$R_m$ ,  $R_s$ ,  $R_a$  are the gas constants for the mixture, steam and air, respectively and  $T$  is the saturation temperature determined from the partial pressure of the steam.

The effective viscosity used in the momentum equations is the sum of laminar and turbulent viscosity.

$$\mu_e = \mu + \mu_t \quad (3.11)$$

Turbulent viscosity may either be constant throughout or allowed to vary with local conditions.

The effective diffusivity is given by

$$D_e = D + D_t$$

$$\frac{D_t}{\mu_t} = \sigma$$

where  $\sigma =$  Schmidt number = 1.

#### **Momentum source terms:**

The interphase friction force term in the x-direction momentum equation is given by

$$F_{ix} = C_f (u_l - u_g) \quad (3.12)$$

$C_f$  is obtained from:

$$C_f = \frac{1}{2} \rho_g f_d A_d | (u_g - u_l) | \quad (3.13)$$

where:

$A_d$  = the total projected area of the droplets in the cell

$$A_d = \frac{1.5 R_l V}{D_d}$$

$D_d$  = droplet diameter

$V$  = volume of a given control volume

$f_d$  = friction factor

Friction factor for spherical objects is obtained from an empirical correlation given by Clift et al.<sup>[15]</sup>, which is

$$f_d = \frac{24}{Re_d} (1 + 0.15 Re_d^{0.687}) + \frac{0.24}{(1 + 4.25 \times 10^4 Re_d^{-1.16})}$$

The Reynolds number,  $Re_d$ , is defined as:

$$Re_d = \frac{\rho_g D_d | (u_g - u_l) |}{\mu_g}$$

Similar relations are involved for the interphase friction force term in the y-direction

momentum equation (the difference being u is replaced by v).

$F_{ui}$  and  $F_{vi}$  are the local flow resistance forces in momentum equations due to the tube bundle, baffles and other internal obstacles,

$$F_{ui} = \xi_{ui} \rho_i u_i U_{pi} \quad (3.14)$$

$$F_{vi} = \xi_{vi} \rho_i v_i U_{pi} \quad (3.15)$$

where  $\xi_{ui}$  and  $\xi_{vi}$  are the pressure loss coefficients. The expressions proposed by Rhodes and Carlucci<sup>[16]</sup> for the loss coefficients,  $\xi_{ui}$  and  $\xi_{vi}$ , are used, namely:

$$\xi_{ui} = 2 \left( \frac{f_{ui}}{P_c} \right) \left( \frac{P_c \beta}{P_c - D_o} \right)^2 \left( \frac{1 - \beta}{1 - \beta_c} \right)$$

$$\xi_{vi} = 2 \left( \frac{f_{vi}}{P_c} \right) \left( \frac{P_c \beta}{P_c - D_o} \right) \left( \frac{1 - \beta}{1 - \beta_c} \right)$$

The friction factors,  $f_{ui}$  and  $f_{vi}$ , are determined by

$$f_{ui} = 0.619 \text{Re}_{ui}^{-0.198} ; \text{ If } \text{Re}_{ui} < 8000$$

$$f_{ui} = 1.156 \text{Re}_{ui}^{-0.2647} ; \text{ If } 8000 \leq \text{Re}_{ui} < 2 \cdot 10^5$$

$$f_{vi} = 0.619 \text{Re}_{vi}^{-0.198} ; \text{ If } \text{Re}_{vi} < 8000$$

$$f_{vi} = 1.156 \text{Re}_{vi}^{-0.2647} ; \text{ If } 8000 \leq \text{Re}_{vi} < 2 \cdot 10^5$$

where:

$\text{Re}_{ui}$  - x-directional Reynolds number ( $= \rho_i u_i D_o / \mu_i$ );

$\text{Re}_{vi}$  - y-directional Reynolds number ( $= \rho_i v_i D_o / \mu_i$ );

**Mass source term:**

The mass source term,  $\dot{m}$ , is the steam mass condensation rate per unit volume. The mass sink term for the gas is equal to the mass source term for the liquid droplets. The steam mass condensation rate per unit volume,  $\dot{m}$ , can be calculated, by equating the phase change enthalpy with the heat transfer rate from the steam to the cooling water flowing in the tubes, as follows:

$$\dot{m} L V = \frac{T - T_w}{R} A \quad (3.16)$$

where:

$L$  = latent heat of condensation;

$V$  = volume of a given control volume;

$A$  = heat transfer area of a given control volume;

$R$  = overall thermal resistance;

The cooling water temperature,  $T_w$ , is obtained by heat balance between the steam and cooling water in each control volume.

$$\frac{T - T_w}{R} A = \dot{m}_w C_{pw} \Delta T$$

where:

$\dot{m}_w$  = flow rate of cooling water through tube;

$\Delta T$  = cooling water temperature difference between the inlet and outlet;

$c_{pw}$  = specific heat of cooling water at constant pressure.

The overall thermal resistance for each control volume,  $R$ , is the sum of all individual resistances which are calculated from various semi-empirical heat transfer correlations,

$$R = R_w \frac{D_o}{D_i} + R_t + R_c + R_f + RS_a \quad (3.17)$$

For the water side thermal resistance,  $R_w$ , the relationship given by Ditus and Boelter<sup>(17)</sup> can be employed,

$$\frac{1}{R_w} = 0.023 \frac{k_w}{D_i} Re_w^{0.8} Pr^{0.4} \quad (3.18)$$

The wall resistance,  $R_t$ , for each tube is calculated from the following expression:

$$R_t = \frac{D_o \ln\left(\frac{D_o}{D_i}\right)}{2 k_t} \quad (3.19)$$

The thermal resistance for condensation heat transfer is denoted by  $R_c$ ,

$$R_c = \frac{1}{\alpha_c} \quad (3.20)$$

where  $\alpha_c$  = the condensation heat transfer coefficient.

There are different correlations available for the calculation of the convection heat transfer coefficient. Four correlations have been used in the present work. These correlations are listed below.

### 1. Modified Nusselt's Equation<sup>[18]</sup>

$$\alpha_c = 0.725 (Gr/H)^{1/4} k/D_o [1 + 0.0095 (Re_s)^{11.8/\sqrt{Nu}}]$$

where:

$$Gr = (D_o^3 g / \mu_c^2) (\rho_c (\rho_c - \rho_s))$$

### 2. Fujii et al.'s Equation<sup>[19]</sup>

$$\alpha_c = K \chi [1 + 0.276 / (\chi^4 Fr H)^{1/4}] Re_m^{1/2} k / D_o$$

where:

K = 0.8 for in-line arrangement

K = 1.0 for staggered arrangement

$$\chi = 0.9(1 + 1/raH)^{1/3}$$

$$Fr = M_v^2 / \rho_s g D_o$$

$$H = c_{pc}(T_s - T_w) / Pr_c L$$

$$Re_m = \rho_s M_v D_o / \rho_c \mu_c$$

$$ra = (\rho_c \mu_c / \rho_s \mu_s)^{1/2}$$

$$Pr_c = c_{pc} \mu_c / k_c$$

$M_v$  = mass velocity of steam through maximum flow area.

### 3. Rose's Equation<sup>[20]</sup>

$$\alpha_c = \left[ \frac{\chi + 0.728 / (Fr H)^{1/2}}{1 + 3.44 / (Fr H)^{1/2} + 1. / (Fr H)^{1/4}} \right] Re^{1/2} k / D_o$$

#### 4. Honda and Fujii's Equation<sup>[21]</sup>

$$\alpha_c = \left[ 1 - 0.27 \frac{(5/FRH)^{1/2} - 1}{(5/FRH)^{1/2} + 1} \right] \frac{1}{(FRH)^{1/4}} Re^{1/2} k/D_o$$

The above correlations are multiplied by an inundation correction factor of  $[w/c]^{0.16}$ .

The fouling resistance  $R_f$  is taken as zero. The resistance from the presence of air film is evaluated via a mass transfer coefficient as reported by Berman and Fuks<sup>[22]</sup>.

$$\frac{1}{R_{s_a}} = \frac{aD}{D_o} Re_s^{0.5} \left( \frac{P}{P - P_s} \right)^b P^{1/3} \left( \rho_s \frac{L}{T} \right)^{2/3} \frac{1}{T - T_{cs}^{1/3}} \quad (3.21)$$

where:

$a = 0.52$  ,  $b = 0.7$  for  $Re_s < 350$ ;

$a = 0.82$  ,  $b = 0.6$  for  $Re_s > 350$ ;

$D$  - diffusivity of air in vapour.

### 3.3 Boundary Conditions

The boundary conditions for inlet, vent and solid walls are stated below.

#### Inlet boundary conditions

- (a) The mass flow rate of the mixture at the inlet is specified.
- (b) The x-component of gas velocity at the inlet is determined based on the mass flow rate at the inlet.

- (c) The y-component of gas velocity at the inlet is zero.
- (d) The x and y-component of liquid droplet velocities at the inlet are zero.
- (e) Pressure and the air mass fraction values are specified at the inlet boundary.

#### **Shell wall boundary conditions**

The shell walls of the condenser are assumed to be non-slip, impervious to flow, and adiabatic.

#### **Vent boundary conditions**

The gas velocities, air mass fraction and the mass flow rate of the mixture at the vent are calculated based on the conservation of mass. According to the conservation of the mass, the amount of the mixture flowing out of the vent must be equal to the difference of the inlet mass flow rate of the mixture entering the domain and the condensation in the tubular region of the corresponding domain.

The value of liquid volume fraction, for region other than the tubular region and the region of the condenser just below the tubular region, is assumed as  $1 \times 10^{-30}$ . The reason for assuming such a low value is that the condensation and hence the droplet formation takes place only after the steam-air mixture enters the tubular region. Hence, there is no liquid in the mixture before entering the tubular mixture. The liquid is present in the domain consisting of the tubular region and the region just below the tubular



region. The condensate exits from the bottom right side of the domain (i.e. from the right side of the region just below the tubular region).

# CHAPTER IV

## NUMERICAL SOLUTION TECHNIQUE

---

In the present study, the finite volume method is used to solve the governing equations presented in the previous chapter. The differential equations are discretized over the domain of interest to yield a set of algebraic equations. The SIMPLEC algorithm<sup>(1)</sup> will be used to solve the discretized equations.

### 4.1 General Form of Differential Equations

The general form of the differential equations for fluid flow and heat transfer in Cartesian coordinates is:

$$\frac{\partial}{\partial x} (R_i \rho_i u_i \phi) + \frac{\partial}{\partial y} (R_i \rho_i v_i \phi) = \frac{\partial}{\partial x} (R_i \Gamma_\phi \frac{\partial \phi}{\partial x}) + \frac{\partial}{\partial y} (R_i \Gamma_\phi \frac{\partial \phi}{\partial y}) + S_\phi \quad (4.1)$$

where:

$x, y$  - Cartesian coordinates in the horizontal and vertical directions, respectively; both

being across the tube bank;

$\rho$  - density;

$\phi$  - variable to be solved for;

$\Gamma_\phi$  - diffusion coefficient;

$S_\phi$  = source of  $\phi$  per unit volume;

$i$  = denotes the phase in question.

The equations for velocities and concentration for the gas phase will contain diffusion terms incorporated in the coefficient,  $\Gamma_\phi$ , defined by:

$$\Gamma_\phi = \frac{\mu_e}{\sigma_\phi}$$

where:

$\mu_e$  = effective viscosity;

$\sigma_\phi$  = effective Schmidt number for concentration equation and unity for the momentum equations.

There will be no diffusion terms in the liquid momentum equations. The general form of the differential equations can be rewritten as:

$$\frac{\partial}{\partial x} (J_x) + \frac{\partial}{\partial y} (J_y) = S_\phi \quad (4.2)$$

where  $J$  represents the total flux of convection and diffusion,

$$J_x = R_i \rho_i u_i \phi - R_i \Gamma_\phi \frac{\partial \phi}{\partial x}$$

$$J_y = R_i \rho_i v_i \phi - R_i \Gamma_\phi \frac{\partial \phi}{\partial y}$$

The discretization procedure requires that the calculation domain be divided into sufficiently small cells, and the distribution of the relevant variables be expressed in terms

of their values at cell center.

## 4.2 Grid Arrangement

In this study, a staggered grid used originally by Harlow and Welsh<sup>[23]</sup>, and also described by Spalding<sup>[24]</sup>, is adopted. Figure 4.1 shows the main control volume, with P as the center, along with the staggered control volumes. All the variables other than the velocities are calculated at the center of the main control volume. These variables are the pressure, temperatures, air-mass fraction, volume fractions etc. The velocity components are calculated for the points that lie on the faces of the main control volumes. Thus, the x-direction velocity  $u$  is calculated at the faces that are normal to the x-direction while the y-direction velocity  $v$  is calculated at the faces that are normal to the y-direction. The main control volume around P has four faces marked n, s, e and w. The velocity grid points have their own control volumes around them. The control volume for the x-direction velocity is staggered only in the x-direction while the control volume for the y-direction velocity is staggered only in the y-direction.

## 4.3 Discretized Equations

The discretized equations are obtained by integrating the corresponding differential equation for the dependent variable  $\phi$  over each control volume in the calculation domain. The piecewise linear profile expressing the variation of  $\phi$  between the grid points is used to evaluate the required integral. When an equation is integrated over the main control

volume surrounding the point P, the resulting equation can be expressed in the following general form:

$$J_e - J_w + J_n - J_s = \bar{S} V \quad (4.3)$$

where:

$V$  = the volume of the control volume;

$J$  = the integrated total flux over the corresponding control volume face;

$\bar{S}$  = the average value of  $S$  over the control volume.

The total fluxes  $J_e$ ,  $J_w$ , etc. in Equation (4.3) can be expressed in terms of the values of  $\phi$  at point P and neighbour points E, W, etc by using some differencing scheme.

The discretization equation then becomes:

$$a_P \phi_P = a_E \phi_E + a_W \phi_W + a_N \phi_N + a_S \phi_S + b \quad (4.4)$$

where  $a_p$ ,  $a_E$ , etc. are non-negative coefficients representing the influences of convection and diffusion and

$$a_P = a_E + a_W + a_N + a_S - S_P \Delta V$$

$$b = S_c \Delta V$$

The source term has been linearized to

$$\bar{S} = S_c + S_P \phi_P$$

Equation (4.4) can be expressed as:

$$a_p \phi_p = \sum a_{nb} \phi_{nb} + b \quad (4.5)$$

There are several differencing schemes that can be put to use during the discretization process. Solution of convective problems using the central difference scheme is limited to low Reynolds number. Otherwise, the central difference scheme may lead to unrealistic results. For the case of zero diffusion, the central difference scheme is unsuitable. The upwind scheme successfully overcomes the above difficulties. The scheme ensures unconditional stability and boundedness. The hybrid scheme described by Spalding<sup>[24]</sup> is indicative of a combination of the central difference scheme and upwind scheme. In the present work the upwind differencing scheme has been used. In the case of liquid momentum equations, the diffusion terms are neglected.

For the SIMPLEC algorithm, a special E-factor is introduced into the discretized governing equations. The discretized equations are solved repetitively, with each of these solutions defined as a cycle. At the beginning of each cycle, the coefficients are evaluated using the  $\Phi$  values obtained in the previous cycle. With the cycle-by-cycle change in coefficients of Equations (4.5), the resulting changes in the  $\Phi$  values can be quite large, and this may cause slow convergence or even divergence. To moderate the changes in consecutive solutions for  $\Phi$ , and thereby improve convergence, under-relaxation is introduced. Under-relaxation is introduced into Equation (4.5) through the under-relaxation factor  $\alpha_r$ .

$$\frac{a_p}{\alpha_r} \phi_p = \sum a_{nb} \phi_{nb} + b + \frac{1-\alpha_r}{\alpha_r} a_p \phi_p^o$$

The discretized equation with the E-factor can now be written as follows:

$$a_p \left(1 + \frac{1}{E}\right) \phi_p = \sum a_{nb} \phi_{nb} + b + \frac{a_p}{E} \phi_p^o \quad (4.6)$$

where the superscript o denotes the values from the previous cycle.

The relationship between E-factor and the under-relaxation factor  $\alpha_r$  is

$$\alpha_r = \frac{E}{1 + E}$$

### 4.3.1 The u-momentum equation

Using the grid arrangement shown in Figure 4.1, the discretized u-momentum equation for the control volume centered at e is written as:

$$a_e u_e = \sum a_{nb} u_{nb} + b + (p_p - p_E) A_e \quad (4.7)$$

where:

$$a_e = \left( \sum a_{nb} - S_p \Delta V \right) \left( 1 + \frac{1}{E} \right)$$

$$b = S_c \Delta V + \frac{a_p}{E} u_e^o$$

The neighbour coefficients,  $a_{nb}$ , account for the combined convection-diffusion influence

at the control-volume faces. The term  $(p_p - p_E)A_e$  is the pressure force acting on the u control volume,  $A_e$  being the area on which the pressure difference acts. Similar discretized equations can be obtained from the v-momentum equation for gas and both the u and v-momentum equations for liquid.

### 4.3.2 The velocity correction equation

The momentum equations can be solved only when the pressure field is given or is somehow estimated. For any guessed pressure distribution  $p^*$ , the velocity  $u^*$  will be obtained from the solution of the following discretization equation:

$$a_e u_e^* = \sum a_{nb} u_{nb}^* + b + (p_p^* - p_E^*) A_e \quad (4.8)$$

The starred velocity field obtained will not satisfy the continuity equation unless the guessed pressure is the correct pressure. The guessed pressure field has to keep on improving until the resulting starred velocity field progressively gets closer to satisfying the continuity equation. Therefore, correction of the guessed pressure by  $p'$  ( $p' = p - p^*$ ) is carried out to get the corrected velocity field  $u$  ( $u = u^* + u'$ ).  $u'$  is the velocity correction corresponding to the pressure correction and  $p$  represents the corrected pressure. Subtracting Equation (4.8) from Equation (4.7), the following relationship is obtained,

$$a_e u'_e = \sum a_{nb} u'_{nb} + (p'_p - p'_E) A_e \quad (4.9)$$

The term  $\sum a_{nb} u'_{nb}$  is subtracted from Equation (4.9). Now we have,



$$(a_o - \sum a_{nb}) u'_o = \sum a_{nb} (u'_{nb} - u'_o) + A_E (p'_P - p'_E) \quad (4.10)$$

The exact equation for  $p'$  is complicated and unsuitable for an economic calculation. In order to obtain a simplified relation, the term  $\sum a_{nb} (u'_{nb} - u'_o)$  on the right-hand side of Equation (4.10) is neglected. Equation (4.10) can now be written as:

$$(a_o - \sum a_{nb}) u'_o = A_o (p'_P - p'_E)$$

$$u'_o = d_o (p'_P - p'_E) \quad (4.11)$$

where,

$$d_o = \frac{A_o}{a_o - \sum a_{nb}}$$

The expression for the corrected velocity  $u_c$  is now written as

$$u_o = u^*_o + d_o (p'_P - p'_E) \quad (4.12)$$

Similar expressions can be obtained from the v-momentum equation for the gas and both the u and the v-momentum equations for the liquid droplet phase.

### 4.3.3 The pressure correction equation

The pressure correction term is calculated by turning the gas phase continuity equation into an equation for pressure correction. The gas continuity equation is integrated

over the main control volume centered at P. The integrated form of the continuity equation becomes:

$$\left[ (R_g \rho_g u_g)_e - (R_g \rho_g u_g)_w \right] \Delta y + \left[ (R_g \rho_g v_g)_n - (R_g \rho_g v_g)_s \right] \Delta x = -\dot{m} \Delta x \Delta y$$

On substituting for all the velocity components by the expressions given by the velocity-correction formulas [such as Equation (4.12)], the following expression for the discretized equation for  $p'$  is obtained,

$$a_P p'_P = a_E p'_E + a_W p'_W + a_N p'_N + a_S p'_S + b \quad (4.13)$$

where:

$$a_P = \sum a_{nb}$$

$$b = [(R_g \rho_g u_g)_w - (R_g \rho_g u_g)_e] \Delta y + [(R_g \rho_g v_g)_s - (R_g \rho_g v_g)_n] \Delta x - \dot{m} \Delta x \Delta y$$

The term 'b' represents a "mass source". If the continuity equation is satisfied by the starred velocities, then 'b' becomes equal to zero and no further pressure correction is needed. The pressure correction,  $p'$ , is obtained by solving the above discretized equation.

The corrected pressure field is then obtained by

$$p = p^* + p' \quad (4.14)$$

#### 4.3.4 The volume fraction equation

The droplet volume fraction is obtained from the liquid continuity equation. The liquid continuity equation is integrated over the main control volume centered at P. The

volume fraction equation is solved only after the corrected velocity field is obtained. Hence, the only unknown in the discretized liquid continuity equation is the droplet volume fraction.

#### **4.4 Solution of the Linear Algebraic Equations**

The solution of the linearized algebraic equations is obtained by the use of an iterative method. In this study the line-by-line iteration method, which employs the TDMA<sup>(25)</sup> (TriDiagonal-Matrix Algorithm), is used.

#### **4.5 The Solution Procedure for One Domain: Sequence of Operations**

1. The pressure field  $p^*$  is guessed.
2. The momentum equations [such as Equation (4.7)] for the gas and the liquid phases are solved to obtain  $u_g^*, v_g^*, u_l^*$  and  $v_l^*$ .
3. The pressure correction equation [Equation (4.13)] is solved to get  $p'$ .
4. The gas and liquid phases velocities  $u_g$ ,  $v_g$ ,  $u_l$  and  $v_l$  are calculated from their starred velocities using the velocity-correction formulas [such as Equation (4.12)].
5. The pressure field is updated [using Equation (4.14)].
6. The air mass fraction equation is solved to get the air mass fraction.
7. Droplet volume fraction is obtained by solving the discretized liquid continuity equation.

8. The auxiliary equation [Equation (3.9)] is solved to get the gas volume fraction.
9. The new volume fractions and air mass fractions are used to update the velocities, pressure and other parameters such as the gas temperature, gas density, temperature of cooling water, condensation rates, momentum source terms etc.
10. If the prescribed accuracy is not obtained, procedure is repeated from step 2, until a converged solution is obtained.

#### 4.6 Convergence Criteria for Each Domain

The convergence criteria for momentum equations and other transport equations such as the air mass fraction equation and the volume fraction equation is as follows:

$$\frac{[\sum (\frac{\phi^0 - \phi}{\phi^0})^2]^{\frac{1}{2}}}{N * M} \leq 10^{-5}$$

where:

$\phi$  = New values of  $u_g$ ,  $v_g$ ,  $u_l$ ,  $v_l$ ,  $\phi$  or  $R_l$

$\phi^0$  = Values of  $u_g$ ,  $v_g$ ,  $u_l$ ,  $v_l$ ,  $\phi$  or  $R_l$  from previous cycle

$M$  = Total number of control volumes in x-direction

$N$  = Total number of control volumes in y-direction

The convergence for the pressure correction equation suggested by Van Doormaal and Raithby<sup>(1)</sup> requires the iteration to continue until

$$\frac{\|\gamma_p\|}{\|\gamma_p^o\|} \leq 0.05$$

where:

$\|\gamma_p\|$  = Euclidean norm of the residual of the pressure correction equation at the present iteration level;

$\|\gamma_p^o\|$  = Euclidean norm of the residual of the pressure correction equation at the previous iteration level.

The Euclidean norm is defined as  $\sqrt{\langle \mathbf{a}, \mathbf{a} \rangle}$  where,  $\langle \mathbf{a}, \mathbf{a} \rangle$  is the inner product,  $\langle \mathbf{a}, \mathbf{a} \rangle = \mathbf{a} \cdot \mathbf{a}$  for any  $\mathbf{a}$ . Thus for the present case  $\|\gamma_p\| = \sqrt{\gamma_p^2}$

#### 4.7 The Overall Solution Procedure

The condenser shell side is divided into a number of domains normal to the cooling water flow direction. Two-dimensional calculations are performed for each domain. Calculations for each domain are made sequentially starting from the cooling water inlet end. The outlet cooling water temperature for the preceding domain is taken as the inlet cooling water temperature for the following domain. Thus the three-dimensional effects due to the cooling water temperature difference are propagated from one domain to the other. The inlet mass flow rate for each domain is used to calculate the inlet gas velocity, which is the inlet boundary condition for the calculation domain. The inlet mass flow rate into each domain is determined by the constraint that the pressure drop from inlet to the vent for all the domains must be identical since the

domains share the same inlet and vent. This is called pressure drop balance concept<sup>[26]</sup>.

Figure 4.2 shows the flow chart of the numerical procedure used for the calculations.

#### **4.8 The Overall Convergence Criteria**

To satisfy the 'Pressure Drop Balance Concept', amendments are made in the inlet mass flow rate to the domains. The numerical procedure is repeated until the maximum difference between outlet pressure for each domain and average outlet pressure is 0.05% of average outlet pressure.

# CHAPTER V

## RESULTS AND DISCUSSION

---

In order to evaluate the capabilities of the present numerical procedure, an experimental steam surface condenser from Al-Sanea et al.<sup>[27]</sup> is employed to verify the numerical procedure.

### 5.1 The Experimental Configuration

The configuration of the experimental condenser is depicted in Figure 5.1. It contains an internal vent located on the horizontal centre line approximately two-thirds of the way into the tube bundle. The tube bank consists of 400 cooling tubes in a triangular pitch arrangement. The position of rows of cooling tubes, for which experimental data are available, is shown in the Figure 5.2. The geometrical and the operating parameters of the experimental condenser are given in Table 5.1 and Table 5.2 respectively.

**Table 5.1 Geometrical Parameters of Experimental Condenser**

Condenser Length (m)	1.219
Tube Outer Diameter (mm)	25.4
Tube Inner Diameter(mm)	22.9
Tube Pitch (mm)	34.9

**Table 5.2 Operating Parameters of Experimental Condenser**

Inlet Temperature of Cooling Water(°C)	17.8
Inlet Velocity of Cooling Water (m/s)	1.19
Inlet Pressure of Steam (Pa)	27670
Inlet Mass Flow Rate (kg/s)	2.032
Inlet Air Flow Rate (kg/s)	$2.48 \times 10^{-3}$

## 5.2 Computational Details

The condenser is subdivided into five domains along the cooling water flow direction. The calculation plane is situated at the center of each domain. A non-uniform grid of 31x34 in the x and y directions respectively is employed in each calculation plane, as shown in the Figure 5.3.

## 5.3 Results

The results obtained using the proposed quasi-three-dimensional, two-phase model are shown in the form of velocity vectors, contours of the primary and secondary variables, and graphs of heat flux variations.

### 5.3.1 Velocity vector plots

Figure 5.4 shows the gas and liquid velocity vectors for the 1 mm droplet case. The steam-air mixture enters from the side and recirculates due to the presence of the end wall and the suction caused by the condensation in the tube bank. The gas velocity,



inside the tube bank, continues reducing as the steam condenses and becomes very small in the central region of the tube bank. An increase in the gas velocity at the entrance to the tube bank is attributed to the sudden decrease in the flow area due to the presence of the tubes.

The liquid velocities come into the picture only after the steam-air mixture enters the tubular region and starts condensing. The x-direction velocity components are dominant at the inlet side of the tube bank, while gravity clearly dominates elsewhere in the tubular region, and the condensate falls nearly vertically. Though the condensate falls under the influence of gravity, it is also subjected to interphase frictional forces which deflect its course.

### **5.3.2 Contours**

The contour maps for gas and liquid velocity magnitudes are shown in Figure 5.5 and Figure 5.6, respectively. The gas velocity contour represents velocities for the complete cross-section of the condenser, while the liquid velocity contour represents the tubular region and the region below it only. In the gas velocity contour, the increase in the gas velocity at the entrance to the tube nest can be clearly seen. In the liquid velocity contour, higher velocities are observed in the region just below the tubular region. The reason for these higher velocities is that high gas velocity in this region forces the liquid along with it.

The air concentration contours are shown in Figure 5.7. The higher air concentration zone lies just above the centreline of the condenser cross-section. The air concentration increases as the steam-air mixture moves ahead in the tubular region, being the maximum at the central region. This is because as the steam moves ahead in the tubular region, the steam starts to condense and the amount of steam in the steam-air mixture reduces. The air concentration is maximum at plane no. 1 and continues reducing for further planes being lowest for the plane no. 5 at the hot end of the cooling water tubes. This is because the condensation rate in plane no. 1 is the highest and decreases reducing for further planes, being the lowest for the plane no. 5.

The contours of heat flux are shown in the Figure 5.8. Corresponding with the higher air concentration region is a region of lower heat transfer. A plausible explanation for the phenomenon of lower heat transfer in the upper tubular region is that the condensate in droplet form sweeps air from the lower areas of the nest thus giving a net gain in performance. The highest heat flux is at the entry to the tube bank, where steam velocities are the highest and air concentration is the lowest. Contrary to the widely held view of a reduction in heat transfer in the lower regions of a condenser tube nest, the heat transfer is higher in the lower part, the lower heat transfer zone being in the upper tubular region. On comparing the heat flux in five different planes, it can be seen that there is a slight decrease in the average heat flux from plane no. 1 to plane no. 5. This reflects the influence of the three-dimensionality of the flow.

The cooling water temperature contour is shown in Figure 5.9. The region of minimum cooling water temperature lies just above the centreline, almost coinciding with the higher air concentration zone.

The condensation rate contour is shown in the Figure 5.10. The condensation rate is highest at the entrance and reduces towards the centre of the tube nest, the lowest value being seen primarily above the centreline. The condensation rates are higher in the lower part of the nest than in the upper part.

The liquid volume fraction contour, for droplet diameter of 0.001 m, is shown in the Figure 5.11. The volume fraction is the highest in the lower part of the tubular region since the amount of liquid is higher there.

The interphase friction force contour, for droplet diameter of 0.001 m, is shown in the Figure 5.12. The contour is drawn for the tubular region and the region just below it. From the contour, it is clear that the interphase friction is prevalent in the lower tubular region where the amount of liquid is high. The variations of the interphase friction forces resemble very closely those of the liquid volume fraction. The contour map of interphase friction force per unit gravitational force, for droplet diameter of 0.001 m, is shown in the Figure 5.13. The contour is drawn for the tubular region and the region just below it. In the lower tubular region, where the liquid density is high, the value of

interphase friction force is comparable to the gravitational force.

### **5.3.3 Effect of droplet size**

The larger droplet size (0.004 mm) has much smaller surface area per unit volume, and hence frictional forces become less significant. The liquid volume fraction contour and the contour for the interphase friction force per unit gravitational force, are shown in Figures 5.14 and 5.15 respectively. The volume fraction contour for the larger droplet size shows similar values near the middle of the tube nest as in the case of smaller droplet size (0.001 mm) considered above. But, there is no build up of water in the lower tubular region as was observed in the 1 mm droplet case. Comparison of the interphase friction force between the two droplet sizes, shows a 10:1 reduction between 1 and 4mm droplet cases. In spite of all the above differences between the two droplet sizes, no significant difference was observed in the condensation rate and the heat fluxes.

### **5.3.4 Comparison with experimental data**

Comparisons between predictions and measurements are made for heat flux distributions. Comparison of heat flux values on five planes along four horizontal tube rows, as shown in the Figure 5.1, is given in Figure 5.16. Since the experimental heat flux at each plane is not available, the experimental values used here are mean values along the cooling water flow direction. The equation used for the calculation of the heat flux is the modified Nusselt's equation.

The values of heat fluxes along all the four tube rows show that the variation is similar to that in the experimental case. The agreement with experiment results is good for the upper three tube rows. There is some over-prediction of heat flux for the bottom-most tube row. On comparing the heat flux variations for a particular tube row for different planes, it can be observed that the average heat flux, in the first plane at the cold end of the cooling water tubes, is more than that in the last plane at the hot end of the cooling water tubes. The average heat flux gradually reduces from first plane towards the last plane, being the highest in the first plane and lowest in the last plane. This is because the steam-air mixture and the cooling water temperature difference is the highest for the plane no. 1. The temperature difference progressively reduces for the next planes, being the lowest for plane no. 5. This brings to light the effect of three-dimensionality of the flow.

#### **5.4 Comparison of Results From Quasi-Three-Dimensional Two-Phase Model and Two-Dimensional Two-Phase Model**

The predictions obtained by the proposed quasi-three-dimensional, two-phase model are compared with those obtained by using two-dimensional, two-phase model proposed by Bush et al<sup>(14)</sup>. The comparisons are given in Figure 5.17. As Bush's model is two-dimensional, data from plane No. 3 is used in the comparison.

The results from the proposed model and the Bush model are similar in the bottom

three tube rows. The main difference is found in the top tube row i.e. the 18th tube row from the bottom. The proposed model gives better prediction for this top tube row. There is a under-prediction of air bubble in the upper part of the tubular region in the case of Bush's model.

### **5.5 Comparison of Results From Quasi-Three-Dimensional Two-Phase Model and Quasi-Three-Dimensional Single-Phase Model**

Results obtained by quasi-three-dimensional single-phase model have been obtained from two methods. These methods are discussed below in details.

#### **Method I**

The velocity calculated here is the average velocity over the whole control surface area and not the actual flow area. The actual velocity of fluid in the tubular region of the condenser is higher than what is calculated by this method.

#### **Method II**

In this method, the velocity calculated is the average velocity over the actual flow area and not the whole control surface area as was the case in method I. In this method some special care has to taken for calculations at and around the boundary of the tubular region because of the change in the flow area.

Method II is used in the proposed two-phase method. The gas velocity calculated

is the average velocity over the actual gas flow area and the liquid velocity calculated is the average velocity over the actual liquid flow area. The comparison of the results, from the plane no. 3, obtained from the quasi-three-dimensional two-phase model and quasi-three-dimensional single-phase model is shown in the Figure 5.18. For the 3rd tube row from the bottom, the results for the single-phase model using both Method I and Method II are not in agreement with the experimental results. There is an under-prediction of heat flux in the central part of the tubular region in the case of both the methods. The liquid has strong influence in the lower part of the tubular region because most of the condensate accumulates there. In the single-phase model, the effect of liquid is not taken into consideration. This is probably the reason for discrepancies in the single-phase model results. In the comparison of predicted heat flux for the 8th tube row from the bottom, similar discrepancies are noticed in the single-phase model results for both the methods.

In the upper two tube rows, i.e. the 13th and the 18th from the bottom, the difference in the results obtained both from the single-phase and the two-phase models is not much. The reason for this is that in the upper tube nest the effect of the liquid is not that significant.

## **5.6 Sensitivity Study of Heat Transfer Coefficient Correlations**

In the present work, sensitivity study of four correlations on the prediction of steam surface condensers is carried out. The four correlations of condensation heat

transfer coefficients are the one proposed by Nusselt<sup>[18]</sup>, Fujii et al.<sup>[19]</sup>, Rose<sup>[20]</sup> and Honda and Fujii<sup>[21]</sup>.

### **5.6.1 Comparison of predicted heat flux for the four correlations**

Figure 5.19 shows the comparison of predicted values of heat flux, along four horizontal tube rows, for the four correlations with the experimental data. As the experimental values are mean values along the cooling water flow direction, average values of the predicted data are used.

In the case of 3rd tube row from the bottom, heat flux values are the highest for the modified Nusselt correlation<sup>[18]</sup>, which is followed by Rose<sup>[20]</sup>, Fujii<sup>[19]</sup> and Honda and Fujii<sup>[21]</sup> in decreasing order of heat flux. In the case of all the other three tube rows, heat flux obtained from the modified Nusselt correlation is highest at the entrance and exit ends of the tubular region. But, it is the lowest in the central part of the tubular region. Overall, the modified Nusselt correlation appears to be the best correlation for the calculation of the heat flux.

### **5.6.2 Comparison of the predicted condensation rates using the four correlations**

Comparison of the predicted condensation rates is done for the case of quasi three-dimensional two-phase models and the two methods of quasi-three-dimensional single-phase models.



**Quasi-three-dimensional two-phase models:**

**Table 5.3 Predicted Total Condensation Rates by Using Different Correlations of Condensation Heat Transfer Coefficient for Quasi-Three-Dimensional Two-Phase Model**

Scheme	Predicted Result	Error (%) <sup>*</sup>
Experimental data	2.021 (kg/s)	–
Modified Nusselt	2.016 (kg/s)	-0.247
Rose	1.993 (kg/s)	-1.385
Fujii et al.	1.983 (kg/s)	-1.880
Honda and Fujii	1.944 (kg/s)	-3.809

<sup>\*</sup> Error = (Prediction-Experimental Data)/Experimental Data \* 100

**Quasi Three-Dimensional Single Phase models:**

**Table 5.4 Predicted Total Condensation Rates by Using Different Correlations of Condensation Heat Transfer Coefficient for Quasi-Three-Dimensional Single -Phase Model (Method I)**

Scheme	Predicted Result	Error (%)
Experimental Data	2.021 (kg/s)	–
Modified Nusselt	2.003 (kg/s)	-0.890
Rose	1.988 (kg/s)	-1.632
Fujii et al.	1.984 (kg/s)	-1.830
Honda and Fujii	1.944 (kg/s)	-3.809

**Table 5.5 Predicted Total Condensation Rates by Using Different Correlations of Condensation Heat Transfer Coefficient for Quasi-Three-Dimensional Single-Phase Model (Method II)**

Scheme	Predicted Result	Error (%)
Experimental Data	2.021 (kg/s)	-
Modified Nusselt	1.993 (kg/s)	-1.385
Rose	1.968 (kg/s)	-2.622
Fujii et al.	1.959 (kg/s)	-3.067
Honda and Fujii	1.924 (kg/s)	-4.799

From the above three tables, it can be inferred that the condensation rates obtained from the Method II are the lowest. The condensation rate for the quasi-three-dimensional two-phase model is higher than Method I for modified Nusselt and Rose correlations. Modified Nusselt correlation gives a higher condensation rate compared to any other correlations. Overall from all the three tables, Modified Nusselt correlation for the case of quasi-three-dimensional two-phase model gives the condensation rate of 2.016 kg/s, which is closest to the experimental value.

# CHAPTER VI

## CONCLUSION

---

### 6.1 Concluding Remarks

A quasi-three-dimensional two-phase numerical model which includes momentum and mass conservation equations for the liquid droplets as well as the steam-air mixture has been developed. Three-dimensional effects due to the increase in the temperature of cooling water have been considered. This approach is only valid for those condensers with partition plates in which the steam flows normally to the cooling water tube bundle.

Calculations have been carried out for an experimental condenser. The numerical model has successfully reproduced the main features of the flow inside the steam condenser. The agreement with experimental results is good in most regions of the tube nest.

The difference in the values of heat flux and air mass fraction for different planes shows the effect of three-dimensionality in the flow. Also, the condensation rate is different for different planes, being highest in the first plane and lowest in the fifth plane

at the hot end of the cooling water tubes. This phenomenon is there also because of the three-dimensional effect of the flow. As seen from the velocity vector plots for the gas and the liquid, the interphase friction between the gas and the liquid droplets plays a significant role in the motion of the liquid flow in the lower part of the tubular region. The present numerical method gives better results than the two-dimensional method of Bush<sup>[14]</sup>, in the upper most tube row. The results are in good agreement in all the other regions of the tube bundle. On comparing the results from the quasi-three-dimensional two-phase model with those from the quasi-three-dimensional single-phase model, it has been seen that the quasi-three-dimensional two-phase model gives better results in the lower part of the tubular region where the liquid plays a major role. In the upper part of the tubular region, results from the two-phase model are similar to those from the single-phase model. This is because the effect of liquid is not much in the upper tubular region. Sensitivity of condensation heat transfer coefficient correlations on the accuracy of the predictions has been studied for the case of the quasi-three-dimensional two-phase model and single-phase model.

## **6.2 Future Work**

Further work is required to incorporate an enthalpy equation for the condensate so that undercooling can be predicted. The liquid phase consists of droplets as well as films. It is therefore required to formulate a numerical algorithm which includes the effects of both the films and droplets. More investigation on the effects of smaller droplet

particles or increased interphase friction should be carried out. However, the results obtained from the present model are very encouraging. The trend towards correct prediction of the experimental case by virtue of the inclusion of the second phase shows that such effects need to be included in future condenser design codes.

## REFERENCES

---

- [1] Van Doormaal, J.P. and Raithby, G.D., "Enhancements of the SIMPLE Method for Predicting Incompressible Fluid Flow", *Numer. Heat Transfer*, Vol.7, 1984, pp.147-163.
- [2] Theodossiou, V.M., Sousa, A.C.C. and Carlucci, L.N., "Flow Field Predictions in a Model Heat Exchanger", *Int. J. Computational Mechanics*, Vol.3, 1988, pp.419-428.
- [3] Carlucci, L.N., Galpin, P.F. and Brown, J.D., "Numerical Predictions of Shell Side Heat Exchanger Flows", in *A Reappraisal of Shell Side Flow in Heat Exchangers*, Eds., W.J. Marner and J.M. Chenoweth, ASME, HTD-Vol.36, New York, N.Y., 1984, pp.19-26.
- [4] Davidson, B.J. and Rowe, M., "Simulation of Power Condenser Performance By Computational Method: An Overview", in *Power Condenser Heat Transfer Technology*, Eds., P.Marto and R.Nunn, Hemisphere, Washington, 1981, pp.17-49.
- [5] Caremoli, C., "Numerical Computation of Steam Flows in Power Plant Condensers", in *Numerical Methods In Thermal Problems*, Eds., R.W.Lewis and K. Morgan, Pineridge Press, Swansea, U.K., 1985, pp.315-325.
- [6] Zhang, C., "Numerical Predictions of Shell Side Fluid Flow and Heat Transfer in Heat Exchangers", Ph.D. Dissertation, U. of New Brunswick, 1989.

- [7] Zhang, Y., "Numerical Analysis of Fluid Flow and Heat Transfer in a Power Plant Condenser", M.A.Sc. Thesis, U. of Windsor, 1992.
- [8] Spalding, D.B., "The Calculation of Free-Convection Phenomenon in Gas-Liquid Mixtures", in Heat Transfer and Turbulent Buoyant Convection, Eds., Afgan and Spalding, Hemisphere, Vol II, 1977, PP.569-586.
- [9] Singhal, A.K. and Spalding, D.B., "Mathematical Modelling of Multi-Phase Flow and Heat Transfer in Steam Generators", in Multiphase Transport: Fundamentals, Reactor Safety, Applications, Vol.3, 1980, pp.373-406.
- [10] Spalding, D.B., "Numerical Computation of Multiphase Fluid Flow and Heat Transfer", in Recent Advances in Numerical Mechanics, Ed., C. Taylor, U. of Swansea, 1978.
- [11] Patankar, S.V. and Spalding, D.B., "A Calculation Procedure for the Transient and Steady- State Behaviour of Shell-and-Tube Heat Exchangers", in Heat Exchangers: Design and Theory Sourcebook, Eds., N.H. Afgan and E.V.Schlunder, McGraw-Hill, New York, 1974, pp.155-176.
- [12] Lee, W.H., "A Pressure Iteration Scheme for Two-Phase Flow Modelling", in

Multiphase Transport: Fundamentals, Reactor Safety, Applications, Vol.3, 1980, pp.407-415.

[13] Al Sanea, S.A., Rhodes, N. and Wilkinson, T.S., "Mathematical Modelling of Two-Phase Condenser Flows", Int. Conference on Multiphase Flow, London, England, 19-21 June, 1985.

[14] Bush, A.W., Marshall, G.S. and Wilkinson, T.S., "A Prediction of Steam Condensation Using A Three Component Solution Algorithm", Proceedings of the Second International Symposium on Condensers and Condensation, U. of Bath, U.K., March 28-30, 1990, pp.223-234.

[15] Clift, R., Grace, J.R. and Weber, M.E., "Bubbles, Drops and Particles", Academic Press, 1978.

[16] Rhodes, N. and Carlucci, L.N., "Predicted and Measured Velocity Distributions in a Model Heat Exchanger", International Conference on Numerical Methods in Nuclear Engineering, Canadian Nuclear Society/American Nuclear Society, Montreal, 1983.

[17] Ditus, F.W. and Boelter, L.M.K., "Heat Transfer in Automobile Radiators of the Tubular Type", U. of California at Berkeley, Publ. in Eng., Vol.2, 1930, pp.443-461.



- [18] Grant, I.D.R. and Osment, B.D.J., "The Effect of Condensate Drainage on Condenser Performance", NEL Report No.350, April, 1968.
- [19] Fujii, T., Uehara, H. and Kurata, C., "Laminar Filmwise Condensation of Flowing Vapour on a Horizontal Cylinder", Int. J. Heat Mass Transfer, Vol.15, 1972, pp.235-246.
- [20] Rose, J.W., "Effect of Pressure Gradients in Forced Convection Film Condensation on a Horizontal Tube", Int. J. Heat Mass Transfer, Vol.27, 1984, pp.39-47.
- [21] Honda, H. and Fujii, T., "Condensation of Flowing Vapour on a Horizontal Tube - Numerical Analysis as a Conjugate Heat Transfer Problem", J. Heat Transfer, Vol.106, 1984, pp.841-848.
- [22] Berman, L.D. and Fuks, S.N., "Mass Transfer in Condensers with Horizontal Tube When the Steam Contains Air", Teploenergetika, Vol.5, No.8, 1958, pp.66-74.
- [23] Harlow, F.H. and Welsh, J.E., "Numerical Calculation of Time-Dependent Viscous Incompressible Flow of Fluid with Free Surface", Phys. Fluids, Vol.8, No.12, 1965, pp.2182-2189.
- [24] Spalding, D.B., "A Novel Finite Difference Formulation for Differential Expressions

Involving both First and Second Derivatives", *Int. J. Numer. Method*, Vol.4, 1972, pp.551-559.

[25] Patankar, S.V., *Numerical Heat Transfer and Fluid Flow*, Hemisphere, Washington D.C., 1980.

[26] Barsness, E.J., "Calculation of the Performance of Surface Condenser by Digital Computer", *Am. Soc. Mech. Eng.*, Paper No.63-PWR-2, 1963.

[27] Al-Sanea, S.A., Rhodes, N., Tatchell, D.G. and Wilkinson, T.S., " A Computer Model for Detailed Calculation of the Flow in Power Station Condensers," in *Condensers: Theory and Practice*, *Int. Chem. E. Symposium Series*, No.75, Pergamon Press, 1983, pp.70-88.

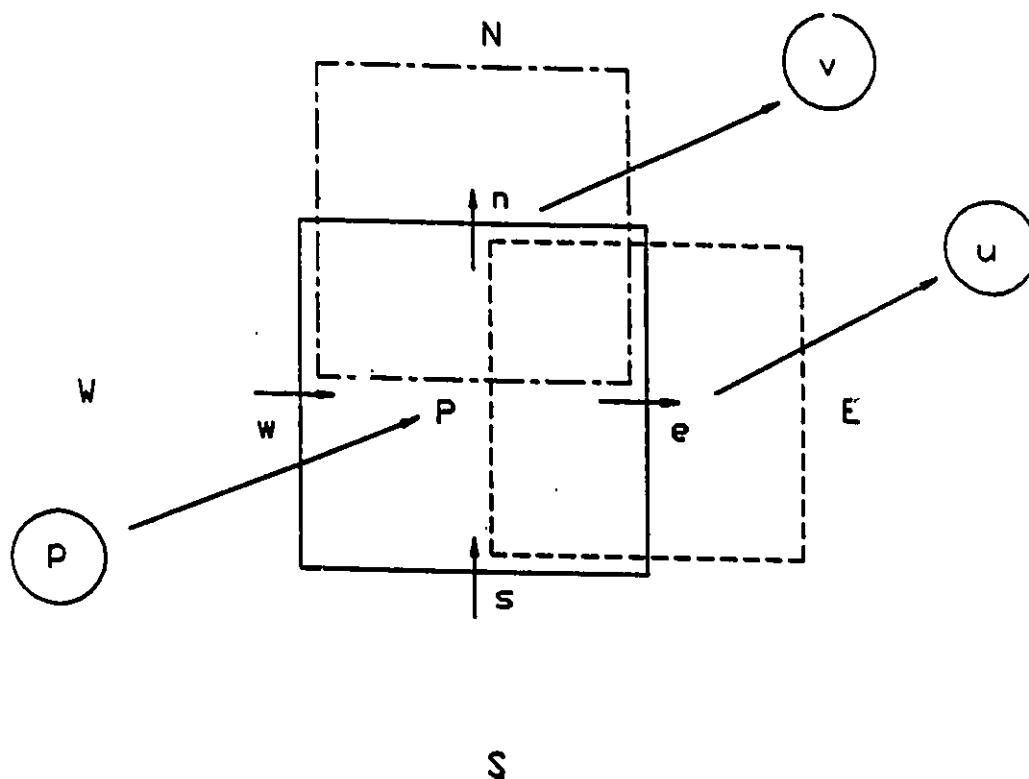


**Figure 4.1 Grid Arrangement**

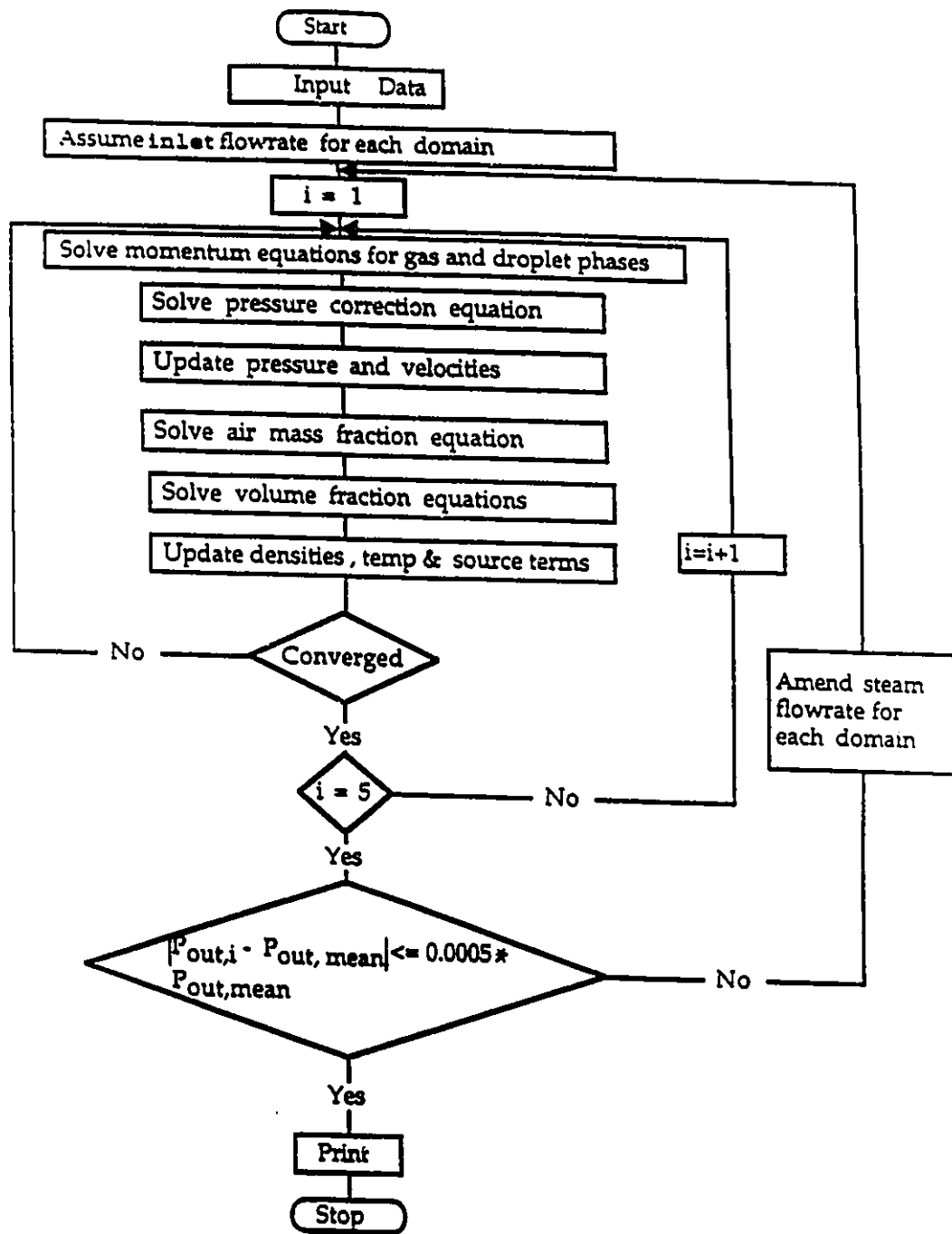
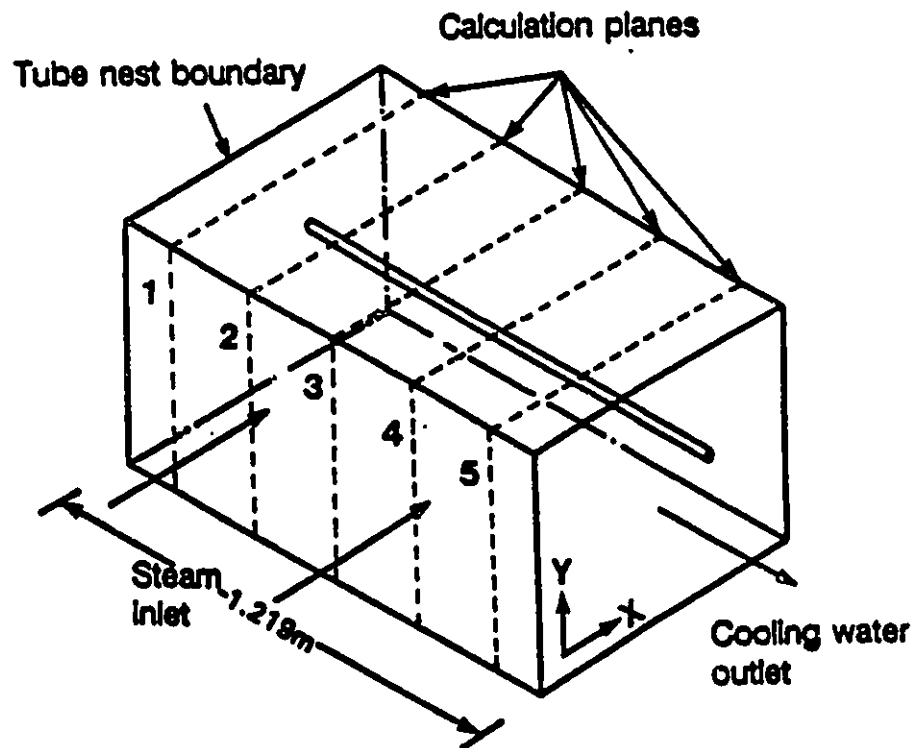
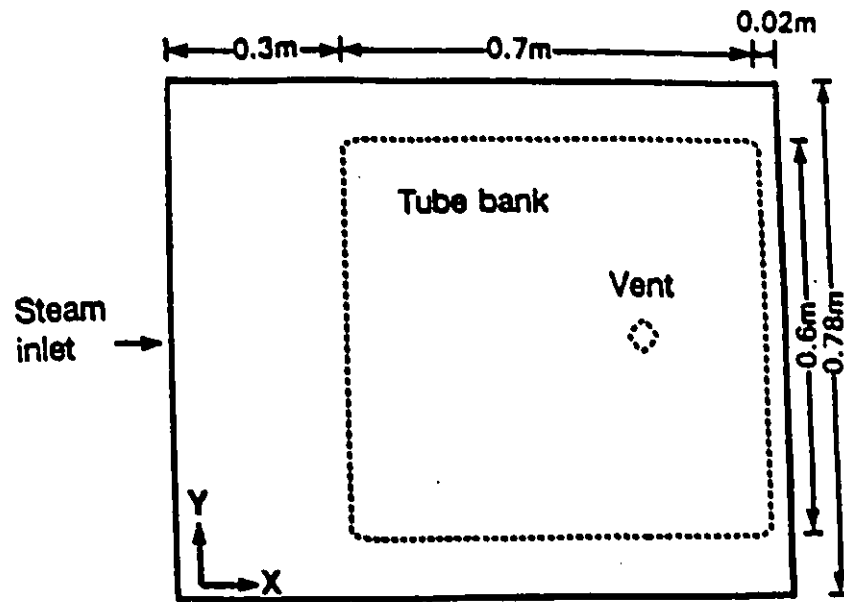
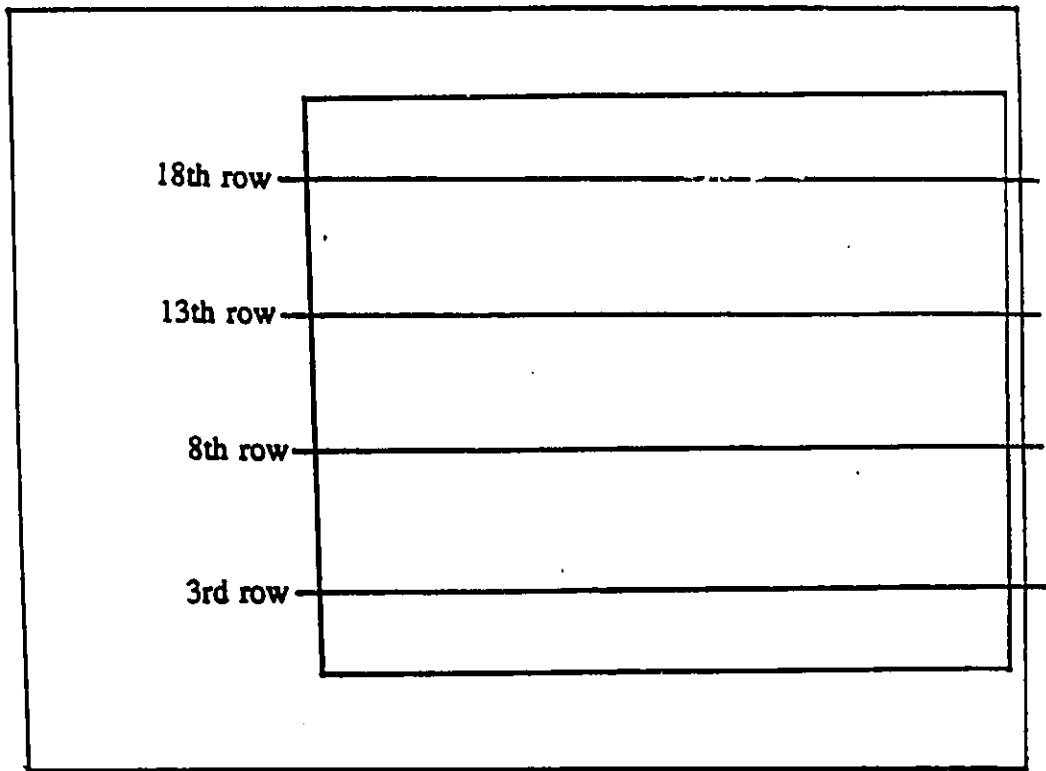


Figure 4.2 Flow Chart



**Figure 5.1 Configuration of the Experimental Condenser**



**Figure 5.2 Position of Tube Rows in the Condenser**

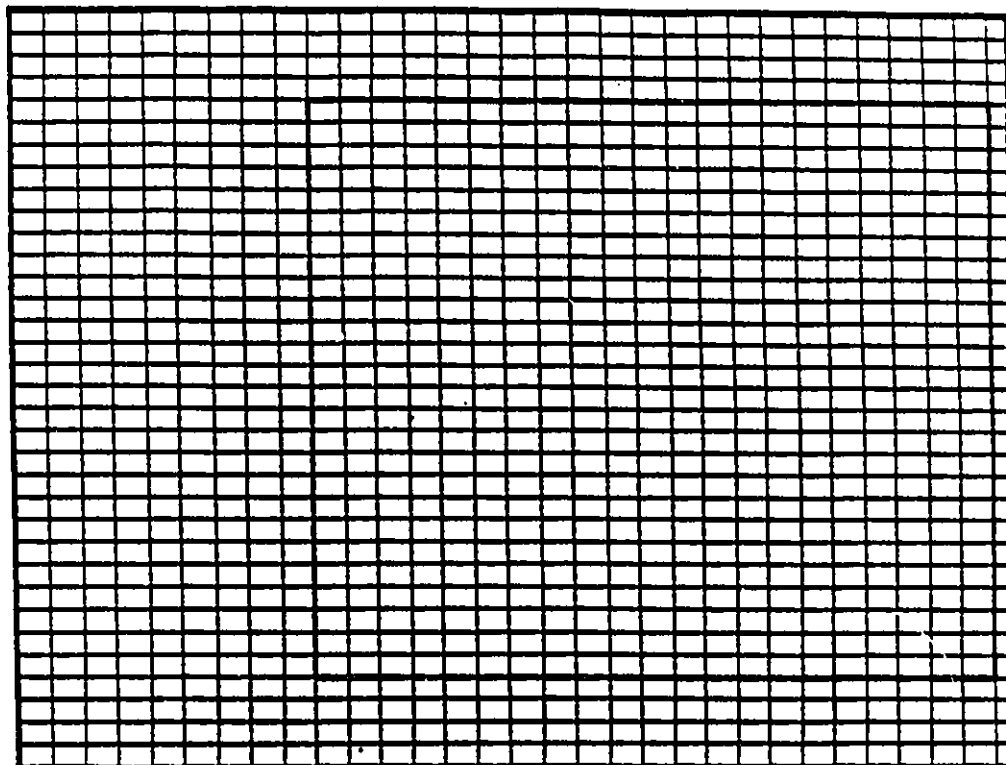
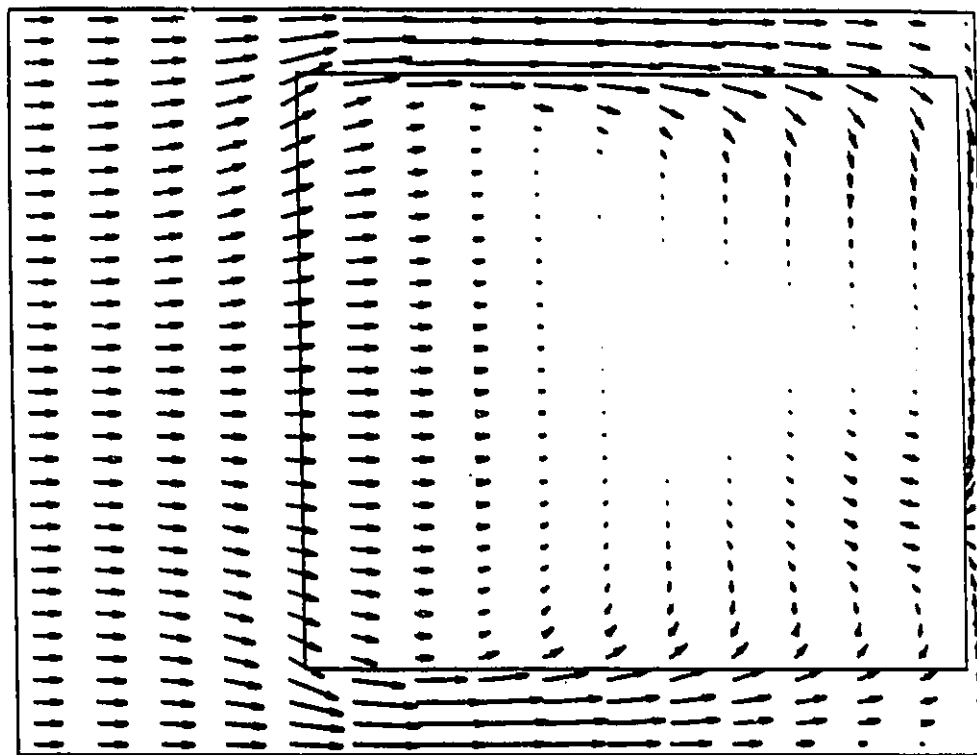


**Figure 5.3 Grid used for the Simulation**

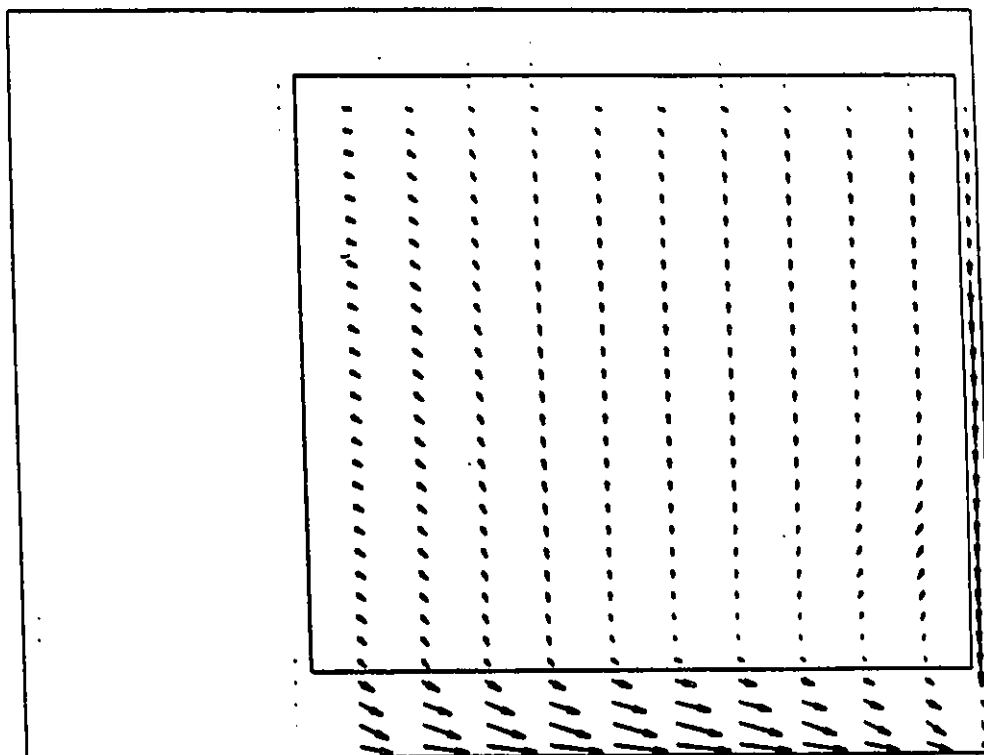


velocity vector scale  $\rightarrow = 10$  (m/s)

(a)

**Figure 5.4 Velocity Vector Plots for Plane no.3**  
**(a) Gas (b) Liquid**





velocity vector scale  $- = 1$  (m/s)

(b)

**Figure 5.4 Velocity Vector for the Plane no.3**  
**(a) Gas (b) Liquid**

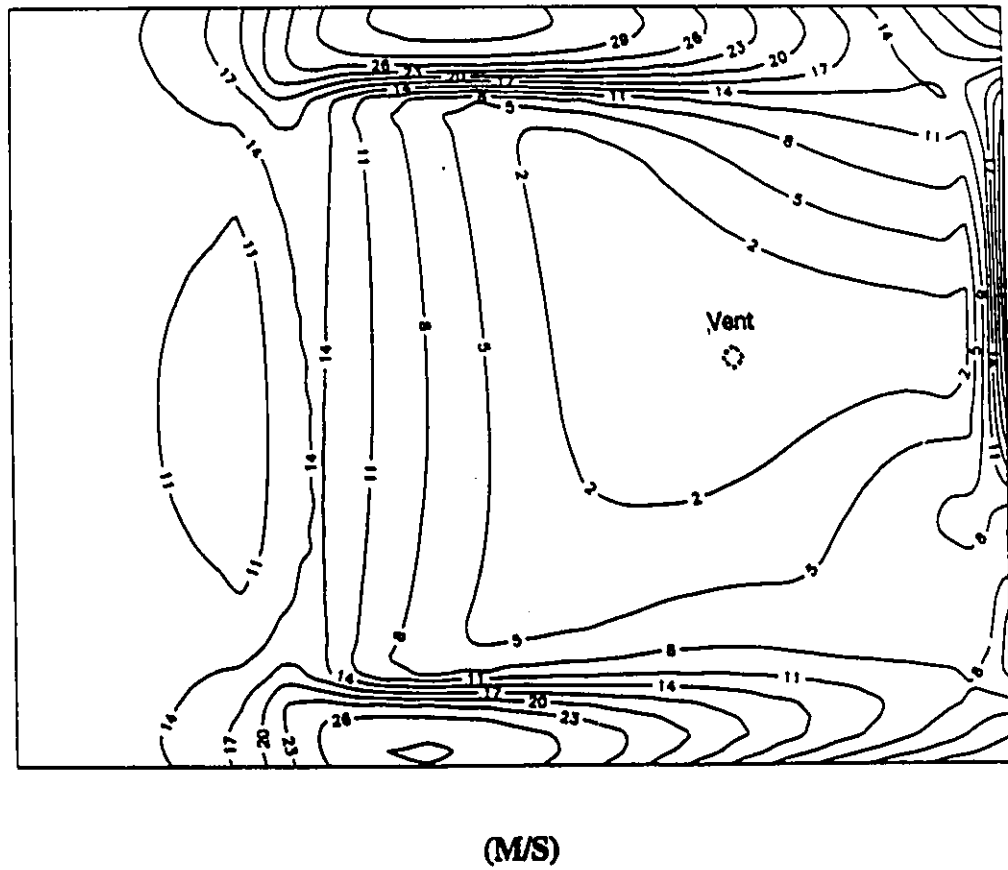
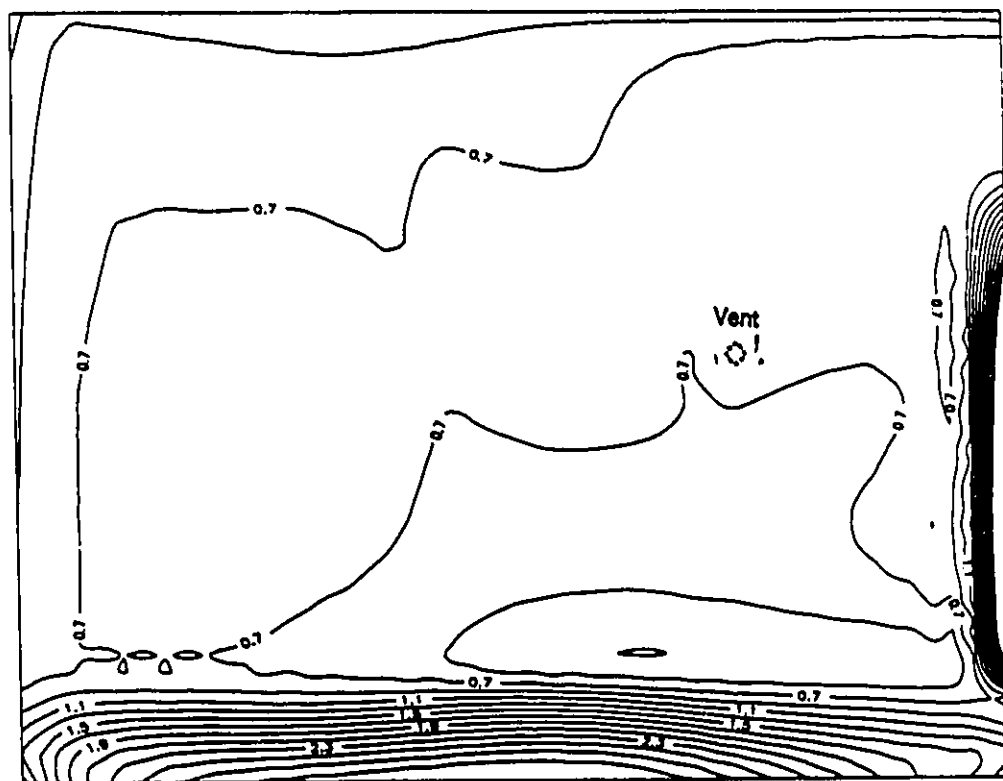


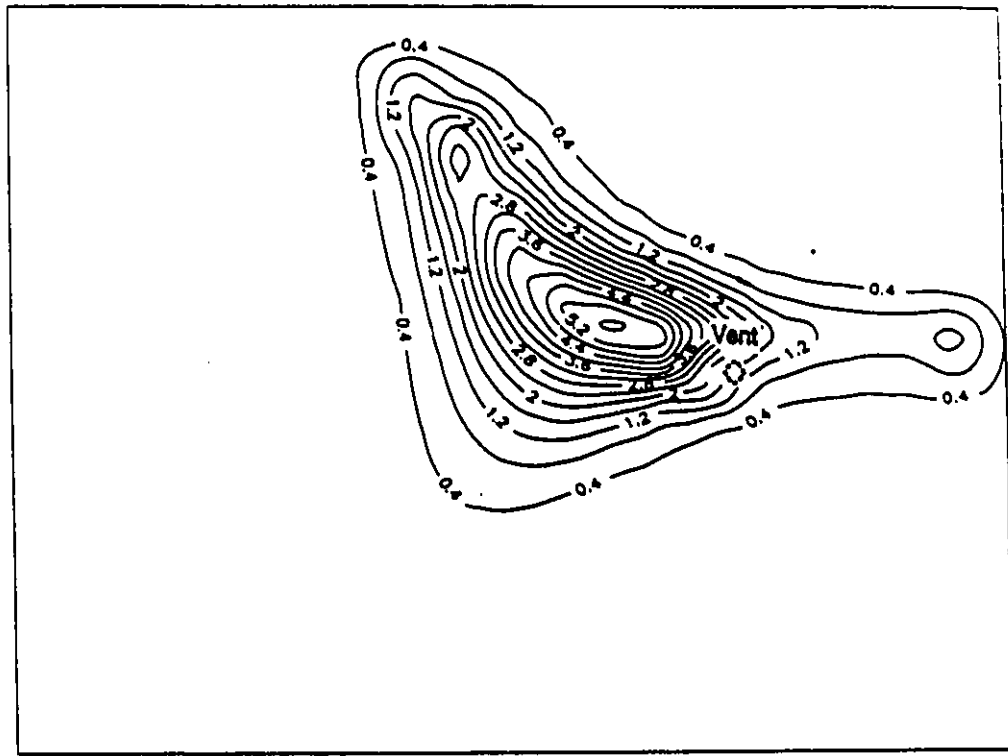
**Figure 5.5 Contour Map of Gas Velocity Magnitude for Plane no.3**



(M/S)

**Figure 5.6 Contour Map of Liquid Velocity Magnitude for Plane no.3**

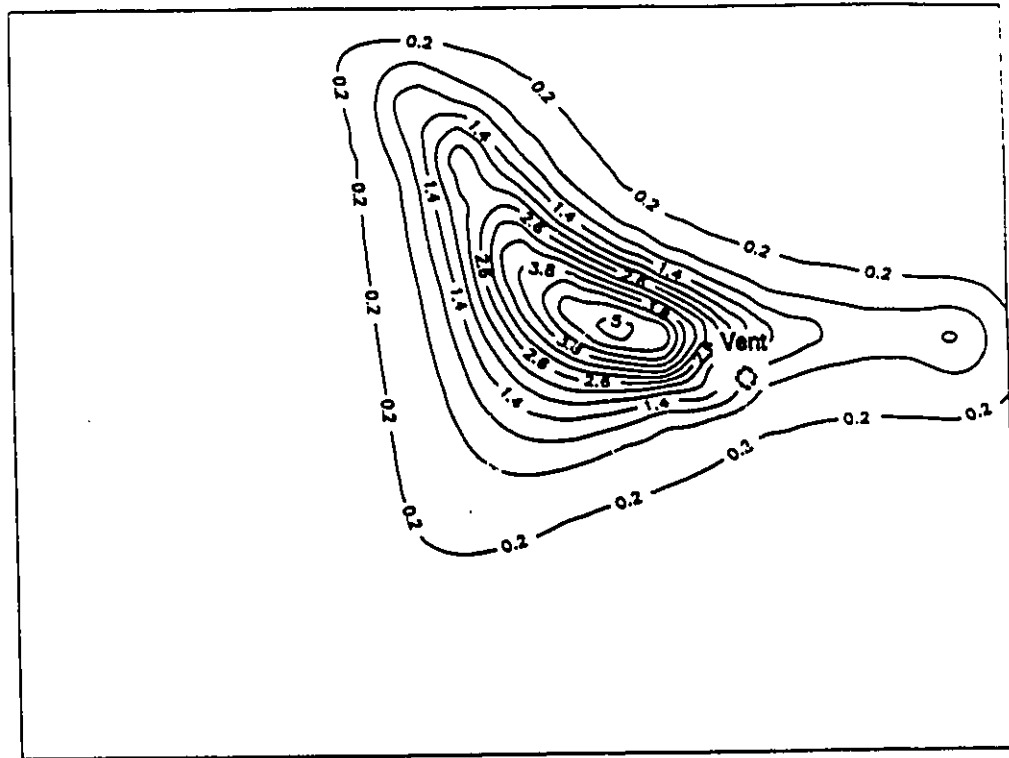




(%)

(b)

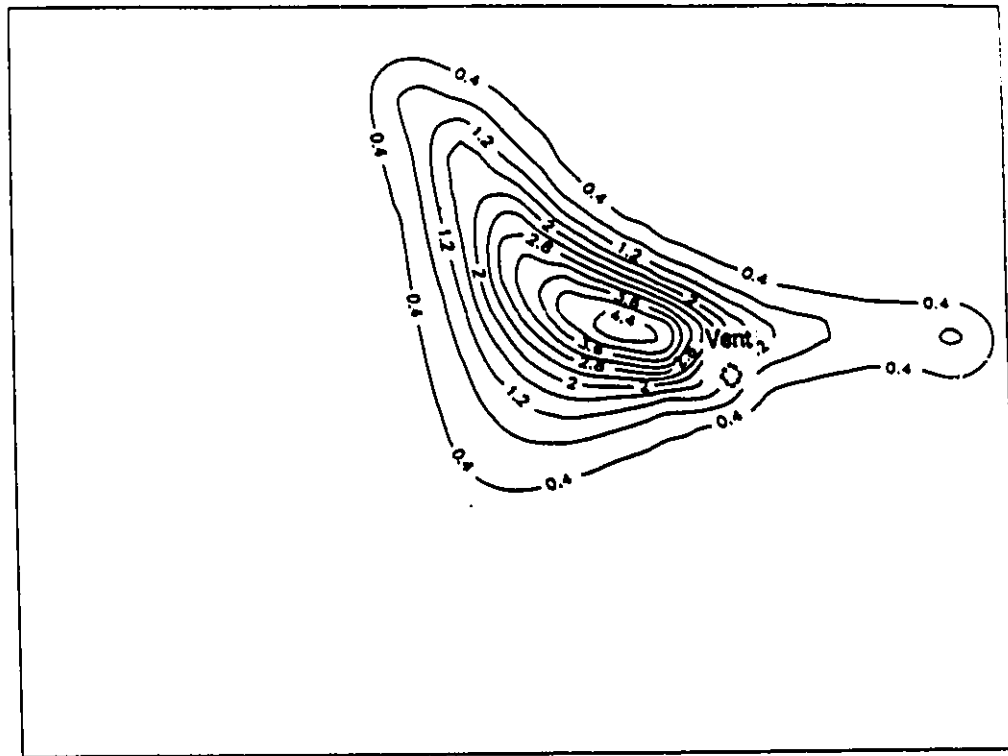
**Figure 5.7 Contour Maps of Air Mass Fraction**  
**(a) Plane no.1 (b) Plane no.2 (c) Plane no.3 (d) Plane no.4**  
**(e) Plane no.5**



(%)

(c)

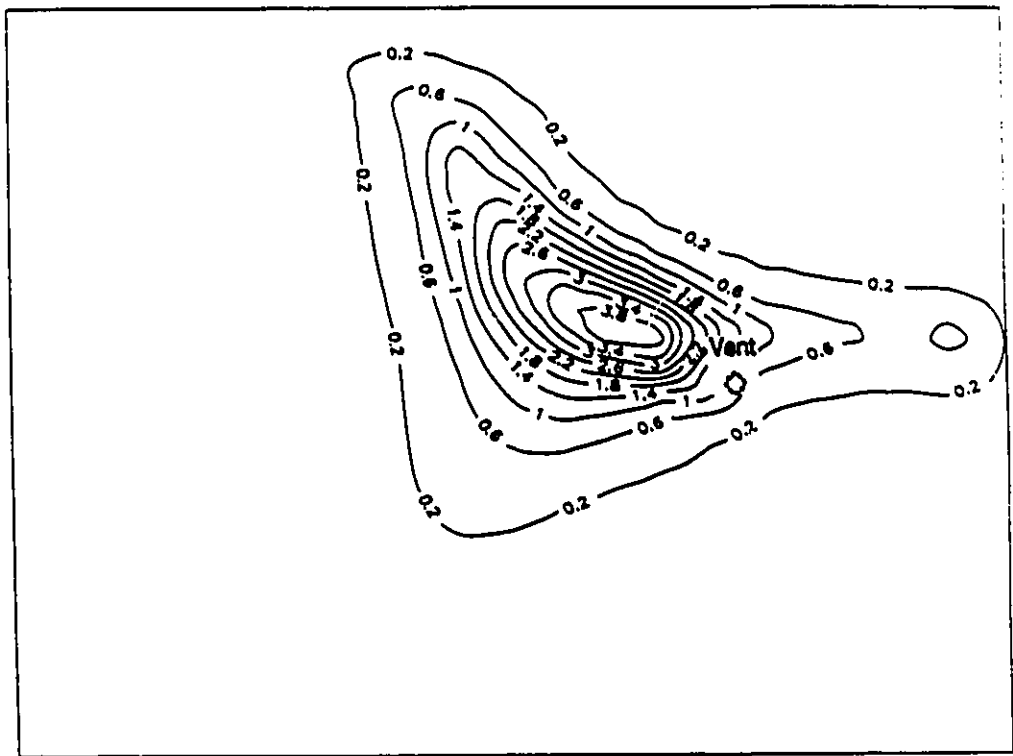
**Figure 5.7 Contour Maps of Air Mass Fraction**  
**(a) Plane no.1 (b) Plane no.2 (c) Plane no.3 (d) Plane no.4**  
**(e) Plane no.5**



(%)

(d)

**Figure 5.7 Contour Maps of Air Mass Fraction**  
**(a) Plane no.1 (b) Plane no.2 (c) Plane no.3 (d) Plane no.4**  
**(e) Plane no.5**

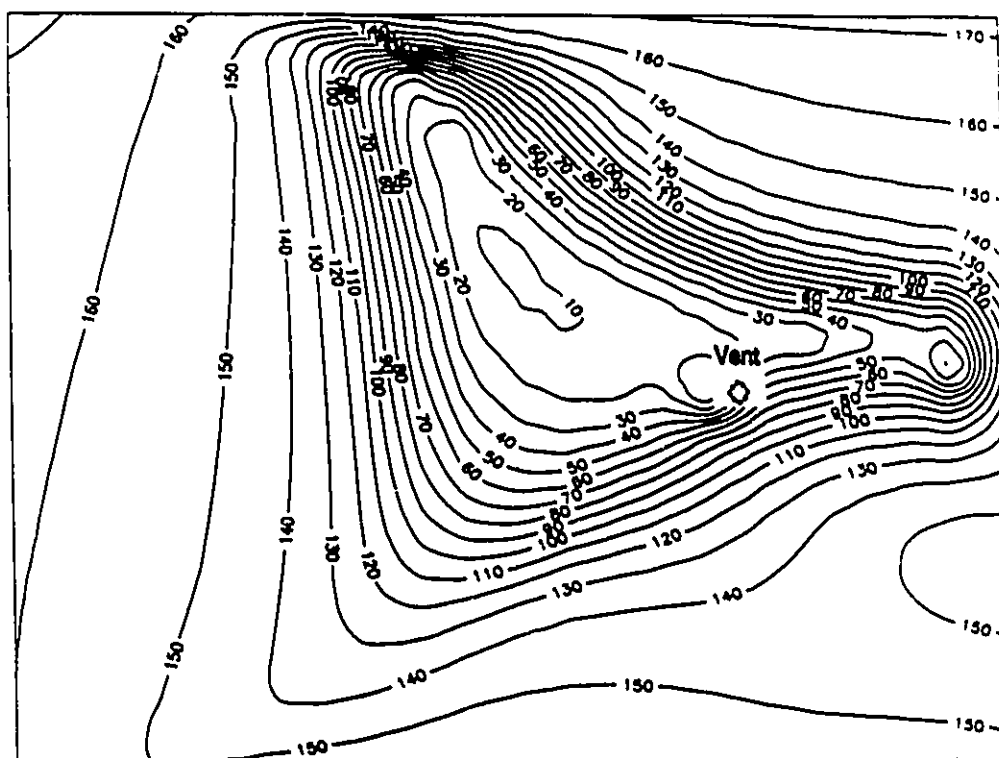


(%)

(e)

**Figure 5.7 Contour Maps of Air Mass Fraction**  
**(a) Plane no.1 (b) Plane no.2 (c) Plane no.3 (d) Plane no.4**  
**(e) Plane no.5**

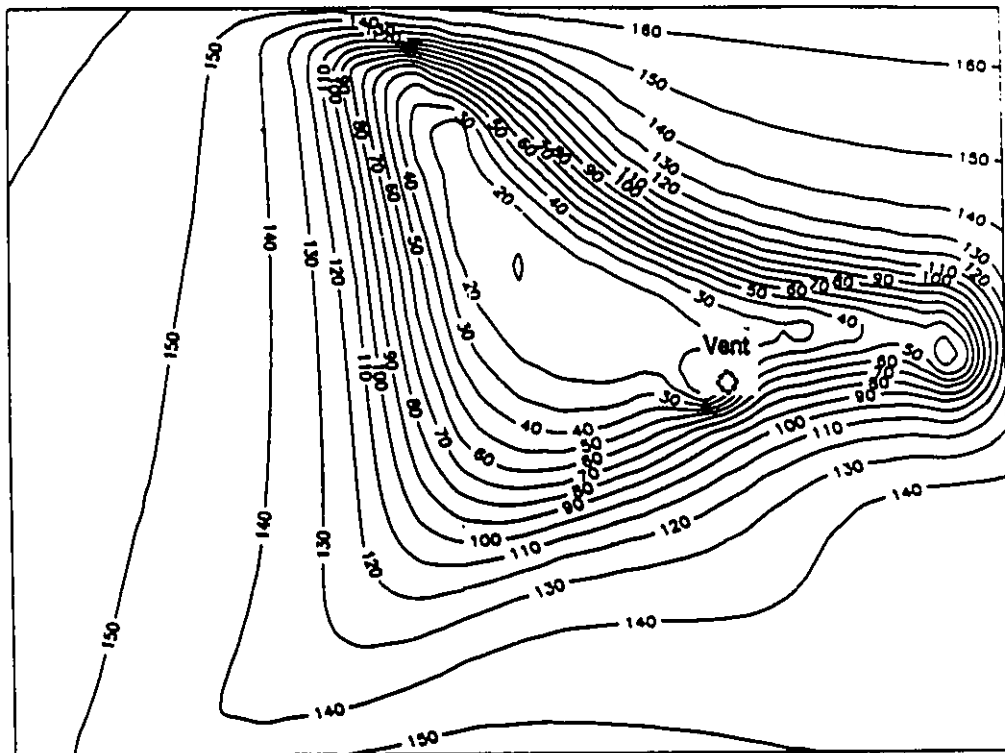




(KW/M<sup>2</sup>)

(a)

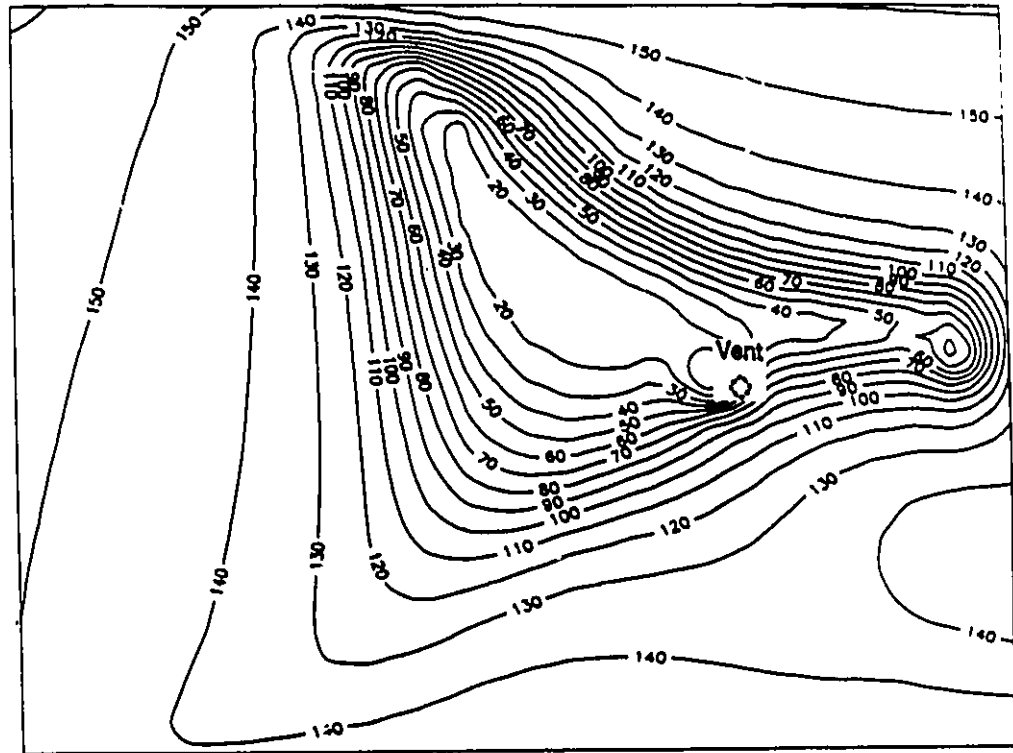
**Figure 5.8 Contour Maps of Heat Flux**  
**(a) Plane no.1 (b) Plane no.2 (c) Plane no.3 (d) Plane no.4**  
**(e) Plane no.5**



(KW/M<sup>2</sup>)

(b)

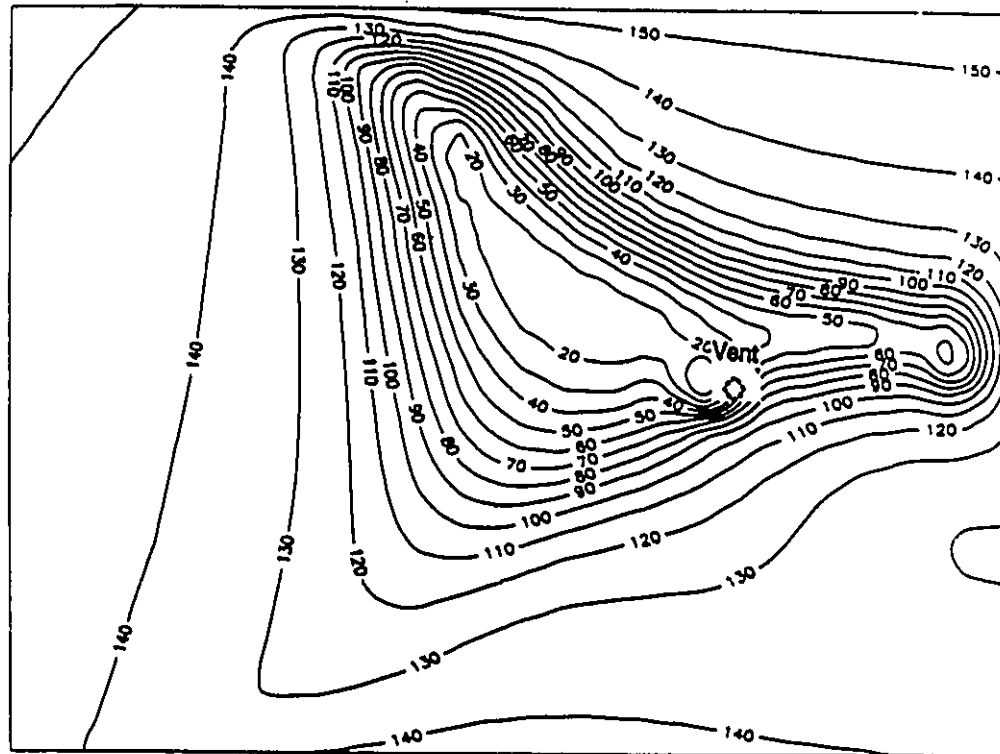
**Figure 5.8 Contour Maps of Heat Flux**  
**(a) Plane no.1 (b) Plane no.2 (c) Plane no.3 (d) Plane no.4**  
**(e) Plane no.5**



(KW/M<sup>2</sup>)

(c)

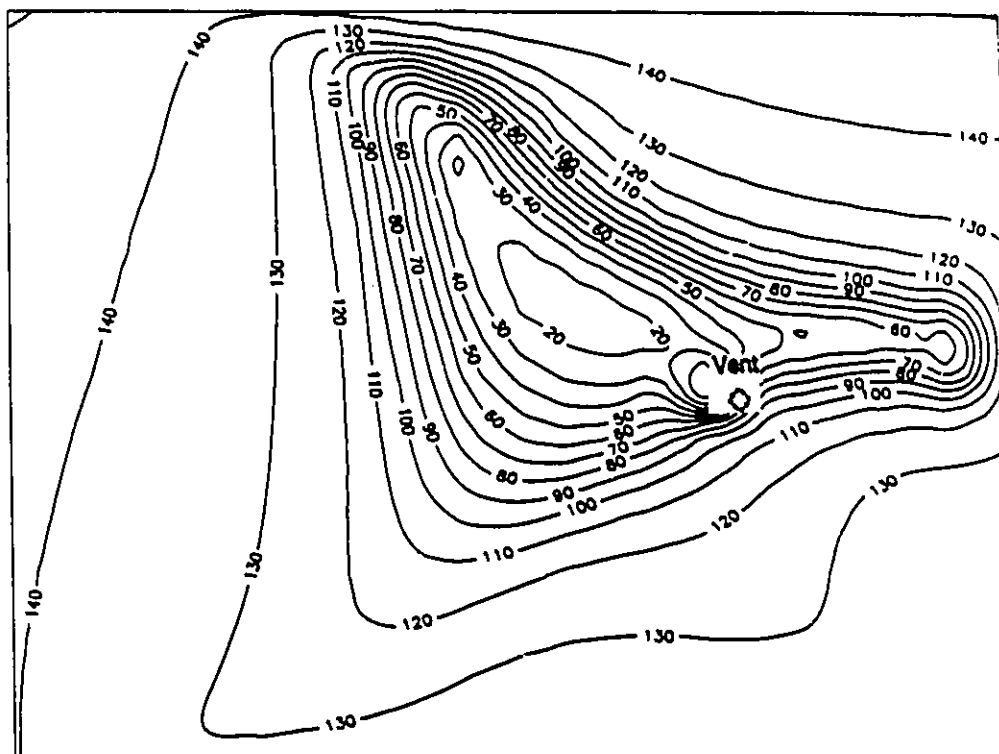
**Figure 5.8 Contour Maps of Heat Flux**  
**(a) Plane no.1 (b) Plane no.2 (c) Plane no.3 (d) Plane no.4**  
**(e) Plane no.5**



(KW/M<sup>2</sup>)

(d)

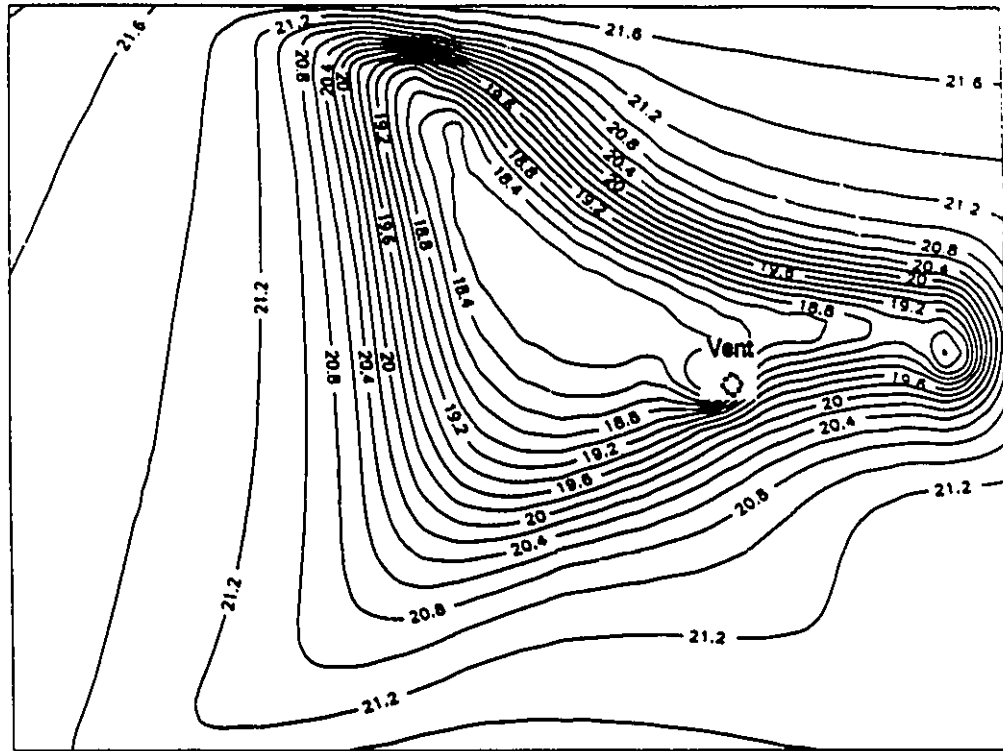
**Figure 5.8 Contour Maps of Heat Flux**  
**(a) Plane no.1 (b) Plane no.2 (c) Plane no.3 (d) Plane no.4**  
**(e) Plane no.5**



(KW/M<sup>2</sup>)

(e)

**Figure 5.8 Contour Maps of Heat Flux**  
**(a) Plane no.1 (b) Plane no.2 (c) Plane no.3 (d) Plane no.4**  
**(e) Plane no.5**



(°C)

**Figure 5.9 Contour Map of Cooling Water Temperature for Plane no.3**

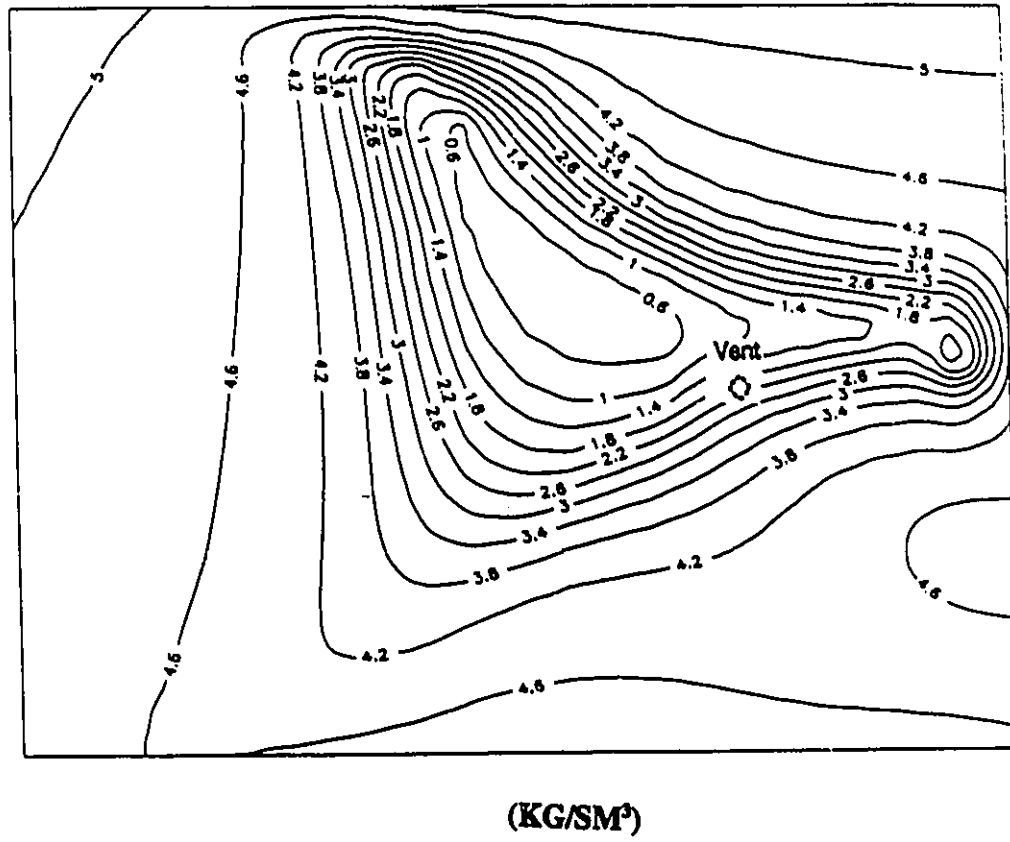


**Figure 5.10 Contour Map of Condensation Rate for Plane no.3**

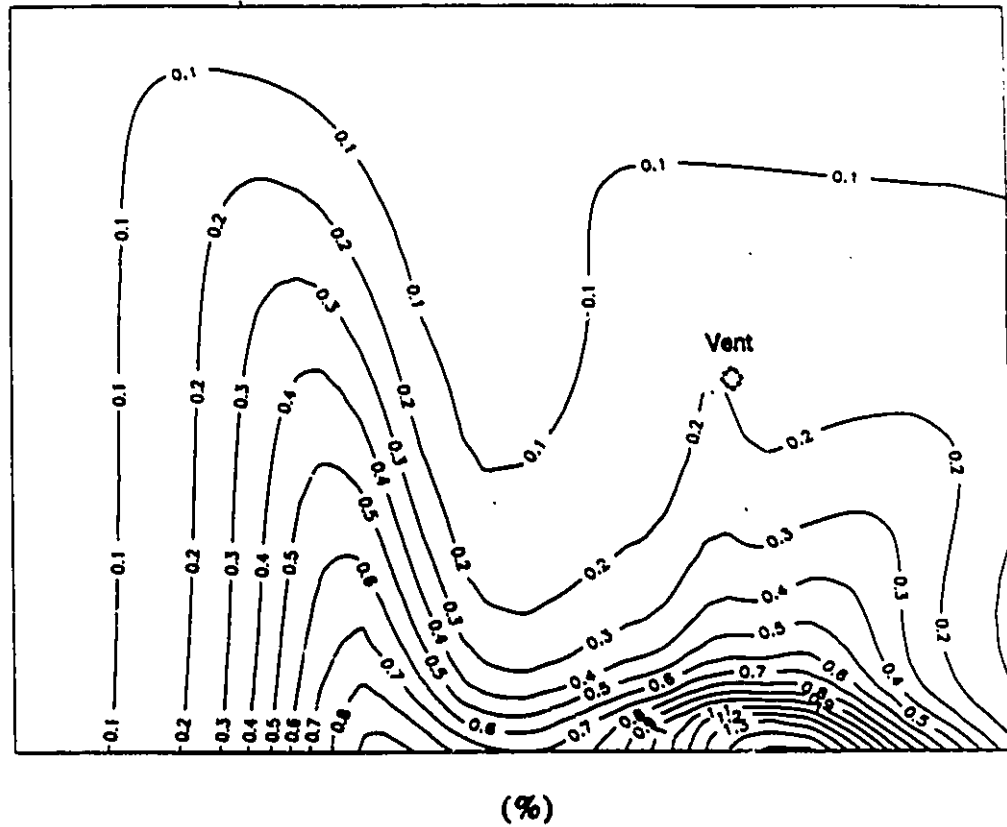


**Figure 5.11 Contour Map of Liquid Volume Fraction for Plane no.3  
(Droplet Diameter=0.001m)**



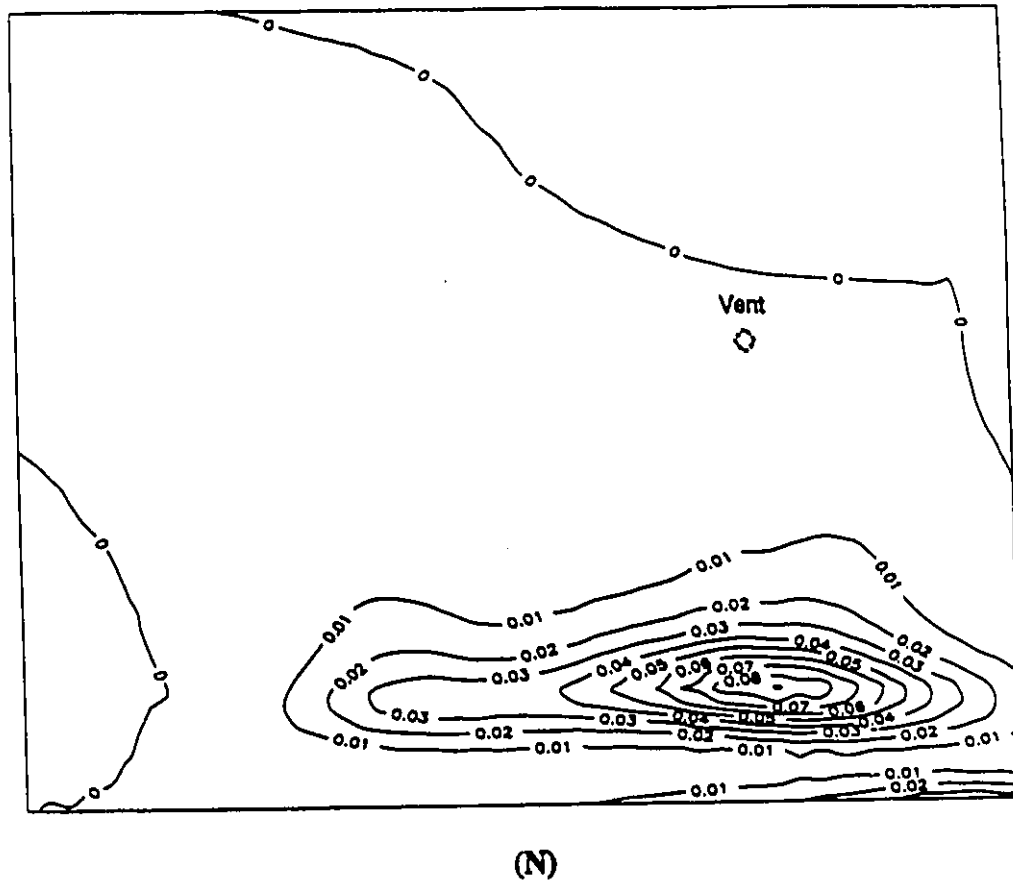


**Figure 5.12 Contour Map of Interphase Friction Force for Plane no.3  
(Droplet Diameter=0.001m)**

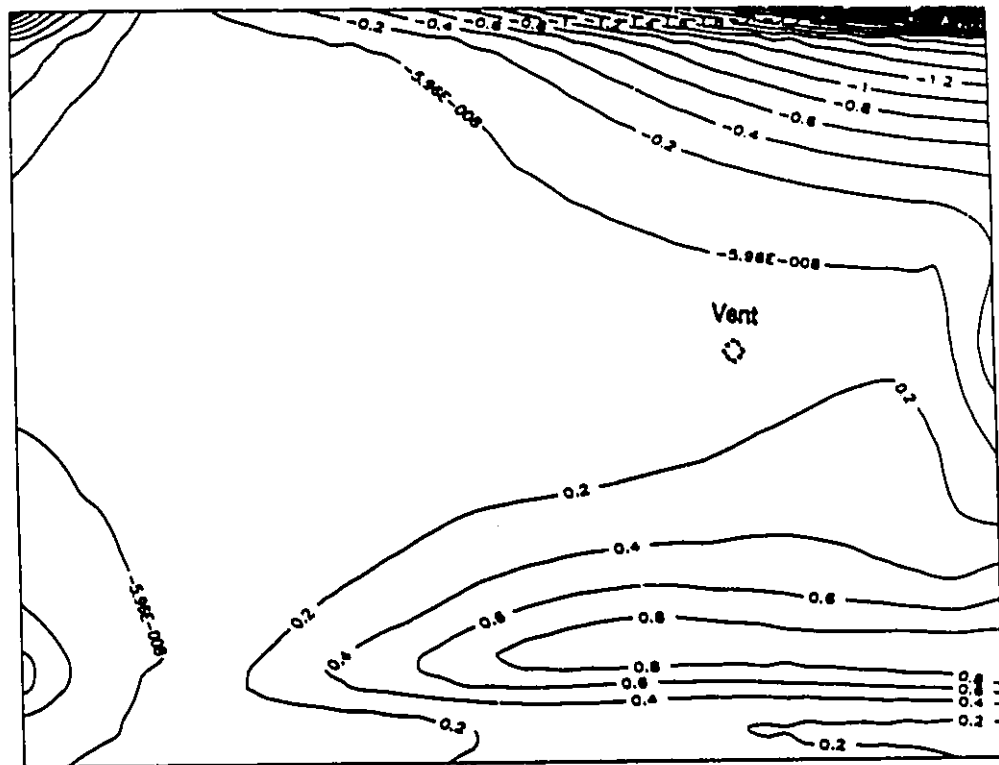


**Figure 5.13 Contour Map of Interphase Friction Force per unit  
Gravitational Force for Plane no.3  
(Droplet Diameter=0.001m)**

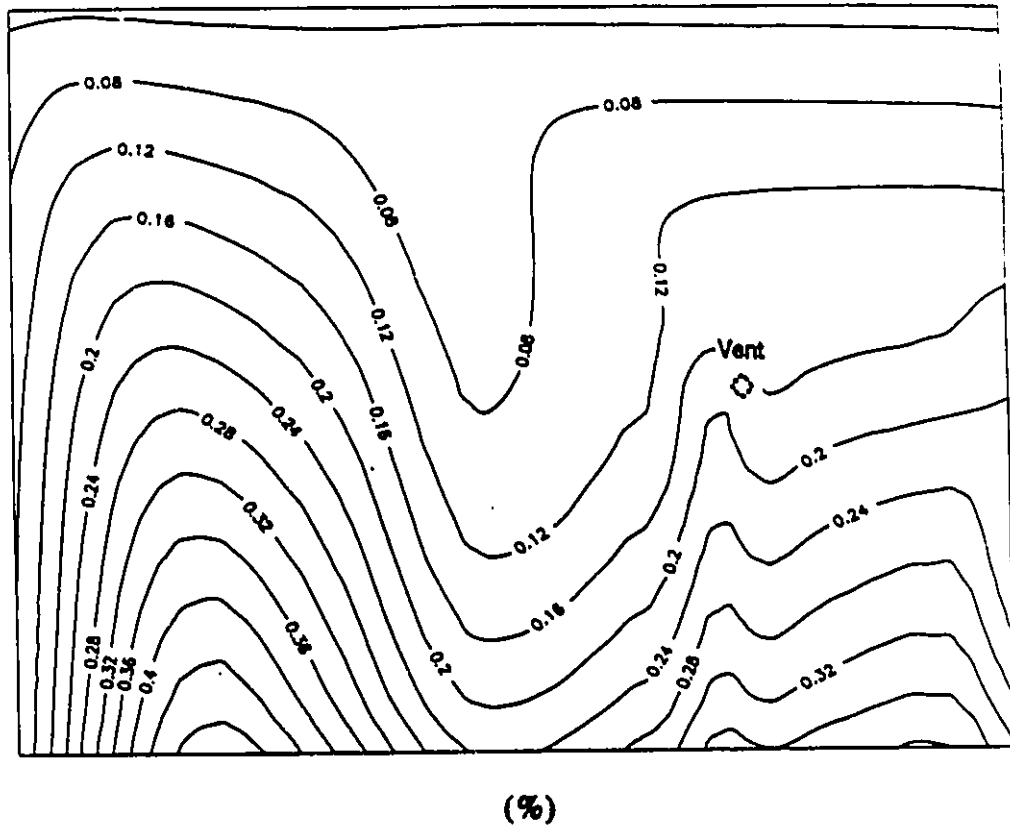


**Figure 5.14 Contour Map of Liquid Volume Fraction for Plane no.3  
(Droplet Diameter=0.004m)**

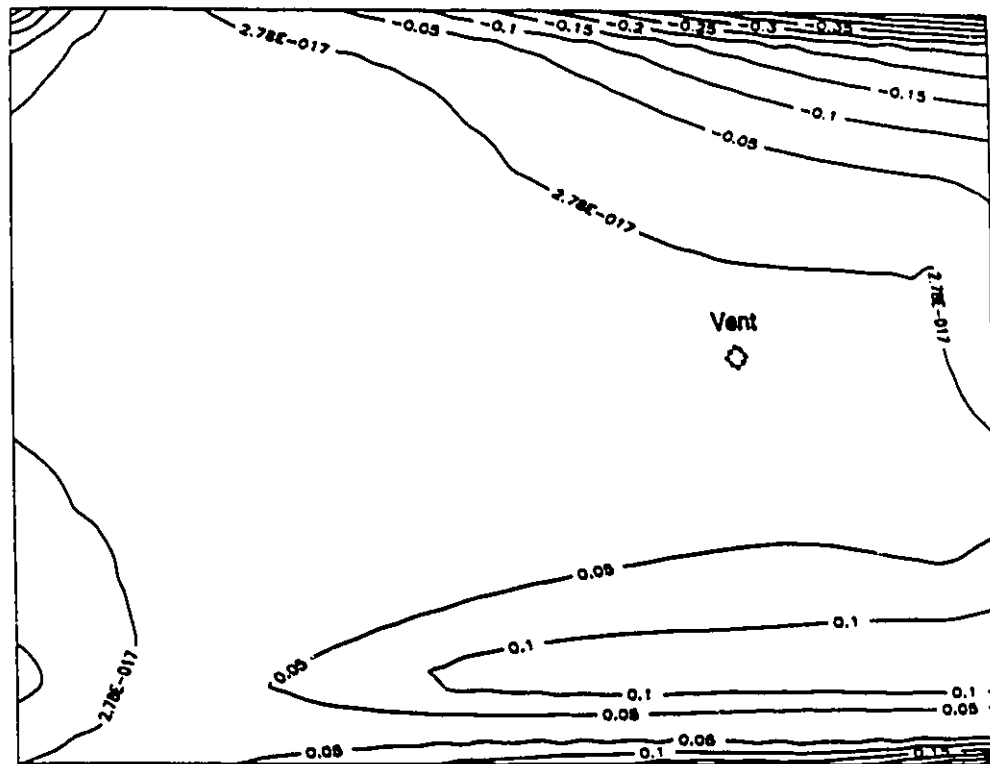
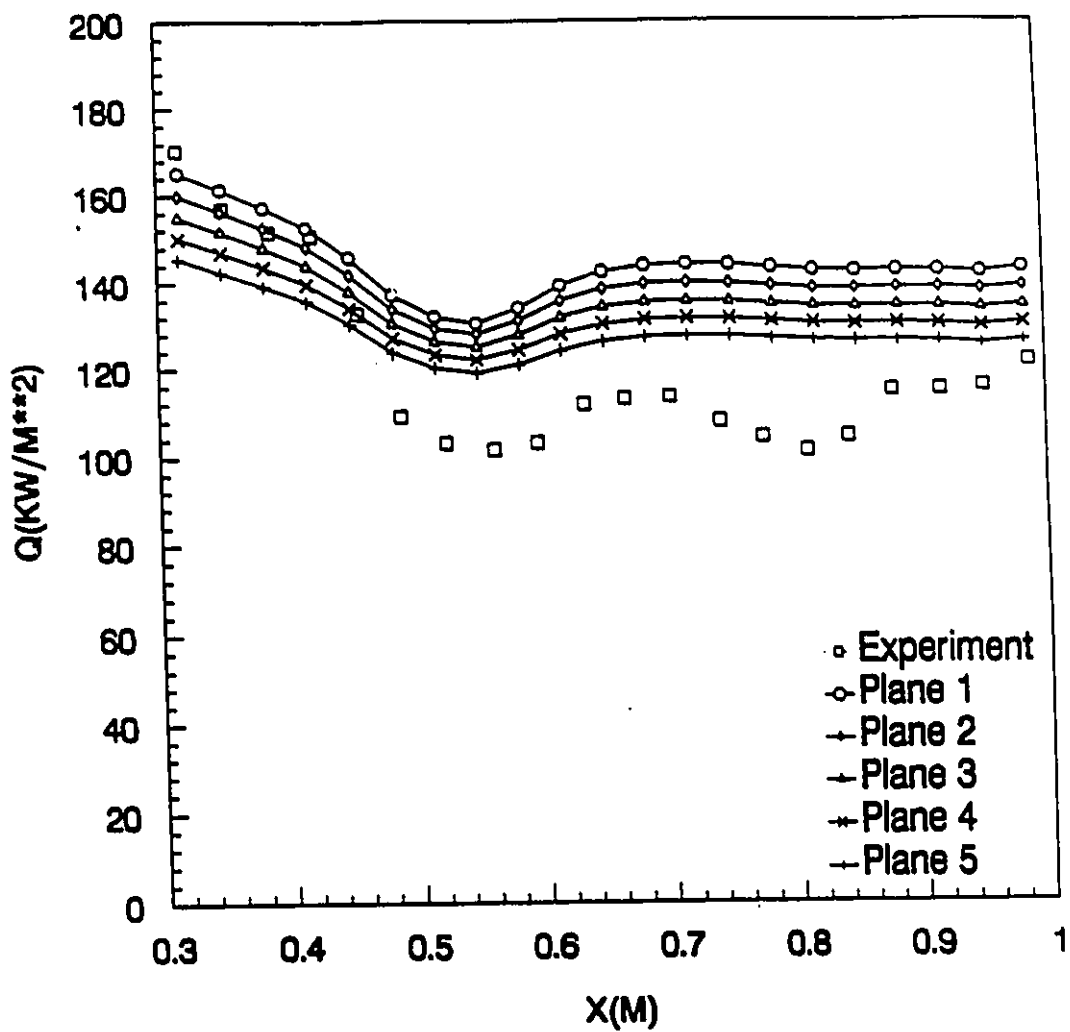


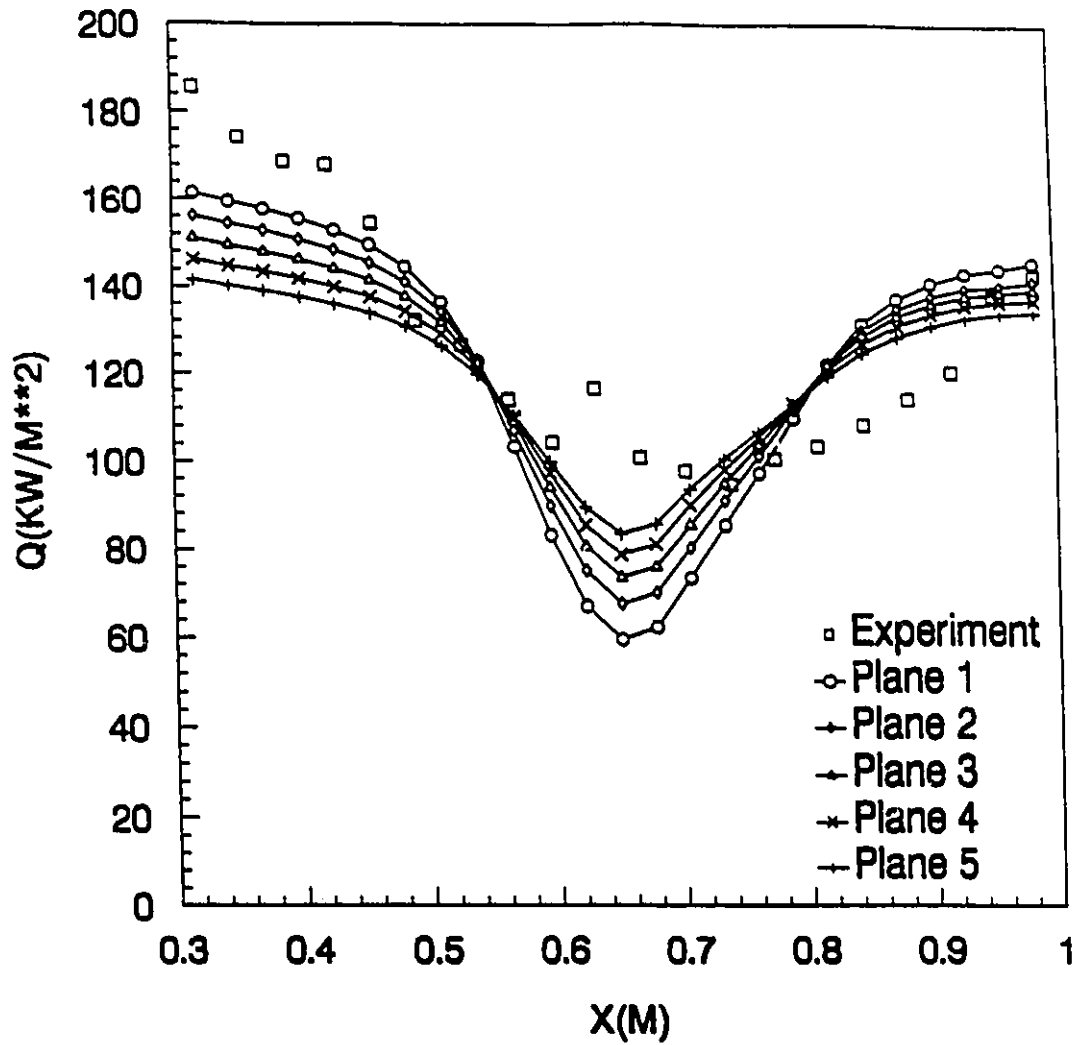
**Figure 5.15 Contour Map of Interphase Friction Force per unit  
Gravitational Force for Plane no.3  
(Droplet Diameter=0.004m)**



(a)

**Figure 5.16 Comparison of Predicted Heat flux with Experimental Data**

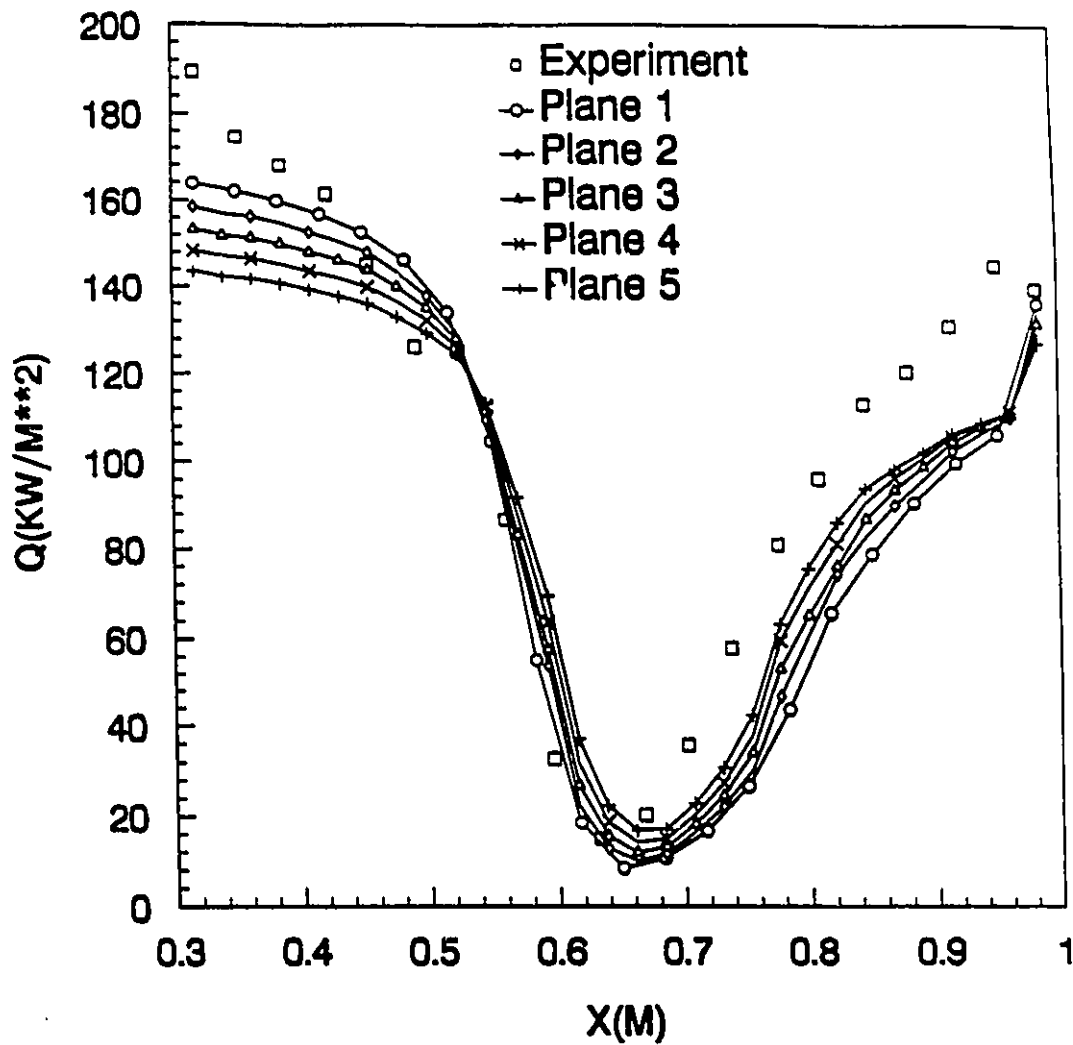
**(a) 3rd Row of Tubes (b) 8th Row of Tubes  
(c) 13th Row of Tubes (d) 18th Row of Tubes**



(b)

**Figure 5.16 Comparison of Predicted Heat flux with Experimental Data**

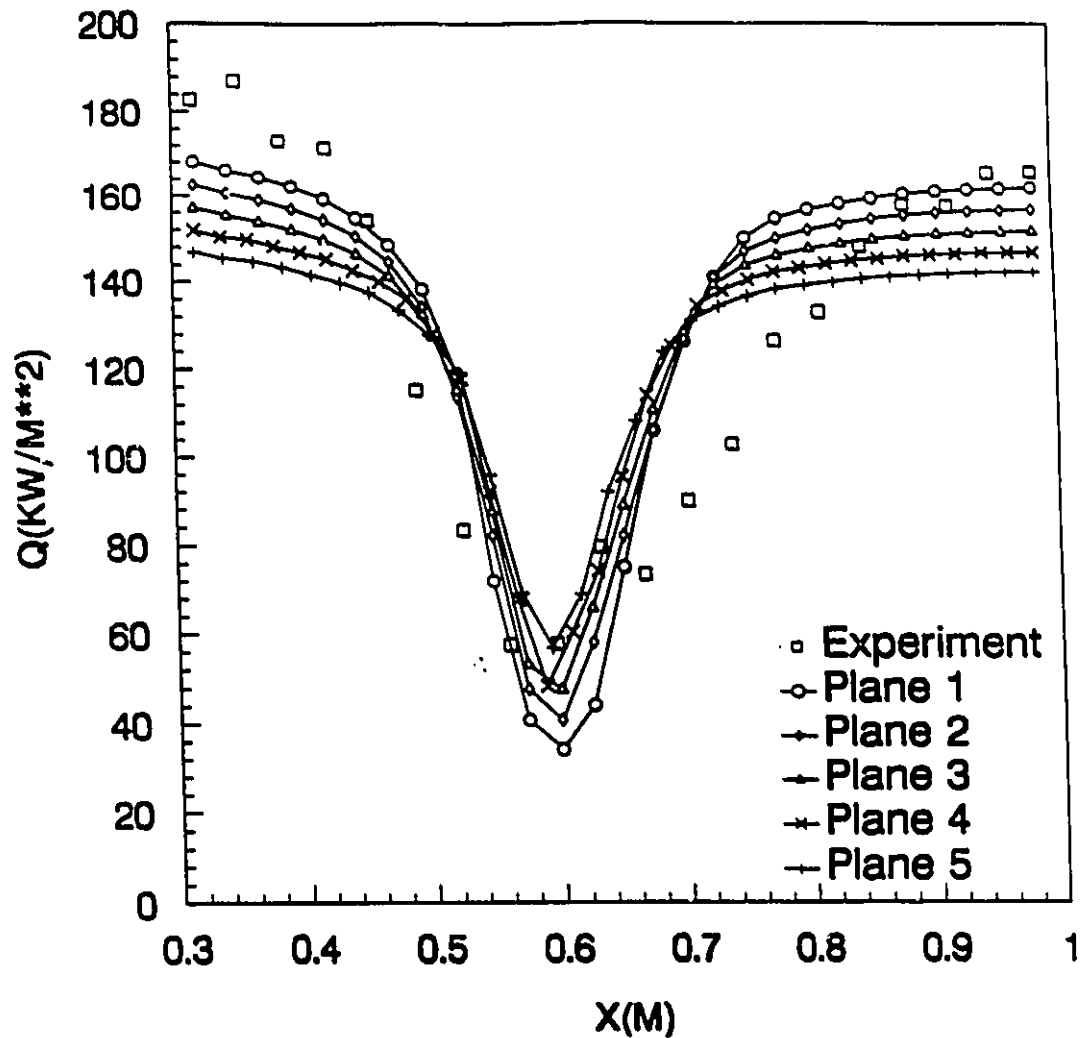
(a) 3rd Row of Tubes (b) 8th Row of Tubes  
 (c) 13th Row of Tubes (d) 18th Row of Tubes



(c)

**Figure 5.16 Comparison of Predicted Heat flux with Experimental Data**

**(a) 3rd Row of Tubes (b) 8th Row of Tubes  
(c) 13th Row of Tubes (d) 18th Row of Tubes**

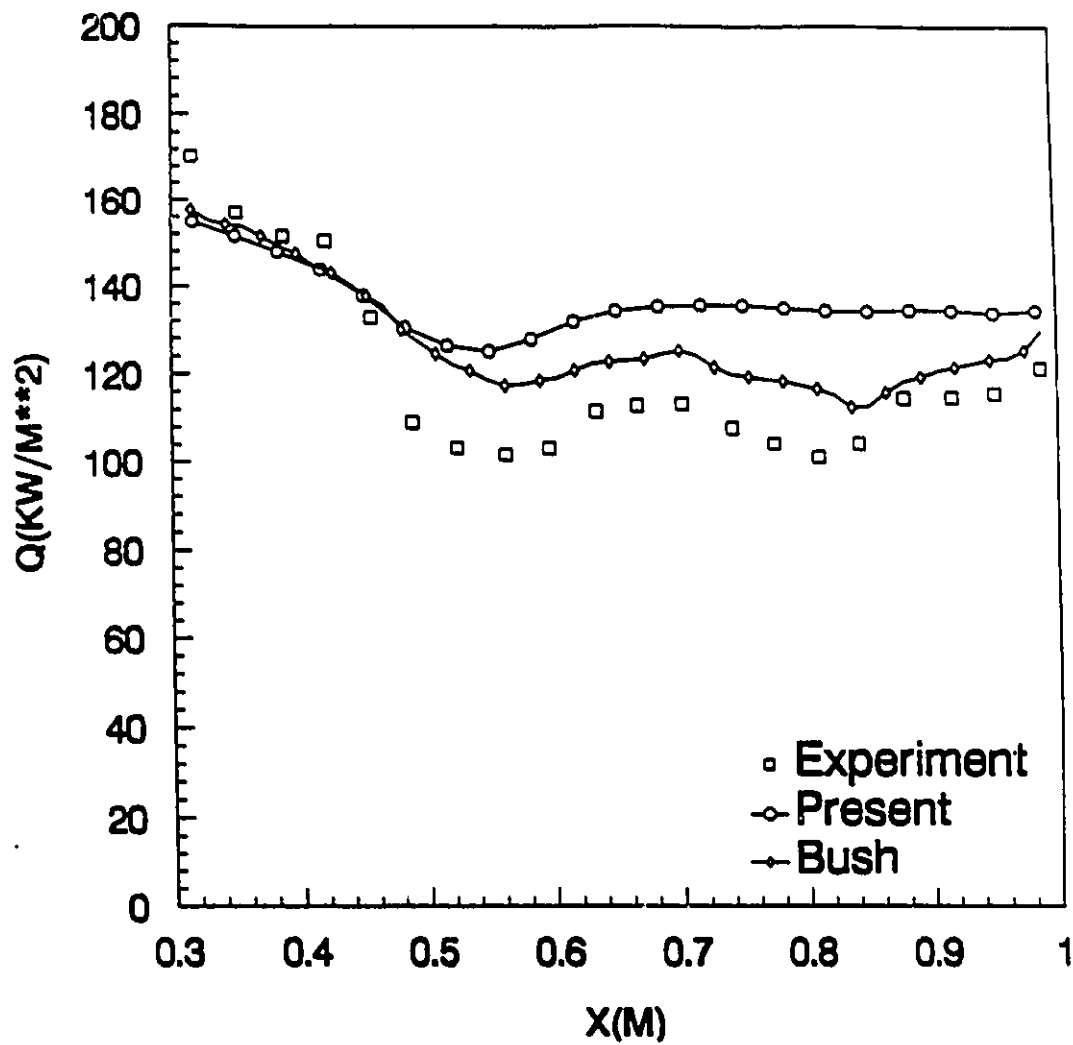


(d)

**Figure 5.16 Comparison of Predicted Heat flux with Experimental Data**

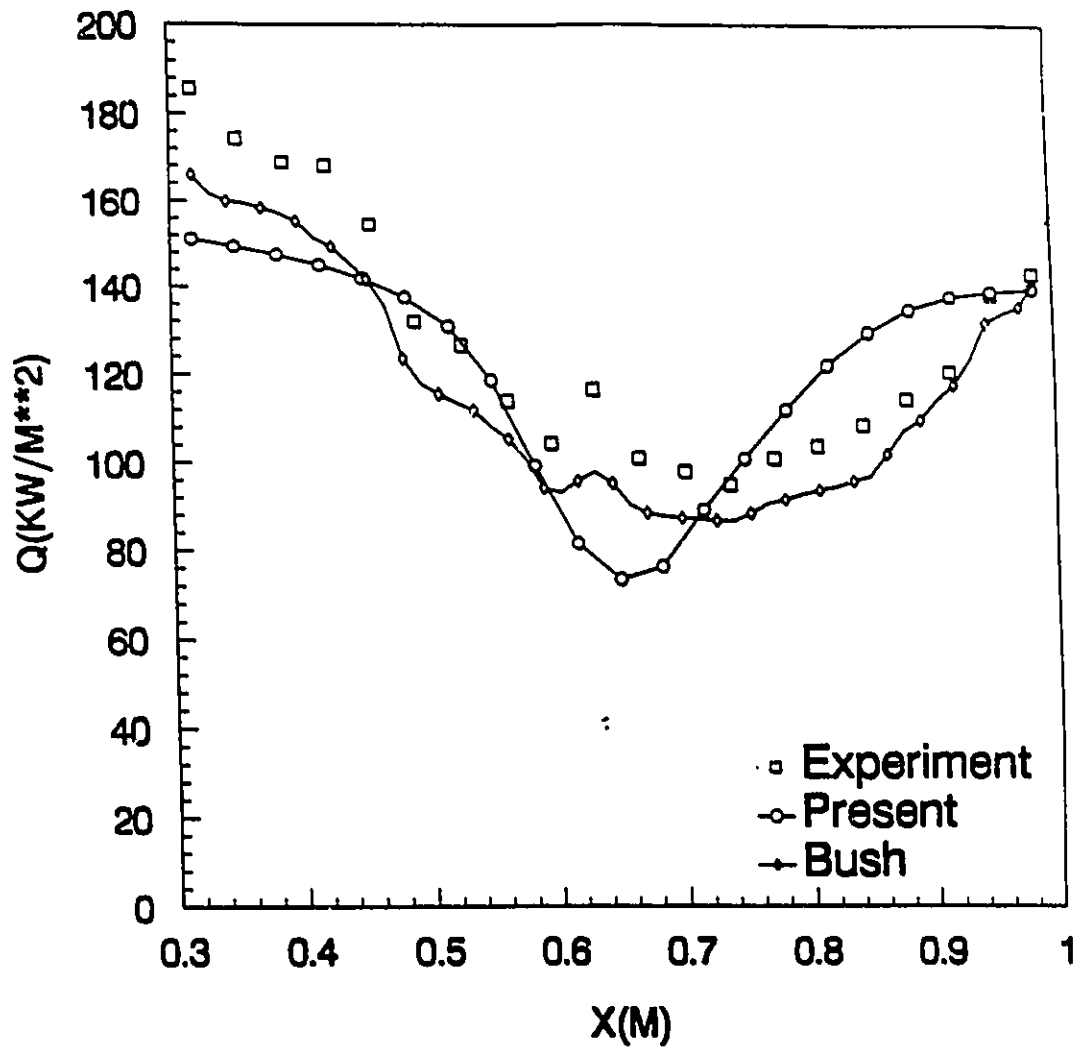
(a) 3rd Row of Tubes (b) 8th Row of Tubes  
 (c) 13th Row of Tubes (d) 18th Row of Tubes





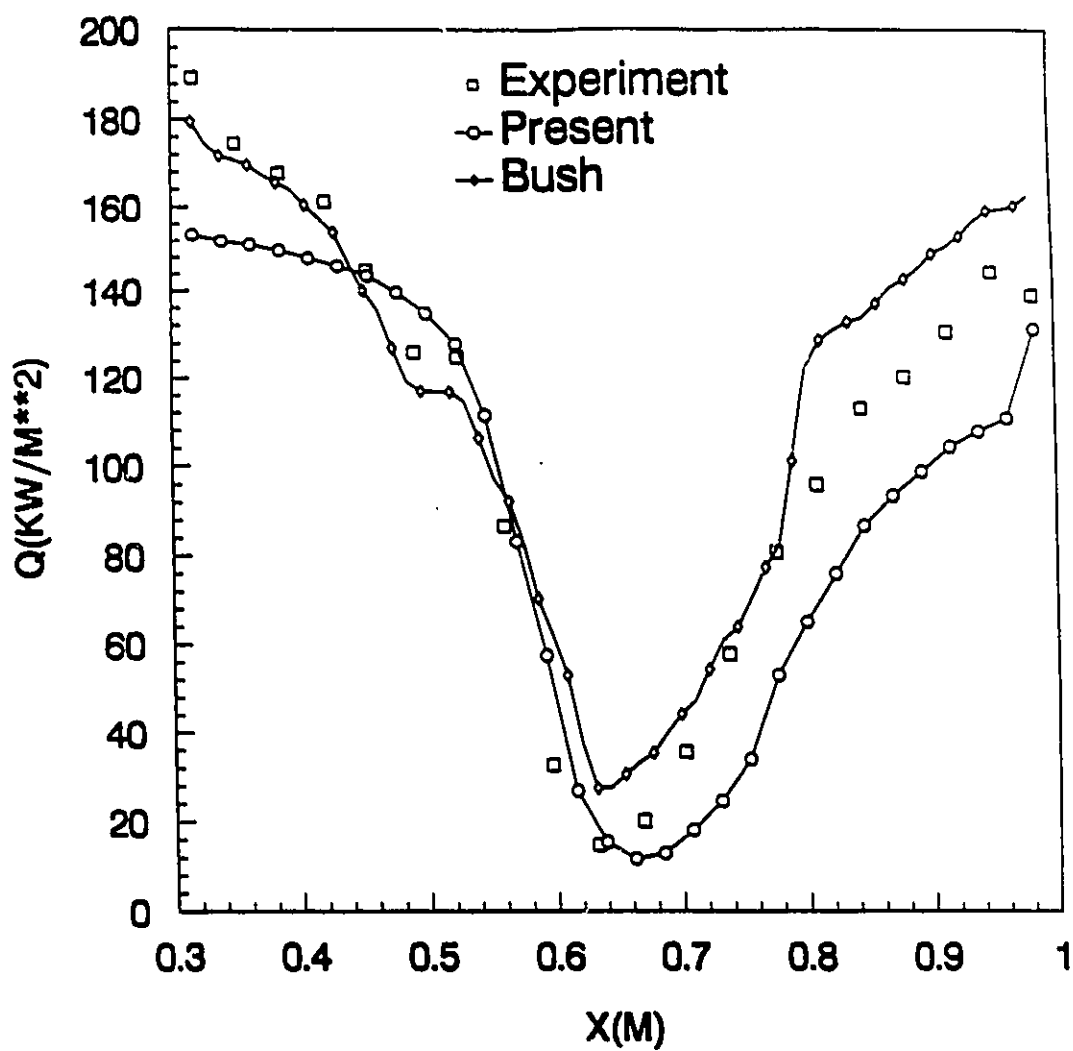
(a)

**Figure 5.17 Comparison of Predicted Heat Flux with Bush's Results**  
**(a) 3rd Row of Tubes (b) 8th Row of Tubes**  
**(c) 13th Row of Tubes (d) 18th Row of Tubes**



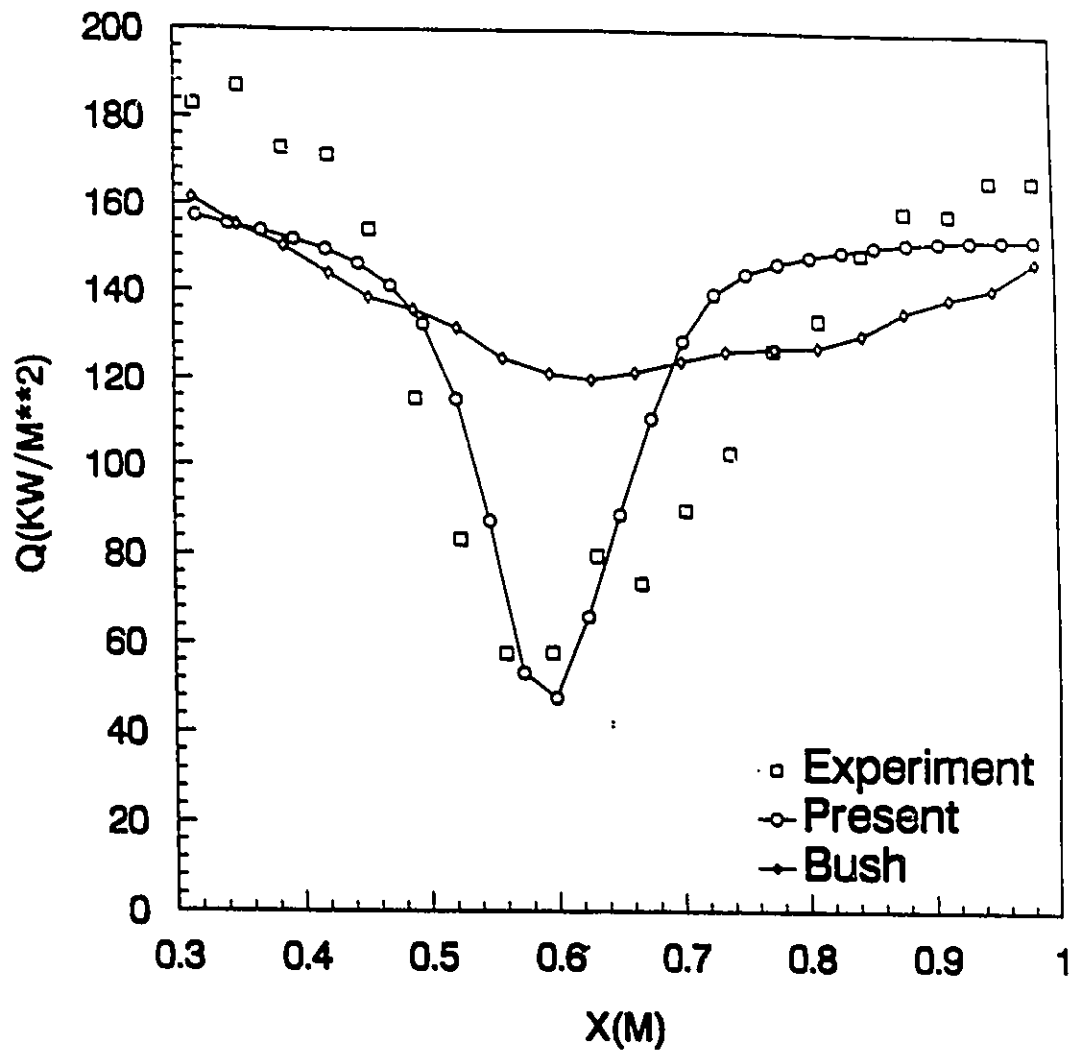
(b)

**Figure 5.17 Comparison of Predicted Heat Flux with Bush's Results**  
**(a) 3rd Row of Tubes (b) 8th Row of Tubes**  
**(c) 13th Row of Tubes (d) 18th Row of Tubes**



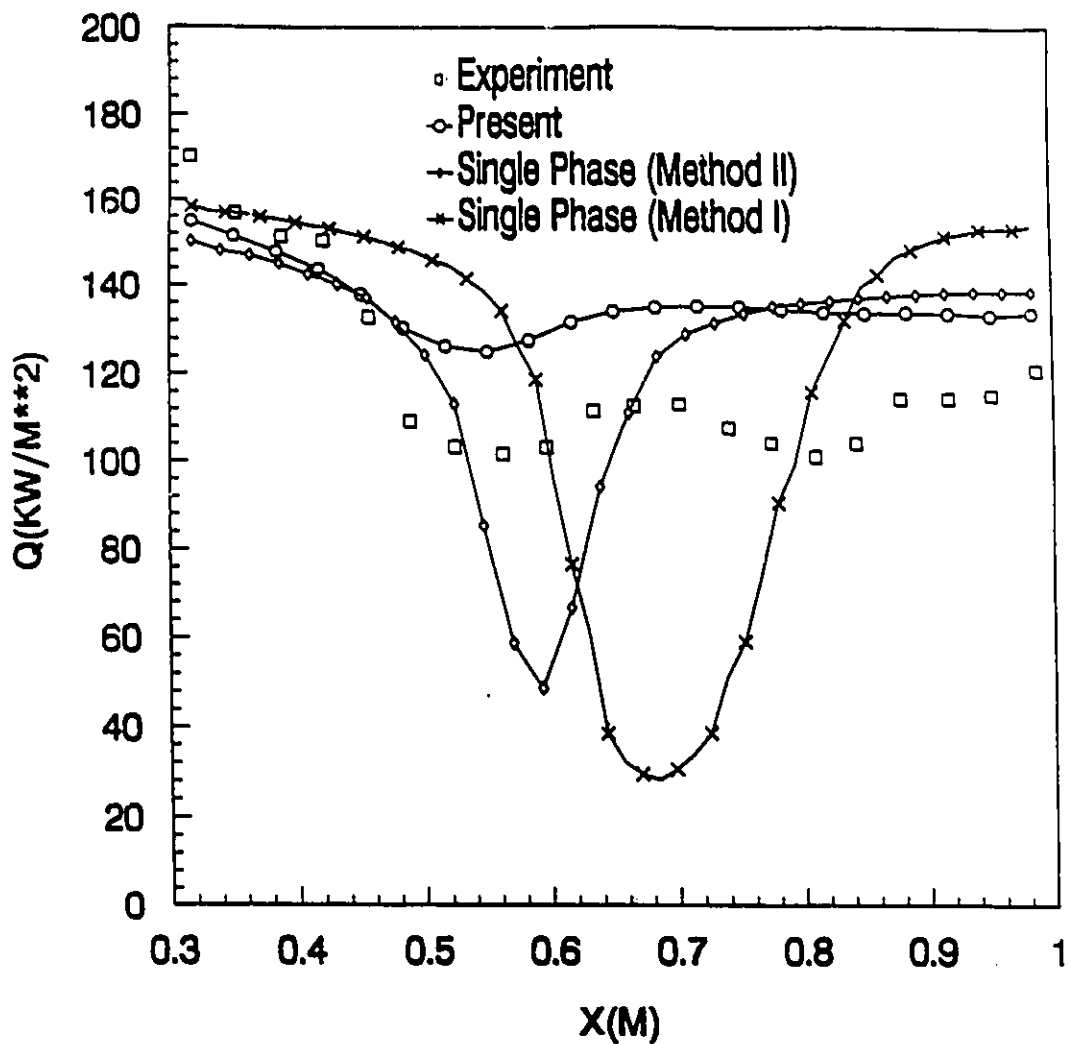
(c)

**Figure 5.17 Comparison of Predicted Heat Flux with Bush's Results**  
**(a) 3rd Row of Tubes (b) 8th Row of Tubes**  
**(c) 13th Row of Tubes (d) 18th Row of Tubes**



(d)

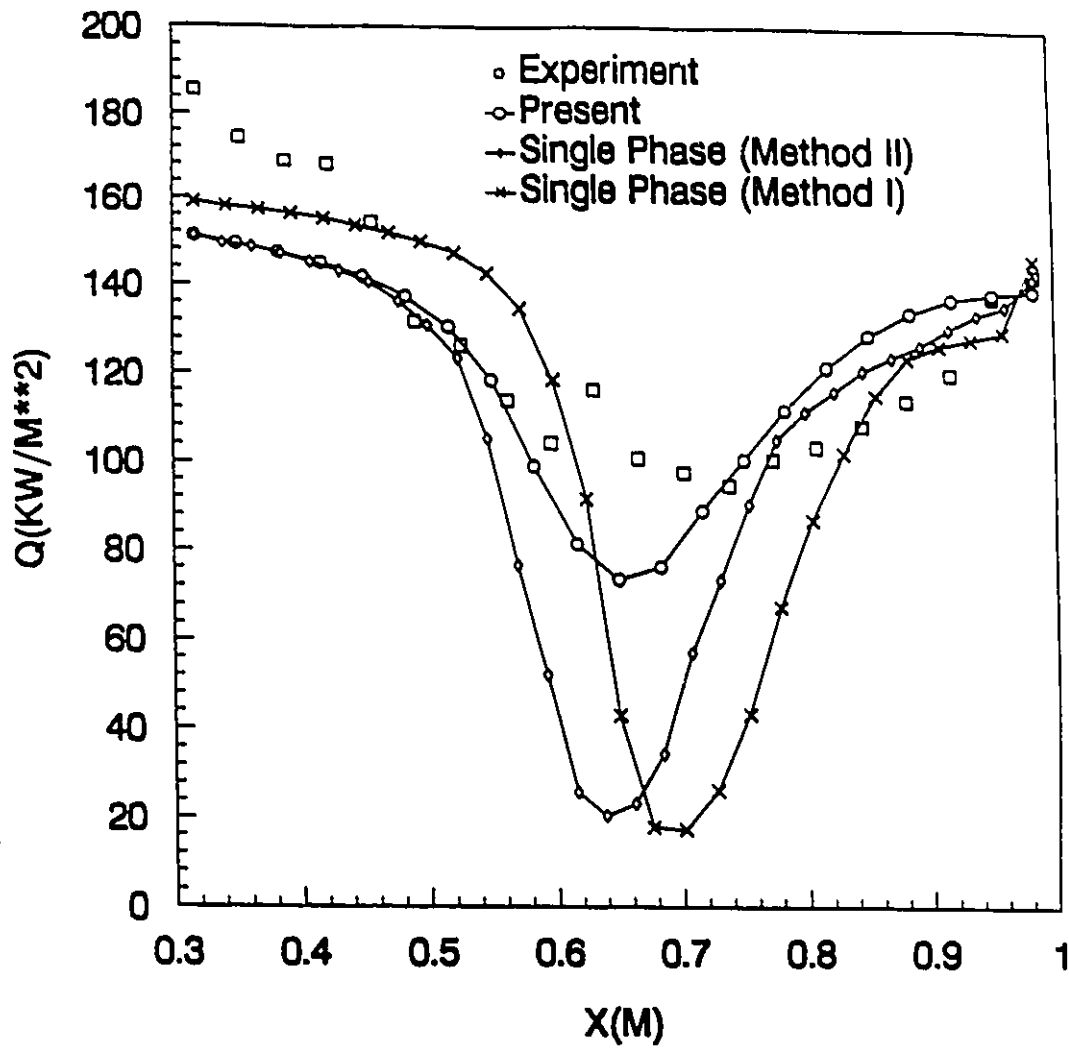
**Figure 5.17 Comparison of Predicted Heat Flux with Bush's Results**  
 (a) 3rd Row of Tubes (b) 8th Row of Tubes  
 (c) 13th Row of Tubes (d) 18th Row of Tubes



(a)

**Figure 5.18 Comparison of Predicted Heat Flux with Results Obtained from Two Different Methodologies of Quasi-Three-Dimensional Single-Phase Model**

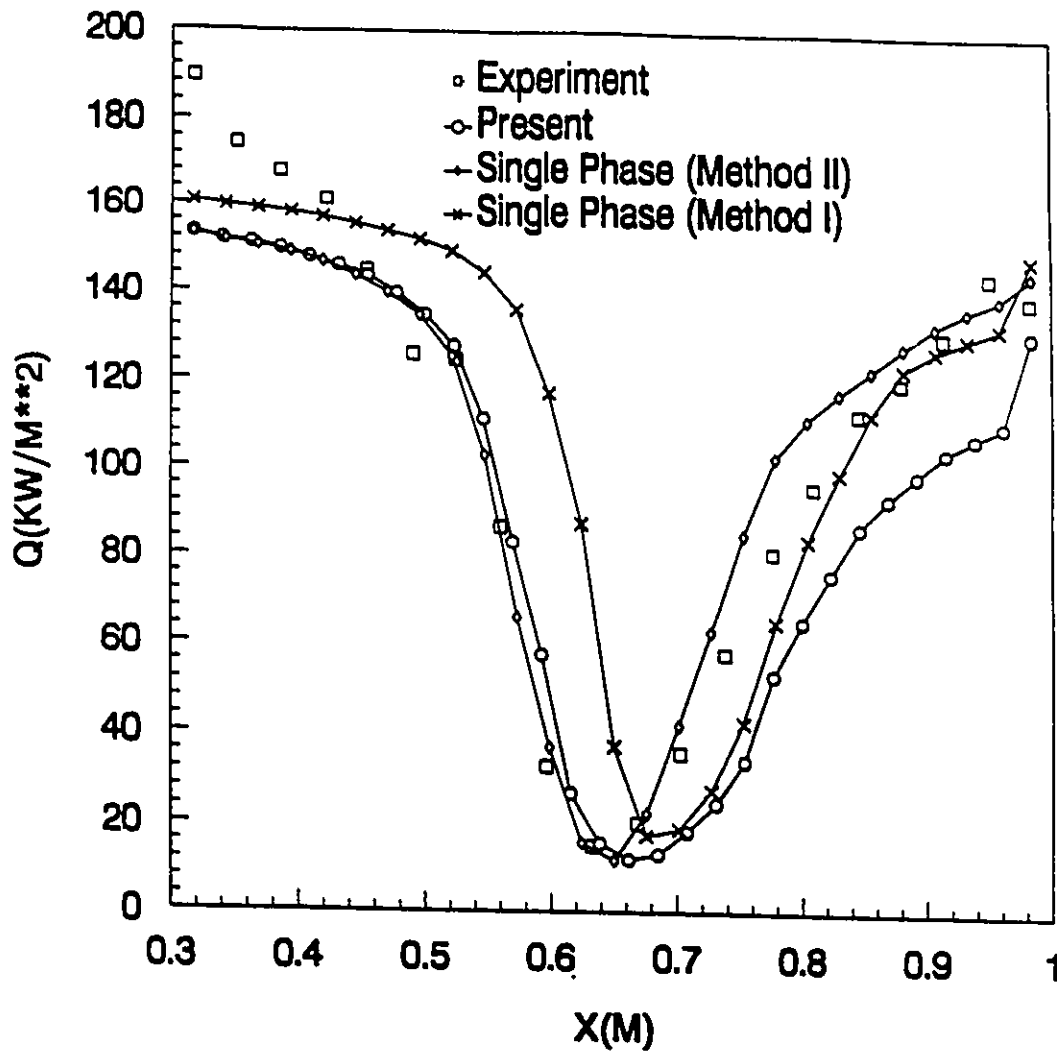
**(a) 3rd Row of Tubes (b) 8th Row of Tubes  
(c) 13th Row of Tubes (d) 18th Row of Tubes**



(b)

**Figure 5.18 Comparison of Predicted Heat Flux with Results Obtained from Two Different Methodologies of Quasi-Three-Dimensional Single-Phase Model**

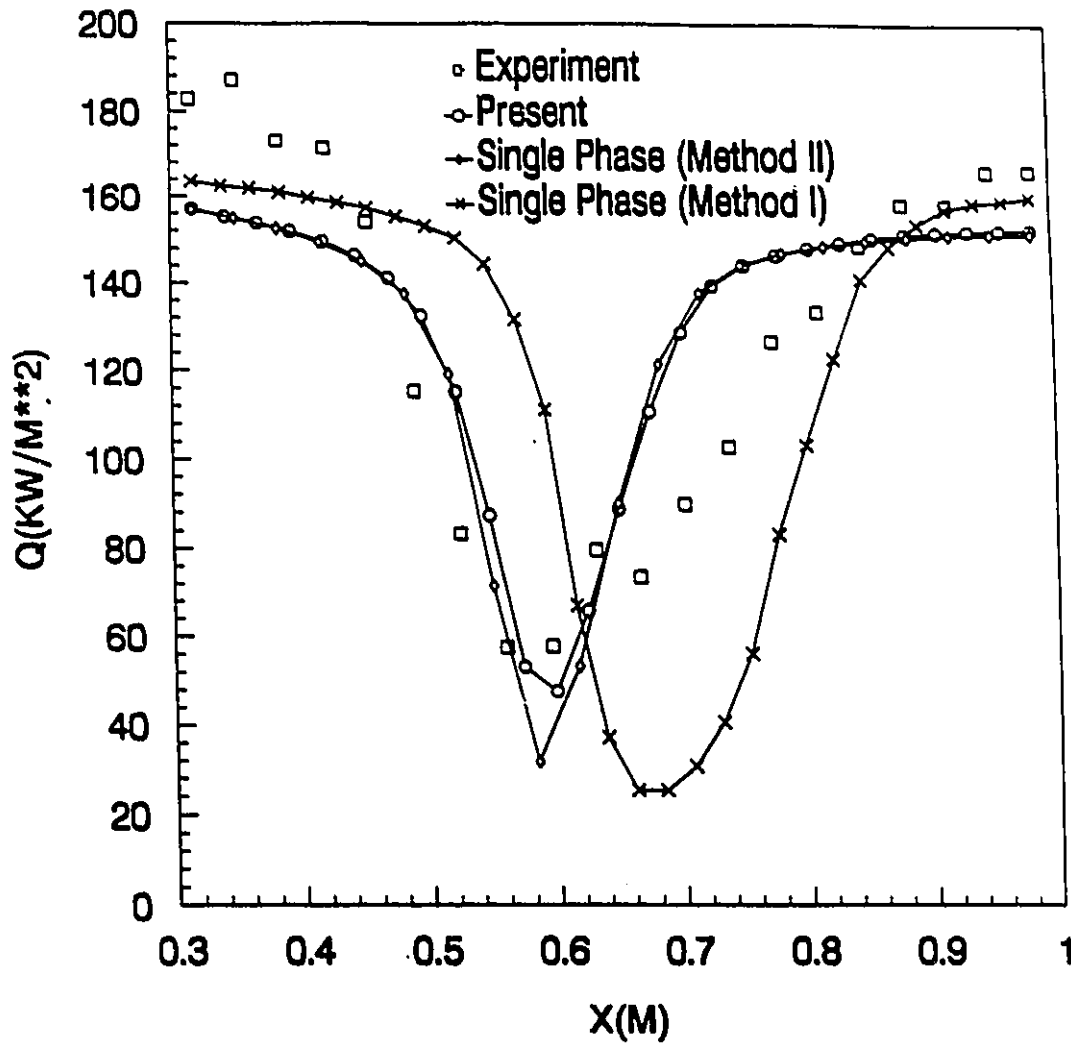
- (a) 3rd Row of Tubes (b) 8th Row of Tubes  
 (c) 13th Row of Tubes (d) 18th Row of Tubes



(c)

**Figure 5.18 Comparison of Predicted Heat Flux with Results Obtained from Two Different Methodologies of Quasi-Three-Dimensional Single-Phase Model**

(a) 3rd Row of Tubes (b) 8th Row of Tubes  
 (c) 13th Row of Tubes (d) 18th Row of Tubes

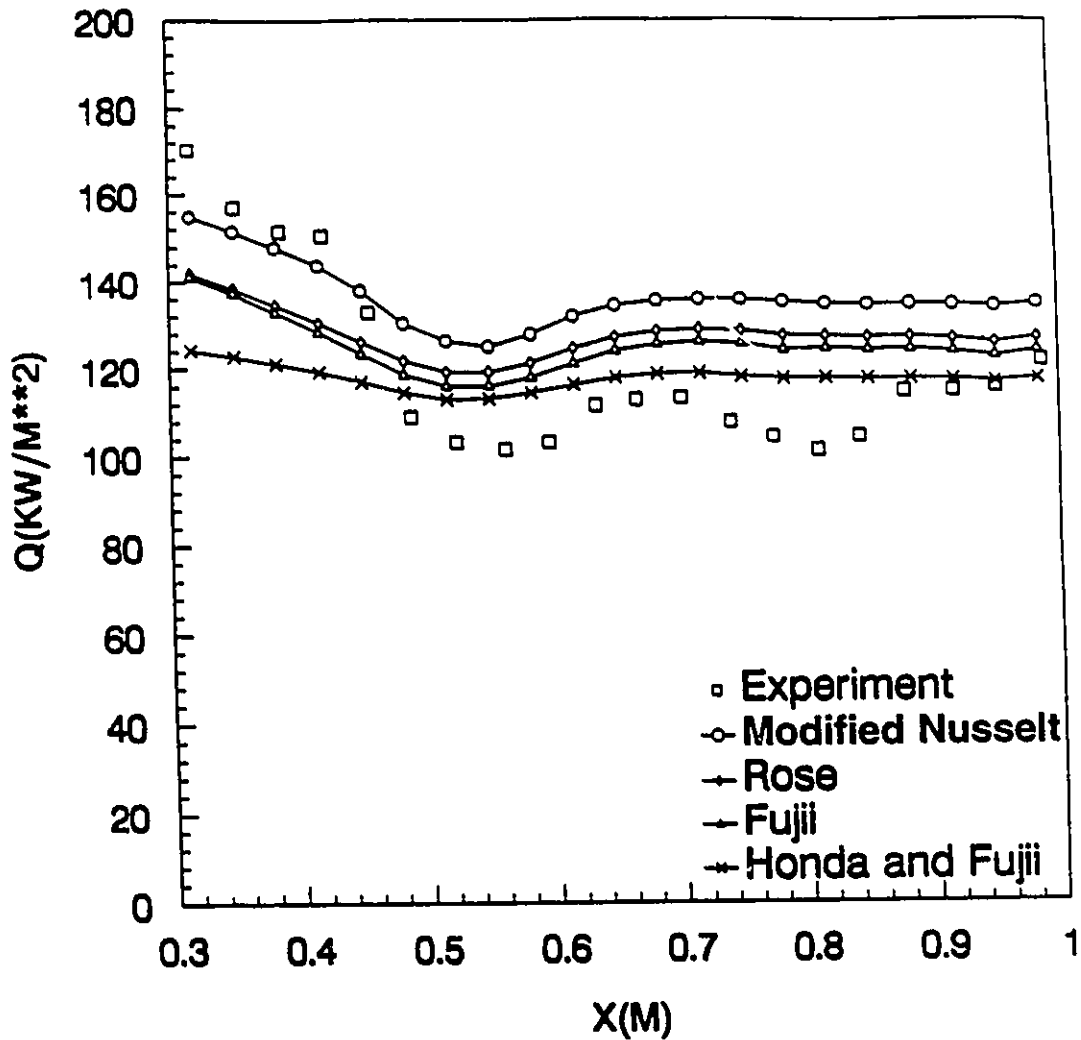


(d)

**Figure 5.18 Comparison of Predicted Heat Flux with Results Obtained from Two Different Methodologies of Quasi-Three-Dimensional Single-Phase Model**

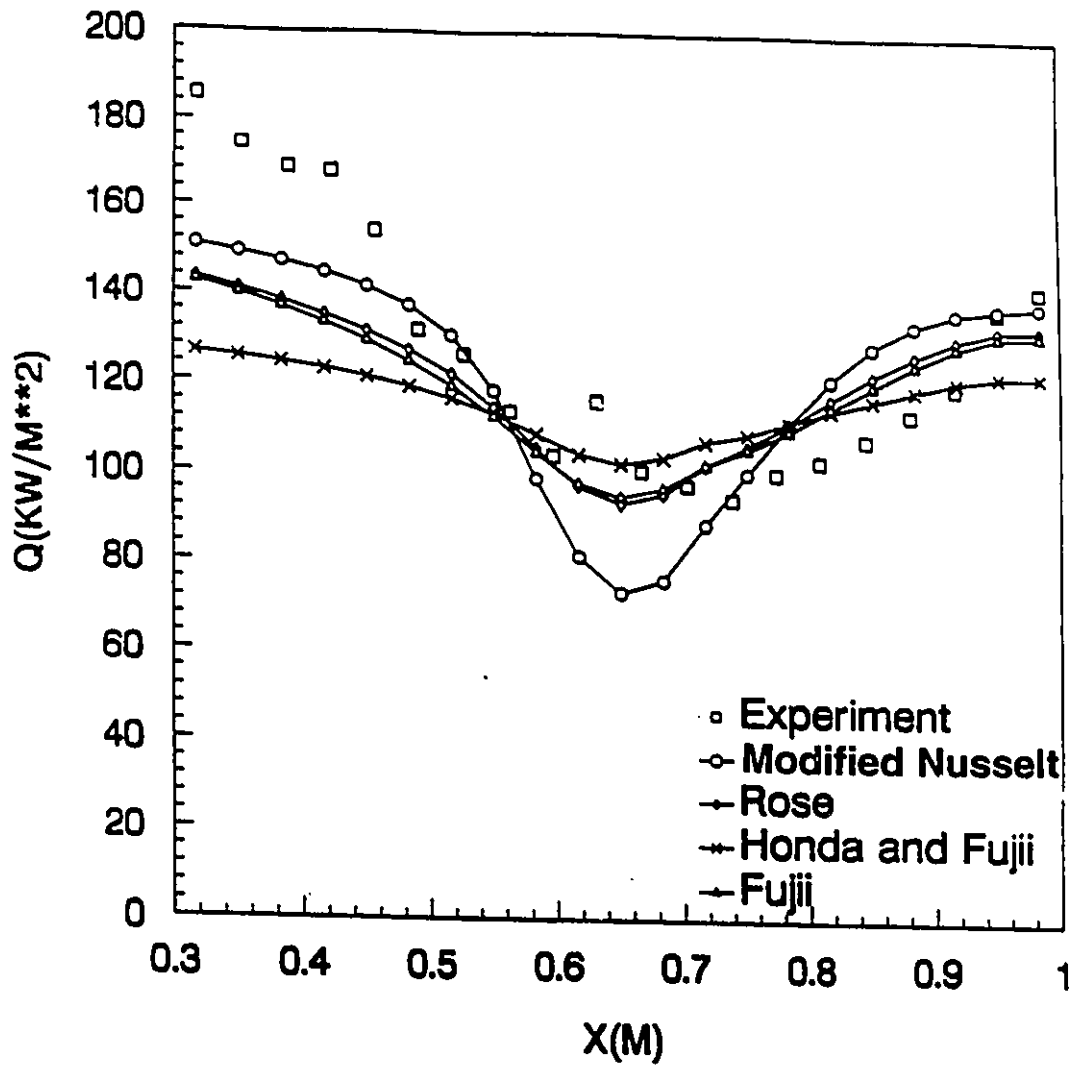
(a) 3rd Row of Tubes (b) 8th Row of Tubes  
 (c) 13th Row of Tubes (d) 18th Row of Tubes





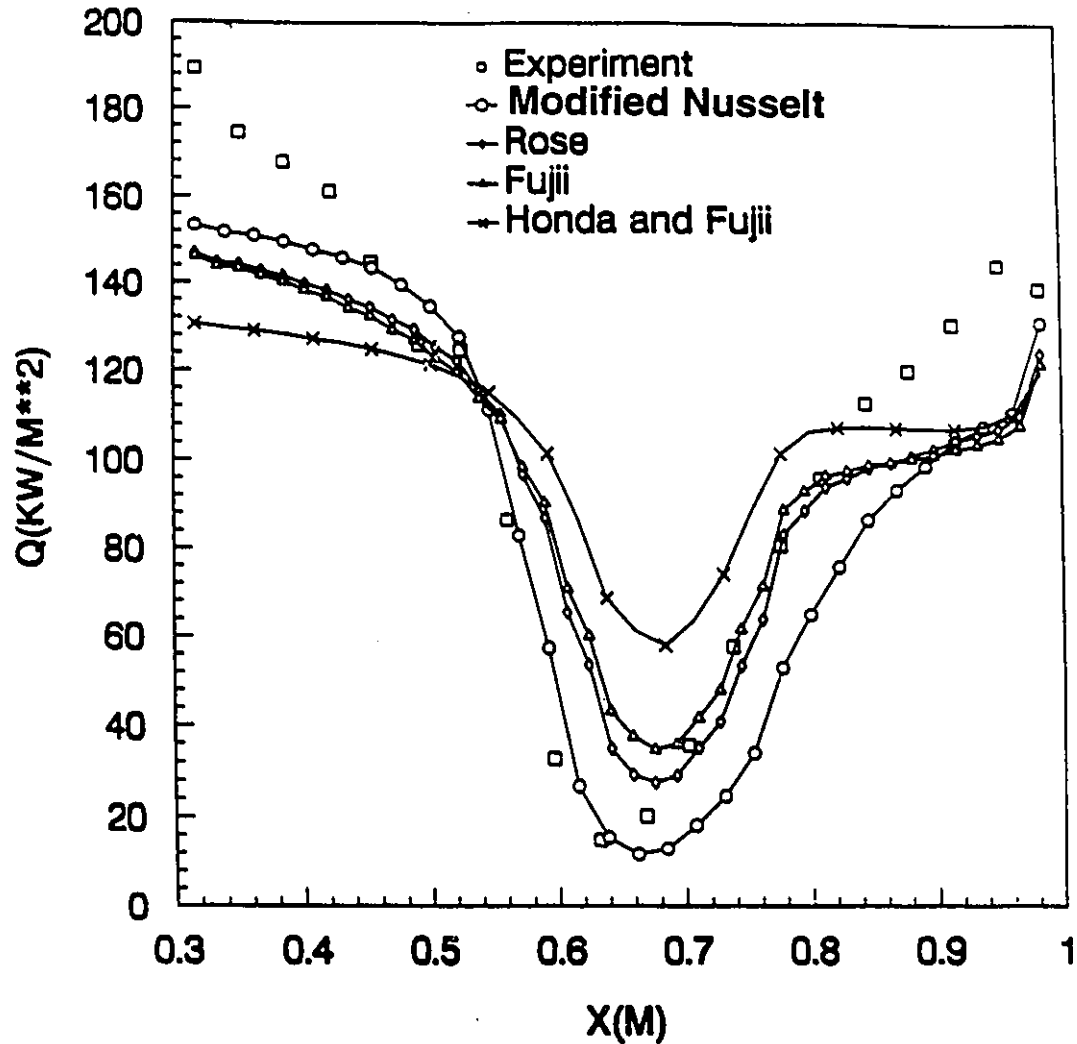
(a)

**Figure 5.19 Comparison of Predicted Heat Flux for Different Correlations of Condensation Heat Transfer Coefficient**  
 (a) 3rd Row of Tubes (b) 8th Row of Tubes  
 (c) 13th Row of Tubes (d) 18th Row of Tubes



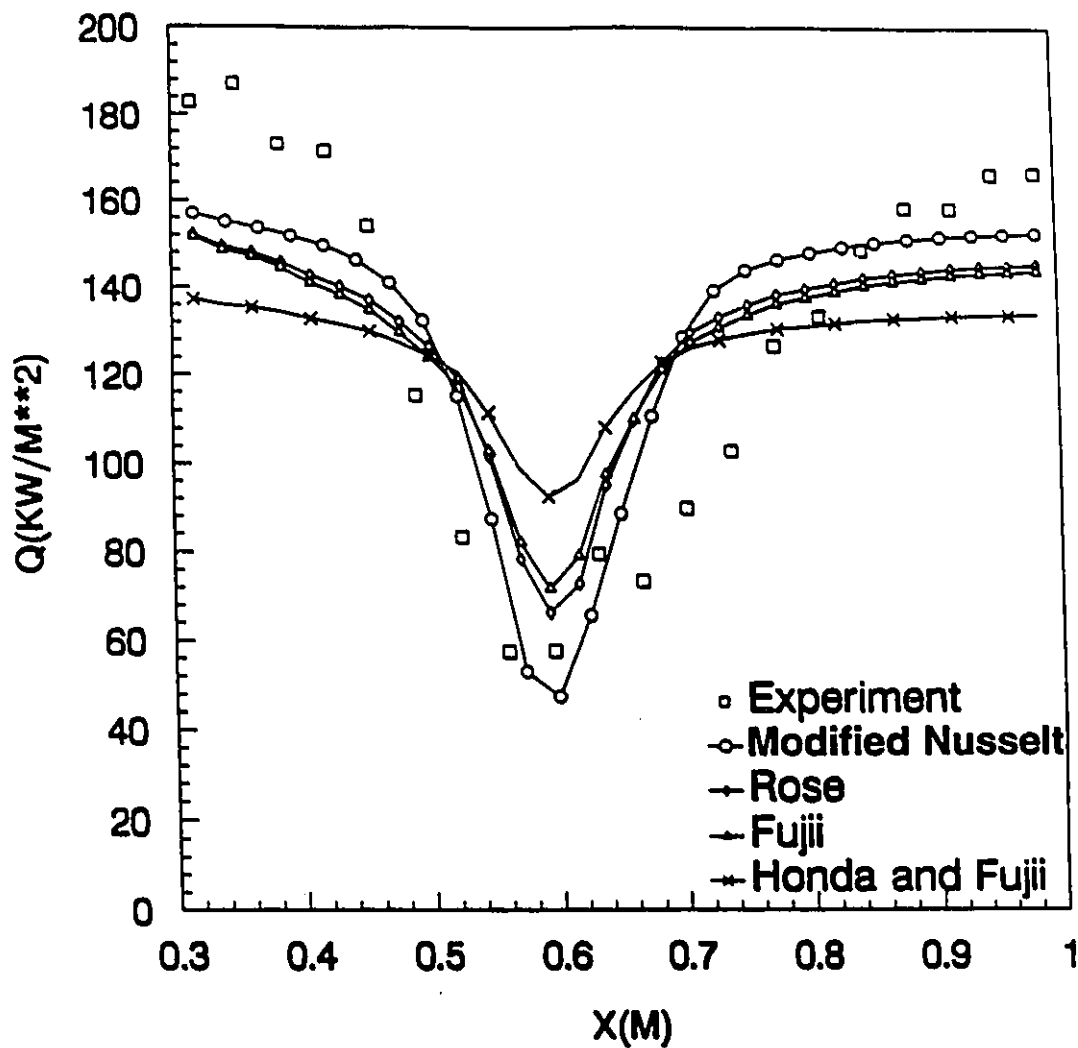
(b)

**Figure 5.19 Comparison of Predicted Heat Flux for Different Correlations of Condensation Heat Transfer Coefficient**  
 (a) 3rd Row of Tubes (b) 8th Row of Tubes  
 (c) 13th Row of Tubes (d) 18th Row of Tubes



(c)

**Figure 5.19 Comparison of Predicted Heat Flux for Different Correlations of Condensation Heat Transfer Coefficient**  
 (a) 3rd Row of Tubes (b) 8th Row of Tubes  
 (c) 13th Row of Tubes (d) 18th Row of Tubes



(d)

**Figure 5.19 Comparison of Predicted Heat Flux for Different Correlations of Condensation Heat Transfer Coefficient**  
 (a) 3rd Row of Tubes (b) 8th Row of Tubes  
 (c) 13th Row of Tubes (d) 18th Row of Tubes

**VITA AUCTORIS**

**NAME:** Atish Bokil

**PLACE OF BIRTH** Windsor, Ontario

**YEAR OF BIRTH** 1971

**EDUCATION** Visvesvaraya Regional Engineering College, Nagpur,  
India.  
1988-1992 B.E. in Mechanical Engineering.

University of Windsor, Windsor, Ontario  
1992-1994 M.A.Sc. Candidate in Mechanical Engineering.